Thermal Stabilization of Nanocellulose by Chemical Modification

2017

Melissa AGUSTIN

Contents

List of Abbreviations

ADM	Adamantoyl
AGU	Anhydro-D-glucose unit
BC	Bacterial cellulose
BNZ	Benzoyl
C10	Decanoyl
C14	Myristoyl
C2	Acetyl
C3	Propanoyl
C8	Octanoyl
CrI	Crystallinity index
DP	Degree of polymerization
DP_n	Number average degree of polymerization
DP_v	Viscosity average degree of polymerization
DP_w	Weight average degree of polymerization
DS	Degree of substitution
FTIR	Fourier Transform Infrared
MW	Molecular weight
MWD	Molecular weight distribution
NBKP	Needle bleached kraft pulp
$NaBH_4$	Sodium borohydride
PIV	Pivaloyl
PyGCMS	Pyrolysis-gas chromatography-mass spectrometry
REs	Reducing ends
TG	Thermogravimetric
TWL	Total weight loss
T_{max}	Temperature at maximum weight loss rate
T_{onset}	Extrapolated onset of degradation temperature
$t_{1\%}$	Time at 1% weight loss
WCNF	Wood cellulose nanofibers
WLT	Weight loss temperature

Chapter 1

General Introduction

1.1. Background of the study

The negative impacts of petroleum-based industries on the environment trigger the global call to develop green technologies, which are based on the utilization of renewable and sustainable materials that have low carbon footprints. This concept of renewability and sustainability has become a stimulus to explore the potential of bio-based materials, and one of these is cellulose.

As a structural polymer, cellulose does not occur naturally as an isolated molecule, but as assemblies of individual cellulose chain-forming fibers (Brinchi et al. 2013). The individual elementary fibrils are part of a hierarchical structure composed of elementary fibrils, which pack into larger units called microfibrils, which are in turn assembled into fibers (Habibi et al. 2010). Because of this fibrillar characteristic, the early application of cellulose, which dates back more than a hundred years ago, has been as a fibrous material in paper and textile industries. Its applications then continuously evolved throughout the past several decades, and the most recent of which are applications that utilize the advantages of the deconstructed cellulose fibers, a material known as nanocellulose. Owing to several unique characteristics, nanocellulose offers a wide range of applications from basic industrial materials like foods, cosmetics, and textiles, to advanced materials such as foldable electronics, high-performance nanocomposites and scaffolds for medical applications (Abitbol et al. 2016; Chattopadhyay and Patel 2016; Gómez H. et al. 2016; Ullah et al. 2016).

Among the various applications feasible for nanocellulose, its use as a reinforcing filler has drawn tremendous interest among researchers. The inherent excellent mechanical properties of crystalline nanocellulose, which was reported to be as strong as Kevlar, make it a good candidate as reinforcing filler in polymer composite preparation. In this field, the application of heat during processing, such as extrusion or melt blending, is inevitable. For example, the polymer matrix in combination with nanocellulose has to be kneaded repeatedly by the action of heat and mechanical force in order to uniformly disperse the nanocellulose into the matrix. In this context, the poor thermal stability of nanocellulose becomes a limiting factor, which prevents their application to polymer

matrices with high melting points such as polyamide or polycarbonate. In order to realize the potential of nanocellulose as a new-generation material that can be used at high-temperature processing of polymer matrices with high melting points (>220^{o}C), this study aimed to improve the thermal stability of nanocellulose by chemical modification.

1.2. Cellulose structure

First discovered and isolated by Anselme Payen in 1838, cellulose is the most abundant biopolymer on earth with an estimated annual production of 10^{11}-10^{12} tons (Krassig 1993; Klemm et al. 2002). It is a ubiquitous structural polymer found mostly in plant cell walls and serves to maintain the cell structure and confers mechanical properties to cells (Habibi 2014). It constitutes about 33% of all plant matter (Eyley and Thielemans 2014); but there are also plants that contain a large amount of cellulose such as hemp, flax, cotton, jute and ramie (Eichhorn et al. 2009). Non-plants sources of cellulose are also available such as those produced by specific bacteria and those present in marine animals like tunicates.

The polymeric structure of cellulose was first elucidated by Staudinger in 1920 (Klemm et al. 2011). Cellulose is a polydisperse, linear homopolysaccharide composed of anhydro-D-glucose units (AGU) linked together by ß(1→4) glycosidic bonds, with cellobiose as a repeating unit, which is a dimer of glucose (Figure 1-1). The number of AGU defines the degree of polymerization (DP), the values of which can vary depending on the source and process of isolation and purification. Each repeating AGU has three free hydroxyl groups at carbon atoms in the 2, 3 and 6 positions, which are capable of forming hydrogen bonds. These hydrogen bonds are formed inter- and intramolecularly and play a major role in directing the crystalline packing and also in governing the physical properties of cellulose (John and Thomas 2008). Furthermore, the terminal groups on the chain ends of cellulose are different. One end consists of the close ring structure called the non-reducing end and another end corresponds to a cyclic hemiacetal known as the reducing end (RE). This cyclic hemiacetal exists in equilibrium with its aliphatic aldehyde form, thus, susceptible to reduction.

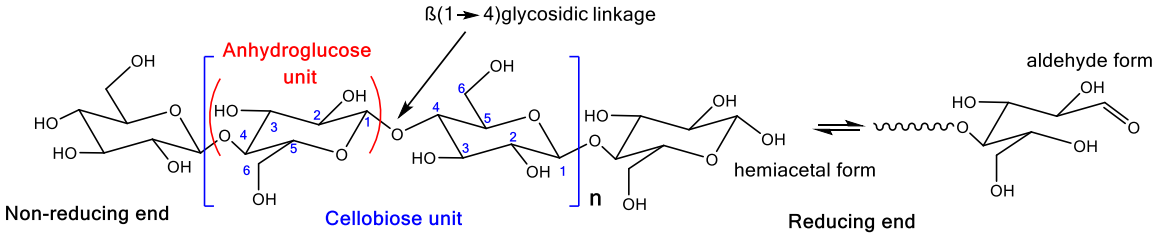

Figure 1-1. Molecular structure of cellulose showing the cellobiose and anhydroglucose unit, along with atom numbering, glycosidic bond, and the two types of terminal groups.

1.3. Nanocellulose: classifications and properties

Nanocellulose, which generally refers to all types of nanometric cellulosic substrates can be classified into three main subcategories on the basis of their dimensions, functions and preparation methods (Klemm et al. 2011; Habibi 2014). (1) Cellulose nanofibers (CNFs) produced by mechanically disintegrating cellulose fiber bundles, typically from wood, into nanoscale fibrils with diameters ranging from 10-100 nm and lengths varying by several micrometers. (2) Cellulose nanocrystals (CNCs) obtained by hydrolyzing the amorphous part of the cellulose with strong acid. CNCs usually consist of elongated highly crystalline rod-like nanoparticles with lengths typically shorter than those of CNFs. CNCs also have lower DP as a result of the cleavage of glycosidic bonds during hydrolysis. (3) Bacterial cellulose (BC), synthesized by several bacterial species in the form of pellicles consisting of a network of randomly assembled ribbon-like fibrils less than 100 nm wide. BC with relatively straight, continuous, and dimensionally uniform (Habibi 2014) nanofibers can also be acid hydrolyzed to produce CNCs.

Recently, there has been significant growth in nanocellulose research, which is evident from the numerous publications and patents involving this material. The worldwide attention paid to nanocellulose can be attributed to its several unique properties. Nanocellulose exhibits large surface area, low density, high mechanical strength, low coefficient of thermal expansion, and wide chemical-modification capacity (Klemm et al. 2011). Owing to several unique characteristics, the potential of nanocellulose as a new-generation material is enormous.

1.4. Nanocellulose as a reinforcing filler and its limitation

Nanocellulose, particularly nanocrystalline cellulose, which contains only a small number of defects, has a theoretical axial Young's modulus which is higher than that of steel and similar to that of Kevlar (Habibi et al. 2010). Because of this excellent toughness, nanocellulose makes a promising material as reinforcing filler in polymer composites. Nanocellulose has been reported to improve mechanical properties, enhance optical transparency and reduce thermal expansion of the resulting composites. One of the pioneering works in this field was the report by Favier et al. (1995) on the reinforcement of poly(styrene-*co*-*n*-butyl acrylate) (PBA) latex films with cellulose whiskers from tunicates. A PBA film with 6% whiskers prepared by casting showed an almost two orders of magnitude higher shear modulus than the non-reinforced PBA film. Yano et al. (2005) pioneered the reinforcement of transparent thermosetting resins by BC nanofibers. The BC nanofiber-reinforced composites were optically transparent, showed a low coefficient of thermal expansion, and exhibited mechanical strength five times that of engineered plastic. Intensive and informative reviews on the application of nanocelluloses as reinforcing fillers have also been published (Eichhorn et al. 2009; Siqueira et al. 2010; Klemm et al. 2011; Abdul Khalil et al. 2012; Brinchi et al. 2013)

Despite remarkable developments in the past decades, the processing technology of polymer reinforced with nanocellulose is restricted to about 200 °C (Azizi Samir et al. 2005) . This limitation is attributed to the poor thermal stability of cellulose which starts to degrade at about 230°C (Klemm et al. 2011). During compounding, the high shearing force needed to attain a good dispersion of the filler into the matrix generates heat that eventually causes the actual temperature of the melt to be higher than the set processing temperature. Thus, to avoid the actual temperature of the melt to increase to as high as the degradation temperature of cellulose, the polymer matrix for nanocellulose has been limited to those with low melting points. To expand the use of nanocellulose to reinforce thermoplastic matrices of high melting point such as polyamide 6, there is a need to produce thermally stable nanocellulose. It is also viewed that having thermally stable nanocellulose can assure long-term durability and performance reliability of the end product. To realize such application and vision, enhancing the thermal stability of nanocellulose is of utmost importance.

The thermal stability of nanocellulose is influenced by several factors and there

have been studies that reported the thermal stability of nanocellulose as affected by drying techniques (Quiévy et al. 2010; Peng et al. 2013; Uetani et al. 2014), mechanical processing (Quiévy et al. 2010; Jacquet et al. 2011), bleaching (Jonoobi et al. 2009), delignification (Okahisa et al. 2011), hydrolysis conditions (Martínez-Sanz et al. 2011; Camarero Espinosa et al. 2013; Yu et al. 2013), and chemical treatments (Kabir et al. 2013). Still, a systematic investigation of the effect of chemical modification, particularly esterification, on the thermal stability of nanocellulose has not been reported.

1.5. Chemical modification of nanocellulose

The properties of cellulose can be tuned to the desired application by chemical modification. The presence of a large number of hydroxyl groups within the cellulose structure offers a unique platform for significant surface modification to graft various types of functional molecules to cellulose (Habibi 2014). The surface hydroxyl groups, which are often exploited for chemical modification, can be converted into esters, ethers, urethanes and siloxanes functions (Belgacem et al. 2011). Similarly, the chemical modifications conducted on cellulose are logically extended also to nanocellulose but often employing necessary precautions to avoid damage to the crystal structure and keep the morphology of the starting nanocellulose. When used as reinforcing fillers, nanocellulose have been chemically modified only on the surface hydroxyl groups and the modification often aims (1) to provide them with an efficient hydrophobic barrier, (2) to compatibilize their surface with that of a non-polar polymer matrix, or (3) to make them reactive with the chosen matrix (Belgacem et al. 2011; Missoum et al. 2012)

One of the most commonly used chemical modifications applied to nanocellulose is esterification, a reaction in which the hydroxyl (OH) groups of cellulose reacts to an acylant usually a carboxylic acid, an acid anhydride or an acyl chloride. Esterification of cellulose can be done either in homogeneous or heterogeneous process. In the homogeneous process, cellulose is either initially dissolved in an appropriate solvent before the reaction (Freire et al. 2006) or solid cellulose is being modified in a reaction media without a solvent or diluent, but the resulting esters gradually dissolves as it is produced (Sassi and Chanzy 1995). The homogeneous process results to the degradation of the supramolecular structure of the cellulose fibers. When the aim is to produce cellulose derivatives that preserved the supramolecular structure of the starting cellulose

fiber, heterogeneous or the “fibrous” process is used. In this process, a solvent or diluent is added to the reaction medium and the resulting cellulose ester remains insoluble (Sassi and Chanzy 1995).

1.6. Objectives of the study

The main objective of the study is to investigate the effect of esterification on the thermal stability of nanocellulose. Specifically, the study aims to:

- evaluate the effect of DP on the thermal stability of BC;
- determine the effect of acetylation on thermal stability of BC with varying DP;
- prepare various types of ester derivatives of BC nanofibers and nanocrystals;
- investigate the effect of the structure of the esters on the thermal stability of BC nanofibers and nanocrystals;
- deduce the events at and propose the mechanism of the initial stage of thermal degradation of BC esters;
- evaluate the resistance against thermally-induced depolymerization and discoloration of BC esters;
- esterify wood-based pulps and nanofibers; and
- investigate the effect of degree of substitution (DS) on the thermal properties of wood-based pulps and nanofibers.

1.7. Outline of the thesis

To meet the objectives of this study, this thesis is organized as follows:

In Chapter 1, the rationale of this study is explained by presenting the current situation of scientific research about nanocellulose. The significance of improving thermal stability of nanocellulose is also explained.

In Chapter 2, the effect of DP on thermal stability was investigated. Nanocellulose with varying DP was prepared by acid hydrolysis of BC which was chosen to eliminate the effect of hemicellulose. The thermal stability was evaluated by thermogravimetric analysis (TGA) and correlated to the DP. Subsequently, acetylation was carried out as a preliminary chemical modification procedure and the thermal stability of nanocellulose acetates with different DP was determined. The improvement in thermal stability after acetylation was correlated to the DP and the dependence of degree of improvement to DP

because of the number of REs was confirmed by sodium borohydride reduction.

In Chapter 3, various types of nanocellulose esters, straight-chain, aromatic, branched, were prepared in order to assess the effect of the structure of the esters on thermal stability. Both dynamic and isothermal heating were used to evaluate thermal stability using TGA. The event at the onset of degradation was deduced using pyrolysis-gas chromatography-mass spectrometry (PyGCMS). By analyzing the structure of the evolved gas during low-temperature pyrolysis, the mechanism of thermal degradation at the initial stage was proposed. The role of alpha hydrogens in the structure of the ester groups on the mechanism of thermal stabilization was established.

In Chapter 4, the change in DP of various types of nanocellulose esters was determined using viscometry and gel permeation chromatography before and after thermal treatment at various temperatures in nitrogen and in air. The effect of the structure of the esters on the resistance against thermally-induced depolymerization was investigated. Furthermore, thermal discoloration was quantitatively evaluated.

In Chapter 5, esterification was extended to wood-based pulps and the effect of DS on thermal properties was evaluated to identify the optimum DS that would possibly esterify the hemicellulose and amorphous cellulose. The ester that gave the highest degree of improvement to NBKP was then chosen to modify wood cellulose nanofibers (WCNF). Consequently, the effect of DS on the thermal stability of WCNF, and the resistance against thermally-induced discoloration and depolymerization was also investigated.

In Chapter 6, the conclusions drawn from the findings of this study are presented.

1.8. References

Abdul Khalil HPS, Bhat AH, Ireana Yusra AF (2012) Green composites from sustainable cellulose nanofibrils: A review. Carbohydr Polym 87:963–979.

Abitbol T, Rivkin A, Cao Y, et al (2016) Nanocellulose, a tiny fiber with huge applications. Curr Opin Biotechnol 39:76–88.

Azizi Samir MAS, Alloin F, Dufresne A (2005) Review of recent research into cellulosic whiskers, their properties and their application in nanocomposite field. Biomacromolecules 6:612–26.

Belgacem MN, Salon-Brochier MC, Krouit M, Bras J (2011) Recent advances in surface chemical modification of cellulose fibres. J Adhes Sci Technol 25:661–684.

Brinchi L, Cotana F, Fortunati E, Kenny JM (2013) Production of nanocrystalline cellulose from lignocellulosic biomass: Technology and applications. Carbohydr Polym 94:154–169.

Camarero Espinosa S, Kuhnt T, Foster EJ, Weder C (2013) Isolation of thermally stable cellulose nanocrystals by phosphoric acid hydrolysis. Biomacromolecules 14:1223–1230.

Chattopadhyay D, Patel B (2016) Synthesis, characterization and application of nanocellulose for enhanced performance of textiles.

Eichhorn SJ, Dufresne A, Aranguren M, et al (2009) Review: current international research into cellulose nanofibres and nanocomposites. J Mater Sci 45:1–33.

Eyley SS, Thielemans W (2014) Surface modification of cellulose nanocrystals. Nanoscale 6:7764–79.

Favier V, Canova GR, Cavaille JY, et al (1995) Nanocomposite materials from latex and cellulose whiskers. Polym Adv Technol 6:351–355.

Freire CSR, Silvestre AJD, Neto CP, et al (2006) Controlled heterogeneous modification of cellulose fibers with fatty acids: Effect of reaction conditions on the extent of esterification and fiber properties. J Appl Polym Sci 100:1093–1102.

Gómez H. C, Serpa A, Velásquez-Cock J, et al (2016) Vegetable nanocellulose in food science: A review. Food Hydrocoll 57:178–186.

Habibi Y (2014) Key advances in the chemical modification of nanocelluloses. Chem Soc Rev 43:1519–42.

Habibi Y, Lucia LA, Rojas OJ (2010) Cellulose nanocrystals: chemistry, self-assembly, and applications. Chem Rev 110:3479–3500.

Jacquet N, Quiévy N, Vanderghem C, et al (2011) Influence of steam explosion on the thermal stability of cellulose fibres. Polym Degrad Stab 96:1582–1588.

John M, Thomas S (2008) Biofibres and biocomposites. Carbohydr Polym 71:343–364.

Jonoobi M, Harun J, Shakeri A, Misra M (2009) Chemical composition, crystallinity, and thermal degradation of bleached and unbleached kenaf bast (*Hibiscus cannabinus*) pulp and nanofibers. BioResources 4:626–639.

Kabir MM, Wang H, Lau KT, Cardona F (2013) Effects of chemical treatments on hemp fibre structure. Appl Surf Sci 276:13–23.

Klemm D, Kramer F, Moritz S, et al (2011) Nanocelluloses: a new family of nature-based materials. Angew Chem Int Ed Engl 50:5438–66.

Klemm D, Schmauder H-P, Heinze H (2002) Cellulose. Biopolymers 6:275–287.

Krassig H (1993) Cellulose, Structure, Accessibility and Reactivity. Gordon and Breach Publishers, PA (USA)

Martínez-Sanz M, Lopez-Rubio A, Lagaron JM (2011) Optimization of the nanofabrication by acid hydrolysis of bacterial cellulose nanowhiskers. Carbohydr Polym 85:228–236.

Missoum K, Bras J, Belgacem MN (2012) Organization of aliphatic chains grafted on nanofibrillated cellulose and influence on final properties. Cellulose 19:1957–1973.

Okahisa Y, Abe K, Nogi M, et al (2011) Effects of delignification in the production of plant-based cellulose nanofibers for optically transparent nanocomposites. Compos Sci Technol 71:1342–1347.

Peng Y, Gardner DJ, Han Y, et al (2013) Influence of drying method on the material properties of nanocellulose I: thermostability and crystallinity. Cellulose 20:2379–2392.

Poletto M, Pistor V, Zeni M, Zattera AJ (2011) Crystalline properties and decomposition kinetics of cellulose fibers in wood pulp obtained by two pulping processes. Polym Degrad Stab 96:679–685.

Quiévy N, Jacquet N, Sclavons M, et al (2010) Influence of homogenization and drying on the thermal stability of microfibrillated cellulose. Polym Degrad Stab 95:306–314.

Sassi J, Chanzy H (1995) Ultrastructural aspects of the acetylation of cellulose. Cellulose 2:111–127.

Siqueira G, Bras J, Dufresne A (2010) Cellulosic bionanocomposites: a review of preparation, properties and applications. Polymers (Basel) 2:728–765.

Uetani K, Watanabe Y, Abe K, Yano H (2014) Influence of drying method and precipitated salts on pyrolysis for nanocelluloses. Cellulose 21:1631–1639.

Ullah H, Santos HA, Khan T (2016) Applications of bacterial cellulose in food, cosmetics and drug delivery. Cellulose 23:2291–2314.

Yano H, Sugiyama J, Nakagaito AN, et al (2005) Optically Transparent Composites Reinforced with Networks of Bacterial Nanofibers. Adv Mater 17:153–155.

Yu H, Qin Z, Liang B, et al (2013) Facile extraction of thermally stable cellulose nanocrystals with a high yield of 93% through hydrochloric acid hydrolysis under hydrothermal conditions. J Mater Chem A 1:3938.

Chapter 2

Improvement in the thermal stability of acetylated nanocellulose: dependence on the degree of polymerization

2.1. Introduction

The thermal stability of nanocellulose is influenced by several factors, from the source to the processing methods (chemical or mechanical treatment) used to isolate the nanocellulose to the post-treatment methods used for purification or modification, which can have profound effects on its thermal properties.

The thermal properties of cellulose differ depending on their origin. Kim et al. (2010) studied the thermal decomposition of cellulose from three different sources, and found that the temperature at the maximum weight loss rate (T_{max}) increased with increasing crystallite size in the order *Halocynthia* (a tunicate) > cotton > Funacel (a commercial microcrystalline cellulose from wood).

Chemical treatments such as bleaching and delignification also affect the thermal properties of nanocellulose. NaOH–anthraquinone pulping followed by three-stage bleaching has been reported to increase the thermal stability of kenaf nanofibers because of the removal of hemicelluloses and lignin and an increase in crystallinity (Jonoobi et al. 2009). Combined acid and alkali treatment followed by mechanical processing (cryocrushing, defibrillation, and homogenization) has also been found to improve the thermal stability of CNFs from wheat straw and soy hull fibers(Alemdar and Sain 2008). Conversely, delignification by acidified sodium chlorite solution could decrease the thermal stability of bamboo nanofibers(Okahisa et al. 2011).

While alkali treatment to remove hemicelluloses has been reported to improve the thermal stability of CNFs,(Jonoobi et al. 2009) hydrolysis using strong acids, especially sulfuric acid, during isolation results in the CNCs being less thermally stable than the original pulp because of the introduction of sulfate groups on the surface of the crystals (Lu and Hsieh 2010; Johar et al. 2012). Gurgel et al. (2012) characterized cellulose residues from extremely low acid hydrolysis of sugarcane bagasse using sulfuric acid. Despite the low concentration of sulfuric acid used, the onset temperature of thermal degradation for hydrolyzed cellulose was lower than the original pulp, and the T_{max} was

found to decrease with decreasing degree of polymerization (DP) of the isolated CNC. The low thermal stability of sulfated CNCs was ascribed to the catalytic effect of sulfuric acid produced when cellulose is desulfated during thermal decomposition.[15] Attempts to improve the thermal stability of CNCs have been made, and include neutralizing the sulfate groups(Wang et al. 2007; Martínez-Sanz et al. 2011) and using milder mineral acids such as hydrochloric acid (Yu et al. 2013) or phosphoric acid (Camarero Espinosa et al. 2013) for hydrolysis.

Post-treatment methods such as drying have also been reported to affect the thermal stability of nanocellulose. Quiévy et al. (2010) investigated the effect of drying on the thermal stability of microfibrillated cellulose produced by high-pressure homogenization. Of the three types of drying techniques (oven drying, freeze-drying, and atomization), freeze-drying resulted in the highest degradation temperature. Peng et al. (2013) recommended spray drying over freeze-drying and oven drying to obtain more thermally stable nanocellulose. The report of Uetani et al. (2014) claimed that drying methods and the bulk density of nanocelluloses have little influence on pyrolysis behavior of nanocelluloses.

Another post-processing technique to change the properties of nanocellulose is chemical modification. There were already numerous chemical modifications reported for nanocellulose but acetylation is considered the simplest and most widely used. Most of the reports on the acetylation of nanocellulose aimed, however, to improve compatibility of the nanocellulose to the matrix (Ashori et al. 2014; Fahma et al. 2014), render the surface of the nanocellulose more hydrophobic (Nogi et al. 2006; Tomé et al. 2011; Ashori et al. 2014; Cunha et al. 2014; Fahma et al. 2014), or propose alternative methods of acetylation (Çetin et al. 2009; Li et al. 2009; Nishino et al. 2011; Hu et al. 2011; Ávila Ramírez et al. 2014; Božič et al. 2015). Only a limited number of papers focused on the thermal stability of acetylated nanocellulose before incorporation to the polymer matrix. Moreover, studies that assessed thermal stability usually dealt with only one type of nanocellulose, CNFs or CNCs alone (Hu et al. 2011; Lee et al. 2011; Ávila Ramírez et al. 2014). So far, the thermal stability of nanocellulose with different DP values before and after acetylation has not been reported. Because DP is directly related to the number of cellulose REs, which was reported to play a catalytic role during pyrolysis (Matsuoka et al. 2014), this chapter investigated the effect of DP on thermal stability. It is viewed that DP, which is one of the properties that differentiates CNCs from CNFs, may play an

important role during chemical modifications because of the reactivity of the REs. Understanding the role of DP in the thermal stabilization of nanocellulose can be helpful in designing chemical modification procedure that will be effective in thermally stabilizing each type of nanocelluloses.

2.2. Experimental

2.2.1. Materials

Unpurified BC pellicles were obtained from Fujicco Co. Ltd (Kobe, Japan). Acetyl chloride and cupriethylenediamine hydroxide (CED) solution were purchased from Sigma-Aldrich Co. (St Louis, MO, USA). *N*-methyl-2-pyrrolidone (NMP), hydrochloric acid, sodium hydroxide, dehydrated pyridine, ethanol, *t*-butanol, L-serine, Na_2CO_3, and $NaHCO_3$ were supplied by Wako Pure Chemicals Industries (Osaka, Japan). Sodium lauryl sulfate, sodium borohydride ($NaBH_4$), and glucose were purchased from Nacalai Tesque Inc. (Kyoto, Japan). The 2,2′-bicinchoninic acid (BCA) disodium salt and copper sulfate pentahydrate were purchased from Alfa Aesar (Ward Hill, MA, USA) and Kanto Chemical Co. (Tokyo, Japan), respectively. All chemicals were of reagent grade and used without prior purification.

2.2.2. BC pre-treatment

Approximately 5 kg of BC pellicles (2×2×2 cm^3) with fiber content of ~0.8% were washed twice with 1 L of 0.05 M NaOH to partially remove the acetic acid present in the absorbed culture media, and then washed repeatedly with distilled water. Every 300 g of BC pellicles was then disintegrated using a Waring blender (Waring Products, USA) operating at 37 000 rpm (maximum speed) for 3 min. The disintegrated BC was then neutralized by 0.5 M NaOH and centrifuged at 7500 rpm for 6 min. The collected BC residue was then heated in 1 L of 2% sodium lauryl sulfate at 80 °C for 1 h with constant stirring using a mechanical stirrer to remove residual proteins and lipids from the culture media. The mixture was then centrifuged, heated in 0.5 M NaOH at 80 °C for 1 h to further remove bacterial cells, and finally washed until pH neutral by repeated centrifugation. The neutralized residue was further suspended in water and vacuum filtered to obtain a BC mat. The percentage of BC in the mat was obtained after subtracting the percent moisture determined by infrared moisture determination balance (FD720, Kett US, Villa Park, CA, USA).

2.2.3. Viscosity-average degree of polymerization (DP_v) measurement

The DP_v was determined by viscosity measurement. In a 50 mL vial, 100 mg of the freeze dried sample of BC was suspended in 10 mL of distilled water and stirred for 30 min under N_2 gas. Then, 10 mL of 1 M CED was added and stirred for 30 min to completely dissolve the BC. The resulting solution was then transferred to a Cannon–Fenske capillary viscometer to determine the intrinsic viscosities of each sample at 25 °C, and the values were then converted to the DP_v using the Mark–Houwink–Sakurada equation $[\eta] = 0.57 \times DP_v$, where $[\eta]$ is the intrinsic viscosity and 0.57 is the solvent–polymer constant between cellulose and CED (Smith et al. 1963).

2.2.4. BC hydrolysis.

Different hydrolysis conditions (Table 2-1) were tested to determine the optimum conditions to provide nanocelluloses with different DP_v. Initially, time series experiments were conducted to monitor the change in the DP_v with time.

Table 2-1. The different acid concentrations and temperatures used for the hydrolysis of bacterial cellulose.

HCl concentration (M)	Temperature (°C)	BC:acid ratio (g/mmol)
4	70	1:300
2	70	1:150
2	50	1:150
2	room temperature	1:150

A 6 g (dry weight) sample of the purified BC was placed in a three-necked flask and was suspended in water to give a final concentration of 1 g BC/25 mL H_2O. The suspension was then stirred to disperse the BC, which was followed by the addition of 300 mL of 3 M HCl to give a final concentration of 2 M HCl. To achieve a final concentration of 4 M HCl in the BC suspension, 300 mL of 6 M HCl was added. The hydrolysis setup was then constructed by attaching a thermometer, condenser, and N_2-containing balloon to the openings of the three-necked flask. It was then placed in a preheated oil bath, and the suspension was stirred continuously during hydrolysis. Samples for DP_v determination were then drawn at specific time intervals. Cold distilled

water (twice the volume of the withdrawn sample) was immediately added to prevent further hydrolysis. The diluted sample was then centrifuged at 10 000 rpm for 10 min twice to remove most of the HCl, neutralized with 0.1 M NaOH, and washed again with distilled water by repeated centrifugation. The residue from the last centrifugation was collected, suspended in water, and finally filtered to form a nanocellulose mat. The nanocellulose mat was then stored in a refrigerator. The percent BC in the mat was obtained after subtracting the percent moisture determined by the infrared moisture determination balance.

2.2.5. Acetylation

Before acetylation, water in the nanocellulose was removed by distillation with NMP (Nakatsubo et al. 2010). To 200 mg BC (dry weight, 1.23 mmol) in a round bottom flask, 60 mL of NMP was added and the suspension was stirred to completely disperse the BC. Distillation was carried out at 150 °C and 65 hPa. The resulting water-free suspension (50 mL) of nanocellulose in NMP was then cooled to room temperature. Pyridine (1.4 mL, 17.8 mmol) and acetyl chloride (1.0 mL, 14.8 mmol) were then added and acetylation was carried out with continuous stirring at room temperature or 50 °C depending on the reactivity of the sample. A 5 mL aliquot of the reaction mixture was drawn at various times, diluted with ethanol, filtered, washed repeatedly with ethanol, solvent exchanged in *t*-butanol, and then freeze-dried. The collected samples were used to monitor the progress of the reaction by determining the DS using the equation derived from the calibration curve, which will be discussed in the next section.

2.2.6. DS determination

A calibration curve that relates DS to the area of the carbonyl group in the Fourier transform infrared (FTIR) spectra of acetylated BC1100 was first constructed to facilitate the rapid determination of DS when monitoring the progress of the reaction during acetylation.

The DS was first determined by the back-titration method. For this purpose, time-series acetylation was carried out in 3.0 g BC1100, and about 300 mg was collected each time and freeze-dried. To 100 mg acetylated BC in an Erlenmeyer flask, 15 mL of ethanol was added and stirred until the BC was uniformly dispersed. Ten milliliters of 0.5 M NaOH was then added, tightly capped, and heated in an oil bath at 70 °C for 30 min. The mixture was cooled and the excess NaOH was titrated with 0.2 M HCl to a

phenolphthalein endpoint. The amount of acetyl groups per gram of sample (mol/g) was then calculated and converted to the DS, which is the number of moles of ester groups (acetyl groups in this study) per mole of anhydroglucose unit. Each acetylated sample was analyzed in duplicate.

To construct the calibration curve, each acetylated BC was subjected to FTIR analysis. A portion of the freeze-dried BC was scanned 16 times at a resolution of 4 cm^{-1} after background correction using a Perkin Elmer Spectrum One spectrometer equipped with a universal attenuated total reflectance accessory. The derived spectra were baseline corrected and normalized before integrating the peak at around 1730 cm^{-1}, which corresponds to the absorption band of carbonyl groups as shown in Figure 2-1. The area (*A*) of the carbonyl group for each sample and the calculated DS in the range of 0.3-1.2 from the back-titration method were then plotted, and the equation was determined from the graph (Figure 2-2). The equation, DS=0.0091A + 0.0264, was then used to calculate the DS of other acetylated nanocelluloses.

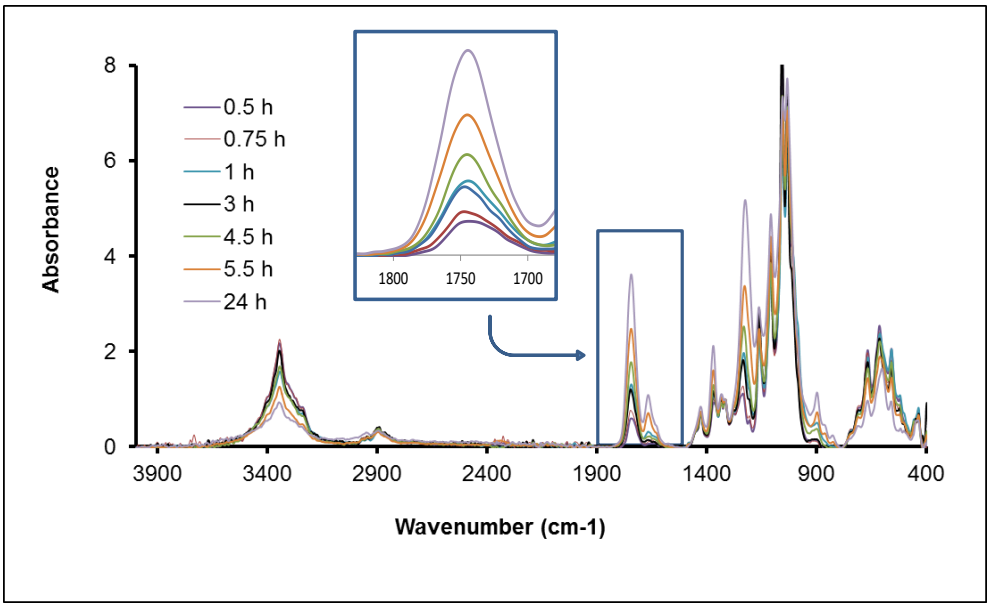

Figure 2-1. FTIR spectra of acetylated BC showing the change in the intensity of the peak at 1730 cm^{-1} with acetylation time. The inset shows the enlarged portion of the peak corresponding to the absorption band of the carbonyl group.

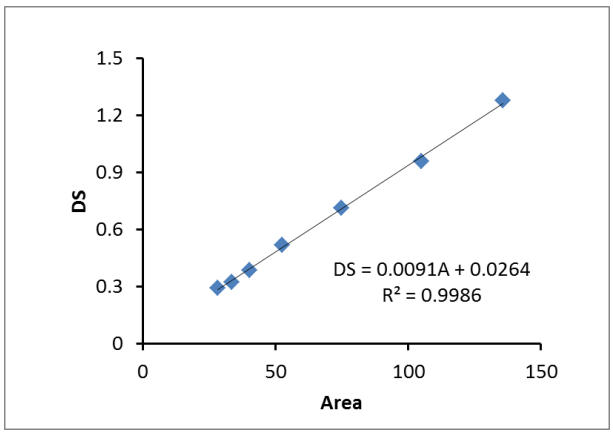

Figure 2-2. Calibration curve obtained by correlating the area of the carbonyl peak from the FTIR spectra with the degree of substitution (DS) obtained by titration.

2.2.7. Microscopy analysis

The morphological changes in BC caused by acid hydrolysis and acetylation were observed with a field-emission scanning electron microscope (JSM-6700F, JEOL Ltd., Tokyo, Japan). One drop of 0.01% nanocellulose (in water or in dichloromethane for non-acetylated and acetylated nanocellulose, respectively) was placed on a glass plate attached to the sample holder. The sample was then allowed to dry at 40 °C, sputter-coated with platinum, and viewed at an accelerating voltage of 1.5 kV.

2.2.8. Crystallinity

X-ray diffraction (XRD) analysis was performed to determine the relative crystallinity of cellulose with different DP_v values before and after acetylation. Acetylated nanocellulose (100mg) was first hydrolyzed in 0.2M NaOH for 1h at 60°C to remove the acetyl groups, cooled, washed with water and freeze dried. Pellets of freeze-dried nanocellulose samples prepared by pressing at 1.4MPa were mounted into the sample holder and irradiated with nickel filtered CuKα (λ = 0.154 nm) radiation generated by UltraX 18HF (Rigaku Corp., Tokyo, Japan) operating at 40 kV and 300 mA. The scattered radiation was detected in the range 5°–40° using an X-ray goniometer that collected data at a scan rate of 1°/min with increments of 0.02° in reflection mode. The crystallinity index was determined from the normalized diffraction profiles using the equation developed by Segal, Creely, Martin, & Conrad (1959).

2.2.9. Reducing end analysis

The number of REs expressed as glucose equivalent in µmol/g was analyzed based on the BCA assay reported by Johnston, Shoemaker, Smith, & Whitaker (1998). The BCA working reagent was prepared similar to the method of Garcia et al. (1993). The nanocellulose suspension was prepared by adding 2 mL distilled deionized water into 2 mg nanocellulose contained in a glass tube. A small magnetic bar was dropped into the solution and the mixture was stirred for 30 min to disperse the nanocellulose. BCA working reagent (2 mL) was then added, the tube was capped, and the mixture was heated at 80 °C in a water bath with continuous stirring for 30 min. The mixture was cooled to room temperature, transferred to centrifuge tubes, and centrifuged at 7500 rpm for 6 min. The absorbance of the supernatant was then read at 560 nm using a U-2910 Hitachi UV–vis spectrophotometer (Tokyo, Japan). The number of REs was determined from the calibration curve obtained from standard glucose solutions (0–50 µM) treated as above.

2.2.10. $NaBH_4$ reduction

The REs of each nanocellulose samples were reduced by treatment with $NaBH_4$ following the procedure reported by Matsuoka et al. (2011a). To 200 mg of freeze dried nanocellulose dispersed in 8 ml of 0.1 M Na_2CO_3 buffer (pH=10) was added 10mg of $NaBH_4$. The mixture was purged with N_2, and the reaction was carried out for 5h at 80°C with occasional stirring. The reaction was terminated by the addition of 1N HCl dropwise until pH 4. The terminated reaction was further heated at 80°C for 30 min before neutralizing with saturated $NaHCO_3$ solution. The $NaBH_4$-reduced nanocellulose was washed repeatedly with 0.001N HCl; then with water; solvent-exchanged to ethanol, acetone and *t*-butanol; and freeze-dried. The REs remaining in the sample after reduction was analyzed following the same BCA method mentioned in the previous section.

2.2.11. Thermogravimetric analysis

TGA was carried out using a TGA Q50 (TA Instruments, Tokyo, Japan). Dynamic and isothermal TGA were performed, each utilizing approximately 5 mg of freeze-dried nanocellulose placed on a platinum pan. The sample was allowed to equilibrate at 110 °C for 10 min to remove bound moisture. Dynamic TGA was done by increasing the temperature from 110 °C to 500°C at a rate of 10 °C/min. Isothermal TGA was carried out by increasing the temperature to 250°C and keeping it isothermally for 1h. The flow rate of nitrogen in both cases was maintained at 100 mL/min throughout the test. Each

sample was run in duplicate.

2.3. Results and Discussion

2.3.1. Acid hydrolysis

Acid-catalyzed hydrolysis of cellulose is a heterogeneous reaction that involves the cleavage of ß(1→4) glycosidic bonds to give hydrolyzed cellulose with reduced DP_v but higher crystallinity (Xiang et al. 2003). As a result of this decrease in DP_v, the intrinsic viscosity of the solutions of hydrolyzed cellulose decreases. Continued hydrolysis would then reach a point where very little change in intrinsic viscosity occurs and the DP_v calculated from this limiting intrinsic viscosity is called the leveling-off degree of polymerization or the LODP (Battista 1944; Nelson and Tkipp 1949). The rate of change of the DP_v during hydrolysis depends on several factors, such as acid concentration, temperature, and the physical state of the cellulose (Xiang et al. 2003). In this chapter, with only BC as the starting material, only the reaction conditions (i.e., temperature and acid concentration) were varied to monitor the change in the DP_v during hydrolysis. As shown in Figure 2-3, different reaction conditions gave different rates of hydrolysis, which is indicated by the change in DP_v with time.

Initially, the pretreated BC had a DP_v of 1100. This BC sample will be referred to as BC1100 in succeeding sections. Hydrolysis in 4M HCl at 70 °C was not suitable to prepare cellulose with different DP_v values. Under these conditions, the DP_v decreased abruptly to 300 and no significant change in DPv was observed with continued hydrolysis. Lowering the concentration to 2M but keeping the temperature at 70 °C also gave a similar result. From these two reaction conditions, the LODP was found to be about 300. Conversely, when hydrolysis was performed at room temperature with 2M HCl, no appreciable change in the DP_v was observed. Hydrolysis at 50 °C in 2M HCl was found to be the optimum conditions to prepare BC with different DP_v values. A gradual change in DP_v was observed, but the LODP was not reached even after 5 h of hydrolysis. Under these conditions, hydrolysis for 4 h was chosen to prepare cellulose with a DP_v of 500, which is in between 1100 and the LODP. This hydrolyzed BC with a DPv of 500 will be referred to as BC500. Although the LODP can be obtained at 70 °C after 0.5 h hydrolysis in 4M HCl, hydrolysis for 4 h was chosen to prepare BC that reached the LODP because visual inspection of the hydrolyzed cellulose after 0.5 h hydrolysis still showed long and

agglomerated fibers. At this stage, the DP_v decreased but the fiber lengths were probably still too large. Lowering the DP_v does not necessarily result in shorter fiber lengths but could result in fracture within the fibers. Thus, to ensure liberation of short cellulose nanocrystals from the fibers, a longer hydrolysis time was chosen, and the sample obtained herein will be referred to in succeeding sections as BC300.

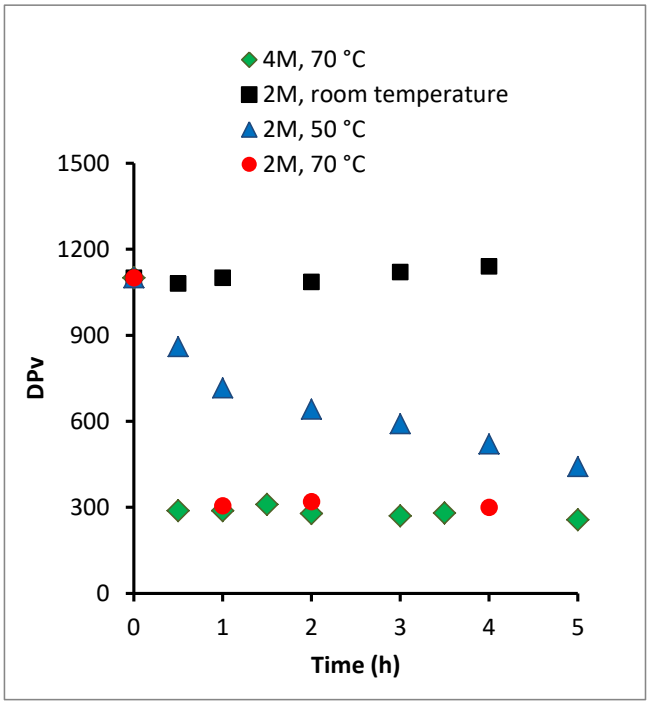

Figure 2-3. The change in DP_v of bacterial cellulose with hydrolysis time at different acid concentrations and temperatures.

2.3.2. Acetylation

To compare the thermal stability of acetylated nanocelluloses, it is important that each material has similar DS value to eliminate the effect of unequal amounts of acetyl groups in a sample. For the purpose of obtaining similar DS, time series acetylation was first carried out and the change in DS was monitored with time.

Figure 2-4 shows the increase in DS of each sample as acetylation progressed. At room temperature, the reactivity of BC1100 and BC500 were nearly the same and slightly higher than that of BC300. In of the first 4 h, the DS of BC1100 and BC500 increased to 0.38 while that of BC300 only reached 0.26. From the observed DS values at room

temperature, the highest value of 0.38 was selected to prepare acetylated nanocelluloses with different DP_v values. It was not attempted to get a DS value higher than 0.38 to avoid possible collapse of the crystalline core of the cellulose associated with higher DS. As reported in the work of Ifuku et al., (2007) the XRD profile of acetylated BC nanofiber at high DS (0.95) showed a diffraction peak of cellulose triacetate and an amorphous halo, while at low DS (0.45) the crystallinity of the original BC nanofiber was maintained. Thus, a DS of 0.38 was a reasonable choice with the assumption that at this value only the surface of the nanocellulose was acetylated and the crystalline core was intact. BC300, however, did not reach a DS of 0.38 at room temperature. It was therefore decided to increase the reaction temperature to 50 °C. As shown in Figure 2-4, the reaction rate of BC300 significantly increased and reached a DS of 0.38 after about 1 h.

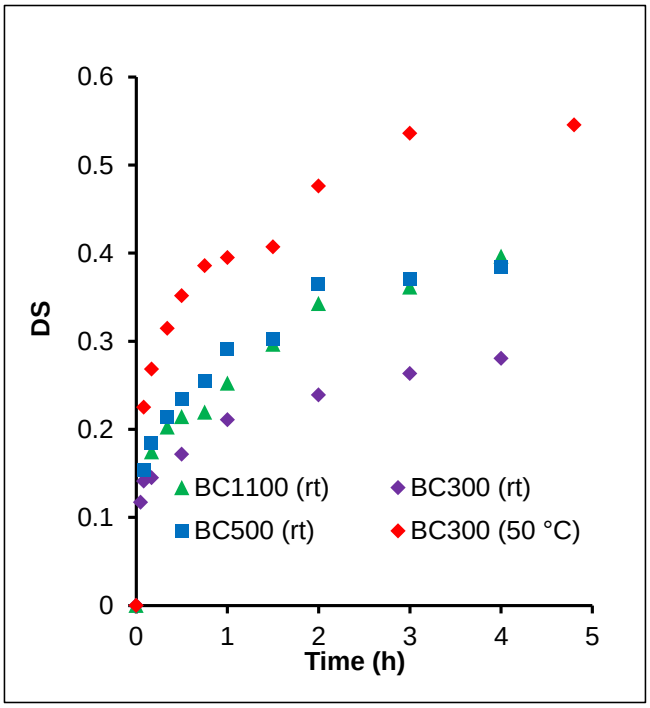

Figure 2-4. The change in DS of nanocelluloses with different DP_v as a function of time during acetylation. Reaction temperatures are indicated inside the parenthesis after the sample code.

2.3.3. Morphology

The morphologies of BC with different DP_v values before and after acetylation are shown in Figure 2-5. BC1100 shows long intertwined nanofibrils, while BC300 shows short rigid rods characteristic of CNCs. Interestingly, BC 500 did not show nanocrystal characteristics but retained the ribbon-like structure of the unhydrolyzed BC1100. The hydrolysis conditions for BC500 must have not been sufficient to cut the nanofibrils into shorter crystalline rods. After acetylation, no change in morphology was observed except for BC300 which showed shorter crystalline rods than the unacetylated ones.

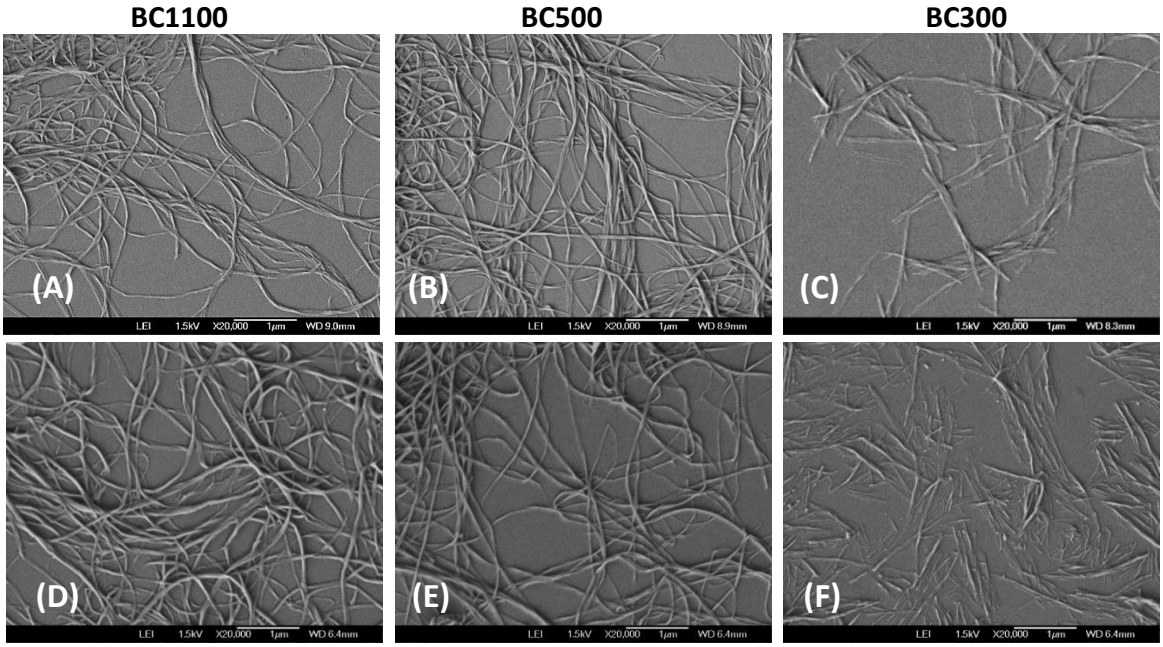

Figure 2-5. Scanning electron micrographs of BC with different average viscosity degree of polymerization before (A-C) and after (D-F) acetylation.

2.3.4. Crystallinity

Crystallinity is an important property that affects physical, mechanical, and chemical properties of cellulose. Tensile strength, dimensional stability, and density are known to increase with increasing cellulose crystallinity, while chemical reactivity and swelling decrease (Agarwal et al. 2010). The crystallinity of cellulosic materials can vary depending on the source and chemomechanical treatment used.

The X-ray diffraction profiles of BC with different DP_v values before and after acetylation are presented in Figure 2-6. The pattern shows three well-defined diffraction

peaks at 2θ = 14.2°, 16.6°, and 22.4°, which were assigned the Miller indices of (100), (010) and (110); respectively; representing a cellulose Iα structure (French 2014). The Miller indices for cellulose Iα were used because it has been reported that 60-70% of the crystal structure in BC is in the form of Iα (Atalla and Vanderhart 1984).

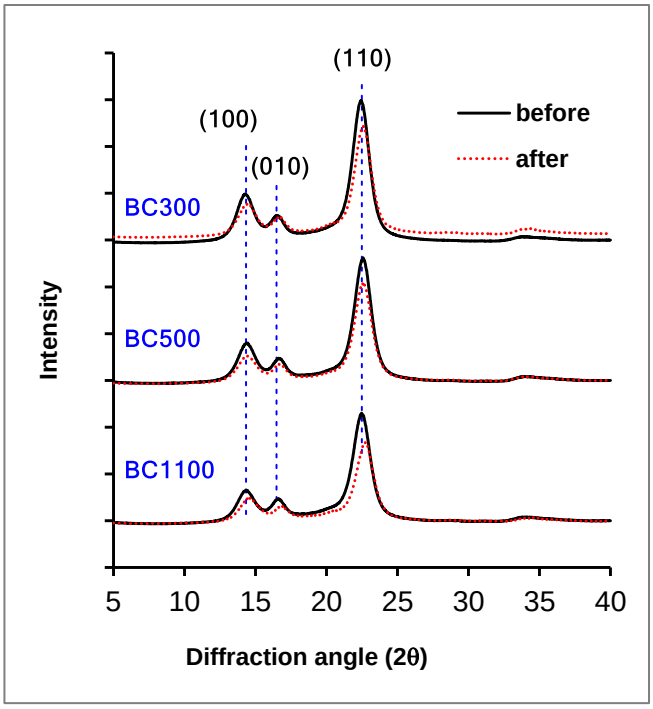

Figure 2-6. X-ray diffraction profiles of BC with different viscosity average degree of polymerization before and after acetylation.

Initially, BC1100 had a crystallinity index of 93.6. After acid hydrolysis, the crystallinity indexes increased to 95.7 and 95.5 for BC500 and BC300, respectively. During acid hydrolysis, the amorphous domains of cellulose are digested, thereby increasing the crystallinity of BC500 and BC300. The different hydrolysis conditions for the preparation of BC500 and BC300 did not seem to affect the crystallinity of the hydrolyzed nanocellulose. Both had almost the same crystallinity index. This result suggests that hydrolysis of BC at similar acid concentration and duration but at different temperatures can digest the amorphous part of cellulose to the same extent but the cleavage of glycosidic bonds occurs at different rates thereby producing hydrolyzed bacterial nanocellulose with similar crystallinity but different DP_v values.

After acetylation, the XRD profiles still showed the same distinct peaks as the original nanocellulose. The result indicates that the acetylation conditions used to reach a DS of 0.38 did not affect the crystalline core of the nanocellulose. The crystallinity indexes for BC1100, BC500 and BC300 after acetylation were 94.1, 96.1 and 95.7, respectively.

2.3.5. Reducing ends

The RE is the terminal end of cellulose that contains the anomeric carbon bearing the hemiacetal hydroxyl (OH), which can be converted to a carbonyl group in the form of an aldehyde and is thus susceptible to reduction and oxidation. Since analysis of REs involves the reduction of a carbonyl group to form OH group, the number of REs was only determined in the nanocellulose before acetylation and after NaBH4 reduction.

With breaking of the ß(1→4) glycosidic bonds during acid hydrolysis, the decrease in the DP_v is accompanied by production of more REs. As shown in Figure 2-7, the number of REs increases as DP_v decreases. The unhydrolyzed BC1100 consisting of long intertwined nanofibrils had an average number of REs of 4.6 μmol/g. Using the equation RE= 106/[(162)DP+18] and assuming ideal condition that the nanocellulose is monodispersed, the theoretical number of REs were calculated by substituting different DP values. The calculated theoretical number of REs agreed well with the experimental values, except for BC300. The discrepancy observed for BC300 can be attributed to the longer hydrolysis time used in the preparation of BC300. As mentioned earlier, several hydrolysis conditions can attain the LODP. As Figure 2-3 showed, LODP can also be reached after an hour of hydrolysis at 70°C in 4M HCl but the 4h hydrolysis time was selected to ensure the liberation of nanocrystalline rods. The continued hydrolysis therefore increased the number of REs without changing the DP_v. An increase in the number of REs without a change in the DP_v was also reported by Daruwalla & Nabar (1956). It was hypothesized that continued treatment with acid after the LODP was reached caused the formation of smaller chain segments that did not contribute to changes in viscosity but were capable of increasing the number of REs.

After $NaBH_4$ reduction, the number of REs decreased and leveled off to an average value of 1.8 (±0.6) μmol/g for all the nanocelluloses. The number of REs decreased by 73.8%, 83.2% and 91.8% for BC1100, BC500, and BC300; respectively. With the aim of completely reducing all the REs in each sample, the $NaBH_4$-reduced nanocelluloses were

again subjected to a second $NaBH_4$ treatment. The number of REs, however, decreased only to an average value of 1.3(±0.4) μmol/g and the percent reduction also did not significantly change in each of the nanocelluloses. The result suggests that the number of REs not accessible for reduction under the reaction conditions used in this study is relatively the same in each of the nanocelluloses.

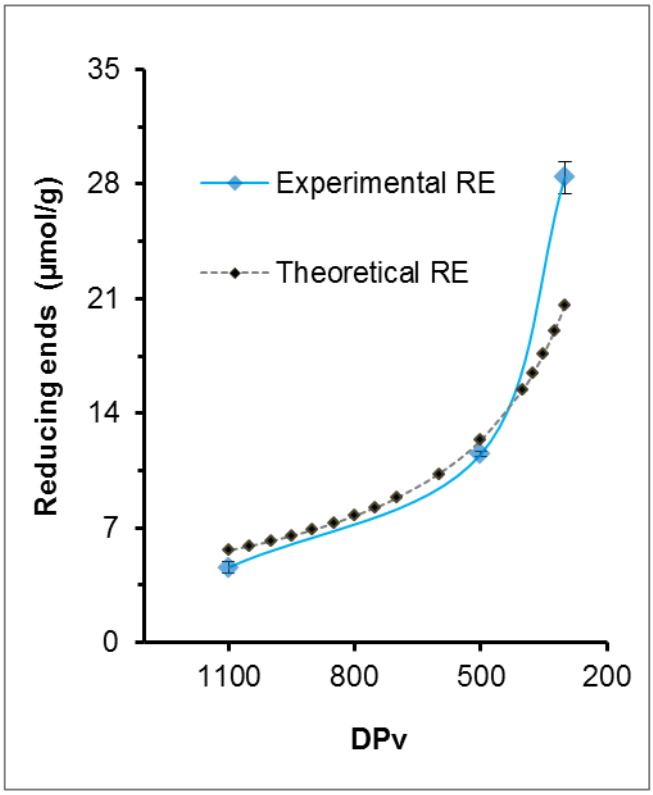

Figure 2-7. Average number of reducing ends (REs) of BC with varying viscosity-average degree of polymerization (DPv) with error bars represented by standard deviation from three measurements, and the theoretical number of REs calculated from different DP values.

2.3.6. Thermal Stability

Because of simplicity and ease of use, TGA is probably the most commonly used method for evaluating the thermal stability of nanocelluloses and their derivatives and composites. The weight loss of a sample is recorded as a function of temperature under dynamic heating or of time at fixed temperature under isothermal heating. Under dynamic heating, the temperature at the onset of degradation can be determined from the

thermogravimetric (TG) curves while the T_{max} can be obtained from the first derivative thermogravimetric (DTG) curves. The weight loss of a sample at a fixed temperature and time is obtained from the isothermal TG curves.

Figure 2-8 shows the thermogravimetric (TG), derivative TG (DTG) curves, the temperature at 5% (5% WLT) and 10% (10% WLT) weight loss, and T_{max}, of the different nanocelluloses before acetylation. All of the nanocelluloses showed typical single-step thermal degradation. Taking the 5% WLT, 10%WLT, and T_{max} values as measures of the thermal stability, the unhydrolyzed BC nanofibers (BC1100) showed the highest thermal stability. After acid hydrolysis, the decrease in the DP_v was accompanied by a corresponding decrease in 5% WLT, 10%WLT and T_{max}, resulting to a decreasing trend in thermal stability with decreasing DP_v.

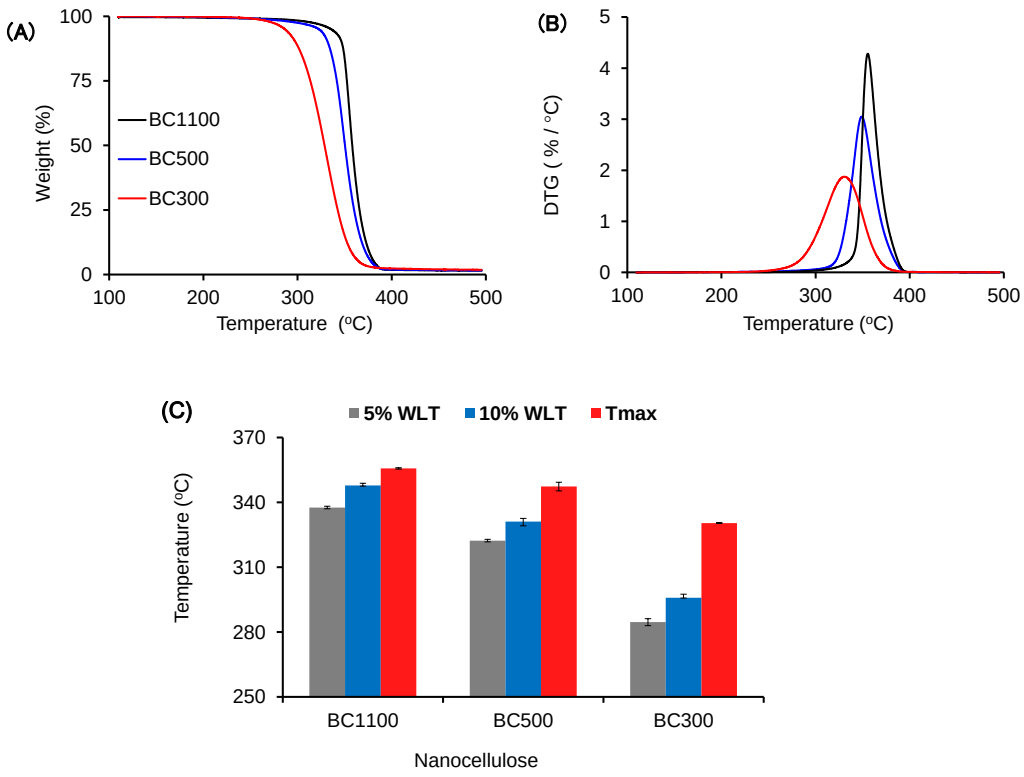

Figure 2-8. Thermogravimetric (A), first derivative thermogravimetric (DTG) (B) curves and the values of 5%WLT, 10% WLT, and T_{max} (C) of BC with different viscosity average degree of polymerization.

A similar trend in thermal stability was also observed by Gurgel et al. (2012) who studied the thermal characteristics of depolymerized residues from extremely low acid hydrolysis of sugarcane bagasse, and by Calahorra et al. (1989) who reported the effect of molecular weight on the thermal decomposition of cellulose obtained by fractionation from a solution of eucalyptus pulp in cadoxen. Calahorra et al. attributed the decrease in thermal stability to the decrease in the crystallinity index with decreasing DP_v. In this study, however, the crystallinity index increased after acid hydrolysis. Moreover, BC500 and BC300 which had the same crystallinity index showed different thermal stability. Thus, the differences in thermal stability cannot be attributed to the change in crystallinity. In this case, the decrease in thermal stability with decreasing DP_v was attributed to the increase in the number of REs. As mentioned in the previous section, the number of REs increased with decreasing DP_v. By plotting the values of 5% WLT, 10% WLT and T_{max} against the number of REs (Figure 2-9), it is clear that there is an inverse relationship between thermal stability and the number of REs. Even though the number of REs is far less than the number of surface OH groups in cellulose, the reactivity of the REs can affect the properties of cellulose. The REs have been reported to be the starting point of various chemical and biochemical reactions, and thermoactivated reactions such as pyrolysis are not an exception. Matsuoka and co-workers (2011a; 2011b; 2014) suggested that the RE is the reactive site in cellulose during low-temperature pyrolysis (<300 °C). From Figure 2-9 with increasing number of REs, the 5% WLT and 10%WLT decreased. BC300, which has the highest number of REs, showed an early stage of degradation at around 250°C (showed in Figure 2-8) and already lost 10% of its initial weight at around 300°C. At this initial stage of decomposition, the REs must play a catalytic role similar to the mechanism proposed by Matsuoka et al. (2014). Accordingly, during the onset of thermal decomposition before significant weight loss occurs, the REs that are initially present in the cellulose or produced by depolymerization activate the crystalline cellulose during pyrolysis, and the activation mechanism is very effective at low temperature.

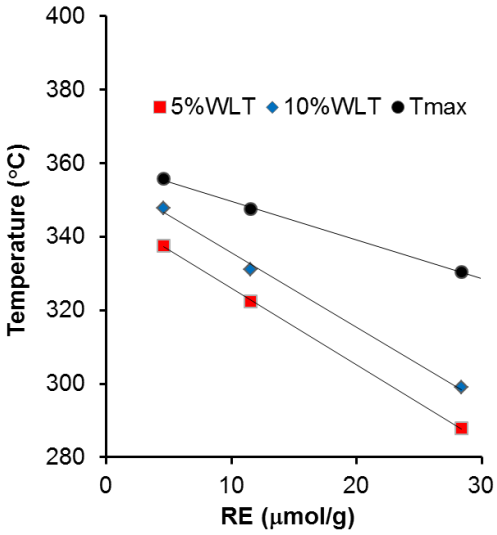

Figure 2-9. Inverse relationship between thermal stability and the number of reducing ends (REs) of BC.

The effect of acetylation on the thermal stability of BC with different DP_v values is shown in Figure 2-10. Acetylation did not change the single-step thermal degradation of BC but only delayed the decomposition, which is reflected by the increase in 5%WLT, 10%WLT and T_{max} after acetylation (Figure 2-11). This indicates that acetylation improved the thermal stability of the nanocellulose, which agrees with the previous findings of Hu et al. (2011) who acetylated BC nanofibers under solvent free conditions and Ávila Ramírez et al. (2014) who also acetylated BC nanofibers by organocatalytic route. The results, however, contradict the report of Lee et al. (2011) who acetylated BC nanofibers using acetic acid in the presence of pyridine and *p*-toluene sulfonyl chloride and Tomé et al. (2011) who acetylated BC nanofibers with acetic anhydride in a non-swelling ionic liquid. The differences in the thermal stability of acetylated BC can be ascribed to different preparation conditions. Pre-treatment processes used to purify the BC or to remove the water in the BC, as well as the reaction conditions during acetylation may have caused improvement or deterioration in the thermal property of acetylated BC.

The increase in thermal stability after acetylation can be attributed to the possible inhibition of inter- and intramolecular hydrogen bond formation when the OH groups are substituted with acetyl groups. Matsuoka et al. (2014) proposed that proton donation to the oxygen at carbon 1 of AGU in cellulose through hydrogen-bond rearrangement or hydrogen bonding with other molecules acts as an acid catalyst that promotes the

depolymerization reaction during pyrolysis.

It should also be noted that the T_{max} value of each acetylated nanocellulose did not show much variation despite the differences in the DP_v. T_{max} values for acetylated nanocelluloses were in the range of 365-371 °C, while a wider range of 330–356 °C was recorded for non-acetylated nanocelluloses (Figure 2-11). The small range in T_{max} values of acetylated nanocelluloses indicates that for acetylated nanocelluloses with similar DS the thermal decomposition temperatures do not show significant variation despite the differences in the DP_v.

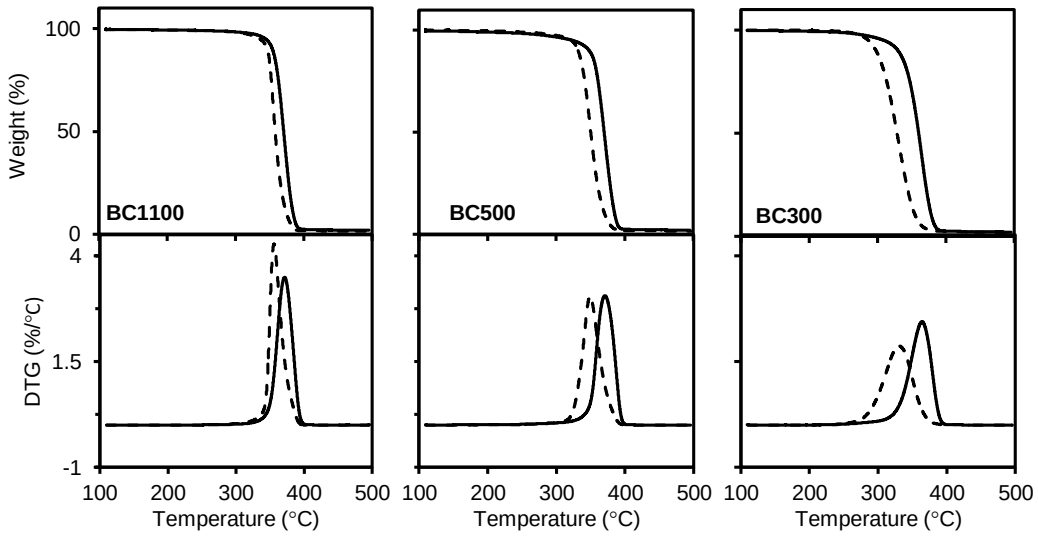

Figure 2-10. Thermogravimetric and first derivative thermogravimetric (DTG) curves of BC with different viscosity average degree of polymerization before (dashed lines) and after (solid lines) acetylation.

Although the T_{max} values did not greatly vary for the acetylated nanocelluloses despite the differences in the DP_v values, the degree of improvement in thermal stability caused by acetylation varied in each of the nanocelluloses. The degree of improvement in thermal stability is defined here as the difference in the values of 5% WLT, 10%WLT and T_{max} before and after acetylation. As shown in Figure 2-11, as the DP_v decreased, the difference in the values of 5% WLT, 10%WLT and T_{max} before and after acetylation increased, and it is reflected by the increase in the height of the white shaded region of each bar. The results indicate that introducing acetyl groups at the same DS to nanocelluloses with different DP_v values does not result in the same degree of

improvement in thermal stability. The degree of improvement was found to increase with decreasing DP_v. This dependence on the DP_v is possibly because of protection of the REs by more stable acetyl groups.

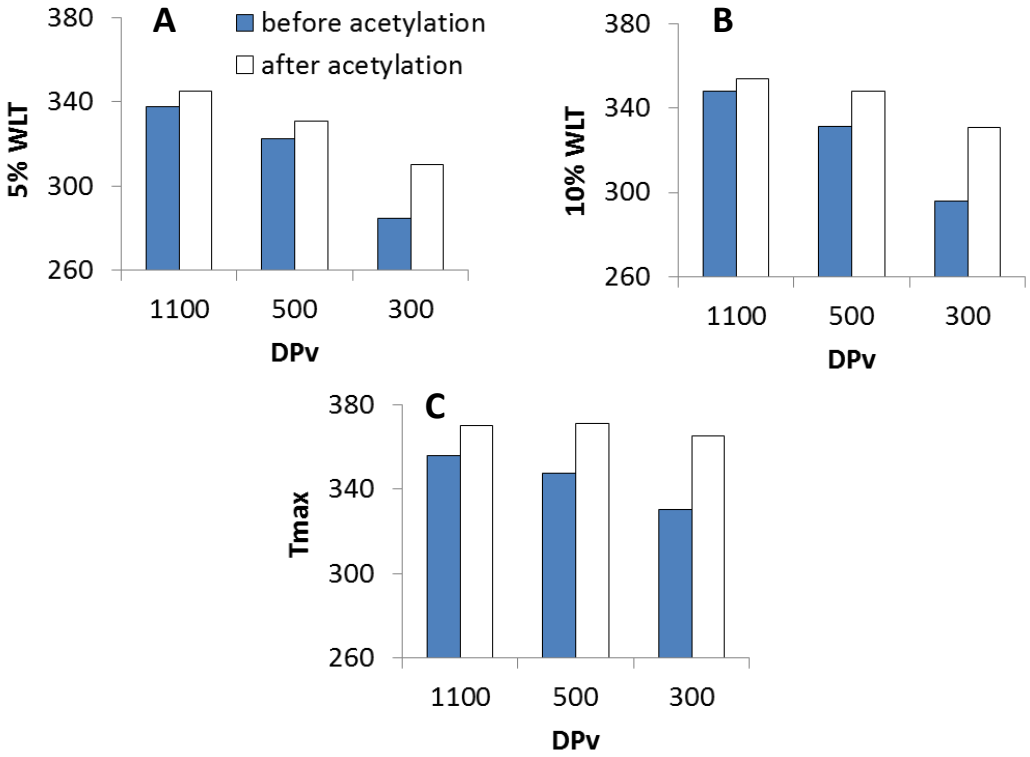

Figure 2-11. The 5% WLT (A), 10% WLT (B) and T_{max} (C) before and after acetylation of BC with different viscosity average degree of polymerization, DPv.

To verify the effect of protecting the REs to the degree of improvement in thermal stability, the REs were converted to its glucitol moiety by $NaBH_4$ reduction. In this manner only the hemiacetal OH was modified leaving the surface OH groups unchanged. $NaBH_4$ reduction has been reported to inhibit thermally-induced discoloration of cellulose (Avicel PH-101) at relatively low temperatures, <300°C (Matsuoka et al. 2011a) and also prolonged the induction period of cellulose during pyrolysis at slow heating conditions (Matsuoka et al. 2014). The induction period is the initial stage during TGA where the cellulose is said to be converted to an active intermediate before significant weight loss occurs (Bradbury et al. 1979). Thus, to observe the effect of $NaBH_4$ reduction, isothermal TGA at the 1% weight loss temperature (1%WLT) of BC300, which is at 250°C, was

performed. The 1%WLT was determined from the TG curves obtained under dynamic heating. Within an hour of isothermal heating at 250°C, differences in the thermal behavior of the untreated nanocelluloses with different DP_v values were observed and the effect of $NaBH_4$ reduction was already evident as shown in Figure 2-12. Before reduction, the percent weight loss increased with decreasing DP_v which again supported the effect of REs to thermal stability, i.e. decreasing thermal stability with increasing number of REs. After $NaBH_4$ reduction, weight loss was inhibited, but only slightly for BC1100 as shown in the small difference in the percent weight loss before and after the treatment. The effect of $NaBH_4$ reduction was more evident for BC300 which has the highest number of REs. Similar result was also obtained by Matsuoka et al. (2014) who also compared the effect of $NaBH_4$ reduction to the weight-loss behavior of Avicel PH-101 and Whatman No. 42.

Considering the difference between the percent weight loss before and after $NaBH_4$ reduction as a measure of the degree of improvement in thermal stability, the degree of improvement also followed the same trend as that of the effect of acetylation. The degree of improvement in thermal stability because of $NaBH_4$ reduction also increased with decreasing DP_v. This result confirms that the improvement in thermal stability is affected by protecting the REs. The thermal stabilization because of acetylation therefore can be ascribed to possible protection of the surface OH and of the REs. Although it has been widely reported that acetylation begins on the accessible surface hydroxyl groups of cellulose, which are in carbon atoms 2, 3 and 6 positions of the AGU, it can be deduced that the two OH groups at each terminal end of the cellulose chains can also participate in the reaction. This is analogous to heterogeneous acetylation of cellobiose in a separate model experiment, where acetylation took place at the six OH groups around the two glucopyranose rings and also at the two terminal OH groups to produce cellobiose octaacetate. The model experiment indicated that, if the terminal OH groups of cellulose are accessible, they can also be acetylated. Therefore, during acetylation, protection of the surface OH and the REs can take place. Furthermore, for nanocellulose with low DP_v values, acetylation of the REs can greatly contribute to improvement in thermal stability.

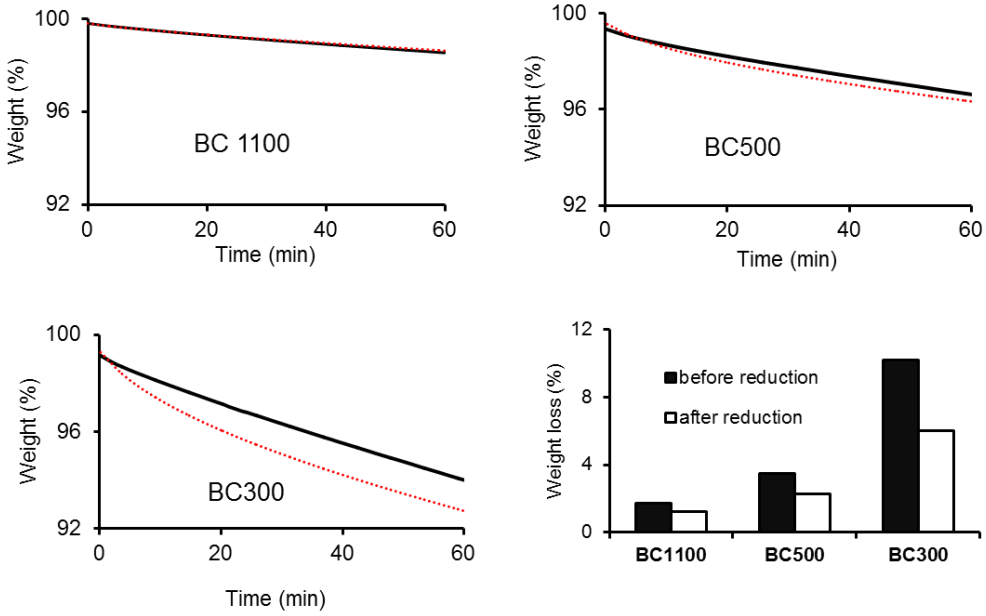

Figure 2-12. The weight loss behavior and the weight loss values before (dashed lines) and after (solid lines) $NaBH_4$ reduction of BC with different viscosity average degree of polymerization during isothermal heating at 250^{o}C for 1h.

2.4. Summary

Acid hydrolysis of BC nanofibers (DP_v =1100) at different temperatures but at the same acid concentration and duration yielded nanocellulose with different DP_v values (500 and 300) and morphologies but similar crystallinity indexes. Of the different characteristics of each of the nanocelluloses prepared, the DP_v was found to significantly affect thermal properties. BC with varying DP_v values showed decreasing thermal stability with decreasing DP_v. The decrease in thermal stability as DP_v decreased is attributed to the increase in the number of REs. Improved thermal stability was achieved by acetylating the nanocelluloses and the degree of improvement increased as the DP_v decreased. The higher stabilization caused by acetylation to CNCs with low DP_v than with high DP_v was attributed to possible protection of the hemiacetal OH groups at the REs by more stable acetyl groups. The effect of protecting the REs to the degree of improvement in thermal stability was also confirmed by $NaBH_4$ reduction. The degree of improvement in thermal stability of $NaBH_4$-reduced nanocelluloses also increased with decreasing DP_v. The recent findings suggest the strong effect of REs to the thermal

stability of nanocellulose. For CNCs characterized by small DP, protection of the REs, apart from surface OH modification, can greatly contribute to its thermal stabilization. For CNFs with high DP and low number of REs, protection of the surface OH improves thermal stability while processes that generate more REs such as acid hydrolysis causes thermal destabilization.

2.5. References

Agarwal UP, Reiner RS, Ralph SA (2010) Cellulose I crystallinity determination using FT–Raman spectroscopy: univariate and multivariate methods. Cellulose 17:721–733.

Alemdar A, Sain M (2008) Isolation and characterization of nanofibers from agricultural residues: wheat straw and soy hulls. Bioresour Technol 99:1664–71.

Ashori A, Babaee M, Jonoobi M, Hamzeh Y (2014) Solvent-free acetylation of cellulose nanofibers for improving compatibility and dispersion. Carbohydr Polym 102:369–375.

Atalla RH, Vanderhart DL (1984) Native cellulose: a composite of two distinct crystalline forms. Science (80-) 223:283–285.

Ávila Ramírez JA, Suriano CJ, Cerrutti P, Foresti ML (2014) Surface esterification of cellulose nanofibers by a simple organocatalytic methodology. Carbohydr Polym 114:416–423.

Battista O (1944) Molecular weight of cellulose. Ind Eng Chem 16:351–354.

Božič M, Vivod V, Kavčič S, et al (2015) New findings about the lipase acetylation of nanofibrillated cellulose using acetic anhydride as acyl donor. Carbohydr Polym 125:340–351.

Bradbury AGW, Sakai Y, Shafizadeh F (1979) A kinetic model for pyrolysis of cellulose. J Appl Polym Sci 23:3271–3280.

Calahorra ME, Cortazar M, Eguiazabal JI (1989) Thermogravimetric analysis of cellulose: effect of the molecular weight on thermal decomposition. J Appl Polym Sci 37:3305–3314.

Camarero Espinosa S, Kuhnt T, Foster EJ, Weder C (2013) Isolation of thermally stable cellulose nanocrystals by phosphoric acid hydrolysis. Biomacromolecules 14:1223–1230.

Çetin NS, Tingaut P, Özmen N, et al (2009) Acetylation of cellulose nanowhiskers with vinyl acetate under moderate conditions. Macromol Biosci 9:997–1003.

Cunha AG, Zhou Q, Larsson PT, Berglund L a. (2014) Topochemical acetylation of cellulose nanopaper structures for biocomposites: Mechanisms for reduced water vapour sorption. Cellulose 21:2773–2787.

Daruwalla EH, Nabar GM (1956) Acid hydrolysis of cellulose. J Polym Sci XX:205–208.

Fahma F, Takemura A, Saito Y (2014) Acetylation and stepwise solvent-exchange to modify hydrophilic cellulose whiskers to polychloroprene-compatible nanofiller. Cellulose 21:2519–2527.

French AD (2014) Idealized powder diffraction patterns for cellulose polymorphs. Cellulose 21:885–896.

Garcia E, Johnston D, Whitaker JR, Shoemaker SP (1993) Assessment of endo- 1 ,4-ß -d-glucanase activity by a rapid colorimetric assay using disodium 2,2' -bicinchoninate. J Food Biochem 17:135–145.

Gurgel LVA, Marabezi K, Ramos LA, Curvelo AADS (2012) Characterization of depolymerized residues from extremely low acid hydrolysis (ELA) of sugarcane bagasse cellulose: Effects of degree of polymerization, crystallinity and crystallite size on thermal decomposition. Ind Crops Prod 36:560–571.

Hu W, Chen S, Xu Q, Wang H (2011) Solvent-free acetylation of bacterial cellulose under moderate conditions. Carbohydr Polym 83:1575–1581.

Ifuku S, Nogi M, Abe K, et al (2007) Surface modification of bacterial cellulose nanofibers for property enhancement of optically transparent composites: dependence on acetyl-group DS. Biomacromolecules 8:1973–8.

Johar N, Ahmad I, Dufresne A (2012) Extraction, preparation and characterization of cellulose fibres and nanocrystals from rice husk. Ind Crops Prod 37:93–99.

Johnston DB, Shoemaker SP, Smith GM, Whitaker JR (1998) Kinetic measurements of cellulase activity on insoluble substrates using disodium 2,2' bicinchoninate. J Food Biochem 22:301–319.

Jonoobi M, Harun J, Shakeri A, Misra M (2009) Chemical composition, crystallinity, and thermal degradation of bleached and unbleached kenaf bast (*Hibiscus cannabinus*) pulp and nanofibers. BioResources 4:626–639.

Kim UJ, Eom SH, Wada M (2010) Thermal decomposition of native cellulose: Influence on crystallite size. Polym Degrad Stab 95:778–781.

Lee K-Y, Quero F, Blaker JJ, et al (2011) Surface only modification of bacterial cellulose nanofibres with organic acids. Cellulose 18:595–605.

Li J, Zhang LP, Peng F, et al (2009) Microwave-assisted solvent-free acetylation of cellulose with acetic anhydride in the presence of iodine as a catalyst. Molecules 14:3551–3566.

Lu P, Hsieh Y-L (2010) Preparation and properties of cellulose nanocrystals: Rods, spheres, and network. Carbohydr Polym 82:329–336.

Martínez-Sanz M, Lopez-Rubio A, Lagaron JM (2011) Optimization of the nanofabrication by acid hydrolysis of bacterial cellulose nanowhiskers. Carbohydr Polym 85:228–236.

Matsuoka S, Kawamoto H, Saka S (2014) What is active cellulose in pyrolysis? An approach based on reactivity of cellulose reducing end. J Anal Appl Pyrolysis 106:138–146.

Matsuoka S, Kawamoto H, Saka S (2011a) Reducing end-group of cellulose as a reactive site for thermal discoloration. Polym Degrad Stab 96:1242–1247.

Matsuoka S, Kawamoto H, Saka S (2011b) Thermal glycosylation and degradation reactions occurring at the reducing ends of cellulose during low-temperature pyrolysis. Carbohydr Res 346:272–9.

Nakatsubo F, Yoshida N, Abe K, Yano H (2010) Chemical surface-modification of cellulose nanofibers in cellulose-compatible solvents. In: 239th ACS National Meeting Technical Program Archive.

Nelson ML, Tkipp VW (1949) Determination of the leveling-off degree of polymerization of cotton and rayon. J Polym Sci X:577–586.

Nishino T, Kotera M, Suetsugu M, et al (2011) Acetylation of plant cellulose fiber in supercritical carbon dioxide. Polymer (Guildf) 52:830–836.

Nogi M, Abe K, Handa K, et al (2006) Property enhancement of optically transparent bionanofiber composites by acetylation. Appl Phys Lett 89:233123.

Okahisa Y, Abe K, Nogi M, et al (2011) Effects of delignification in the production of plant-based cellulose nanofibers for optically transparent nanocomposites. Compos Sci Technol 71:1342–1347.

Peng Y, Gardner DJ, Han Y, et al (2013) Influence of drying method on the material properties of nanocellulose I: thermostability and crystallinity. Cellulose 20:2379–2392.

Quiévy N, Jacquet N, Sclavons M, et al (2010) Influence of homogenization and drying on the thermal stability of microfibrillated cellulose. Polym Degrad Stab 95:306–314.

Roman M, Winter WT (2004) Effect of sulfate groups from sulfuric acid hydrolysis on the thermal degradation behavior of bacterial cellulose. Biomacromolecules 5:1671–7.

Segal L, Creely JJ, Martin AE, Conrad CM (1959) An empirical method for estimating the degree of crystallinity of native cellulose using the X-Ray diffractometer. Text Res J 29:786–794.

Smith DK, Bampton RF, Alexander JW (1963) New solvents for evaluating chemical cellulose for the viscose process. Ind Eng Chem Process Des Dev 2:57–62.

Tomé LC, Freire MG, Rebelo LPN, et al (2011) Surface hydrophobization of bacterial and vegetable cellulose fibers using ionic liquids as solvent media and catalysts. Green Chem 13:2464.

Uetani K, Watanabe Y, Abe K, Yano H (2014) Influence of drying method and precipitated salts on pyrolysis for nanocelluloses. Cellulose 21:1631–1639.

Wang N, Ding E, Cheng R (2007) Thermal degradation behaviors of spherical cellulose nanocrystals with sulfate groups. Polymer (Guildf) 48:3486–3493.

Xiang Q, Lee Y, Pettersson PO, Torget RW (2003) Heterogeneous aspects of acid hydrolysis of alpha-cellulose. Appl Biochem Biotechnol 107:505–514.

Yu H, Qin Z, Liang B, et al (2013) Facile extraction of thermally stable cellulose nanocrystals with a high yield of 93% through hydrochloric acid hydrolysis under hydrothermal conditions. J Mater Chem A 1:3938.

Chapter 3

Implications of low-temperature pyrolysis on the mechanism of thermal stabilization of nanocellulose esters

3.1. Introduction

The esterification of nanocellulose is one of the most common techniques of modifying the properties of nanocellulose. In the view of using nanocellulose as reinforcing filler, esterification under heterogeneous condition is often favored to preserve the structural morphology and crystallinity of the starting material. Various esters of nanocellulose have been heterogeneously synthesized and reports on the effects of esterification on different properties have also been reported. Tomé et al. (2011) esterified the surface of BC using acid anhydrides of varying number of carbon chains (2-6) and the cyclic alkenyl succinic anhydride in ionic liquid. An increase in hydrophobic character in all of the esterified BC was observed after measuring the contact angle with water. Vuoti et al (2013) reported an increase in the hydrophobic character of nanofibrillated cellulose (NFC) esterified with various types of acyl chlorides including those containing aromatic rings and different number of carbon chains. Butyl esters of cellulose nanocrystals (CNCs) were also found to be highly hydrophobic and show liquid crystalline behavior (Abraham et al. 2016). Apart from increased hydrophobic character, improvement in the compatibility of nanocellulose to the matrix has also been reported. Acetyl esters of nanocellulose have been shown to exhibit better compatibility to polylactic acid (Tingaut et al. 2010) and polychloroprene (Fahma et al. 2014) than the unmodified nanocellulose. The dispersion of ramie whiskers in low-density polyethylene was also found to improve after esterification of the whiskers with long chain acyl chlorides (Menezes et al. 2009). Interaction of the ester groups with other additives such as sulfur in the processing of natural rubber was also observed for nanocellulose esterified with unsaturated oleic acid chloride (Kato et al. 2015). The crosslinking reaction between sulfur and the double bonds in oleic acid during vulcanization of natural rubber was found to improve the reinforcing capability of nanocellulose.

Despite several reports about nanocellulose esters, very few studies have reported the effect of esterification on the thermal stability of nanocellulose. Uschanov et al.

(2011) esterified microcrystalline cellulose and whiskers from cotton linters with different kinds of long-chain fatty acids and reported a decrease in thermal stability of the modified nanocellulose. Lee et al. (2011) introduced ester groups with varying chain length on the surface of the BC and observed a decreasing trend in 10% WLT with increasing number of carbon chain length. An increase in extrapolated onset of degradation temperature (T_{onset}) and T_{max} was observed by Ávila Ramírez et al. (2014) after esterification of the BC with short-chain carboxylic acids using organocatalytic method.

In this chapter, the effect of varying the type of ester groups on the thermal stability of BC with different DP_v was investigated. Although, there have been reports on the thermal stability of nanocellulose esters with different type of ester groups, particularly those with varying chain length, this chapter included other bulky ester groups including benzoyl (BNZ), pivaloyl (PIV), and adamantoyl (ADM). The thermal stability of these bulky nanocellulose esters have not been previously reported and studied in detail. Moreover, previous reports only assessed thermal stability using thermogravimetric analysis (TGA) which basically measures thermal stability in terms of resistance to weight loss. TGA results alone cannot provide enough information to understand why a material is resistant or susceptible to weight loss. Thus, in this chapter, PyGCMS was used in addition to TGA to study the thermal properties of various types of nanocellulose esters. Through low-temperature pyrolysis and subsequent identification of the evolved gas using PyGCMS, the thermal events at the early stage of thermal degradation of nanocellulose esters were investigated. The structure of the evolved gas during low-temperature pyrolysis enabled a deeper understanding of the effect of the structure of the esters on the initial stage of thermal weight loss observed in TGA.

3.2. Experimental

3.2.1. Materials

BC1100 and BC300 were prepared according to the procedure given in Chapter 2. Propanoyl (C3), octanoyl (C8), tetradecanoyl (C14) and pivaloyl (PIV) chlorides were purchased from Wako Pure Chemicals Industries (Osaka, Japan). Adamantoyl (ADM), benzoyl (BNZ), decanoyl (C10), and acetyl (C2) chlorides were supplied by Tokyo Chemical Industry Co., Ltd. (Tokyo, Japan), Kanto Chemical Co. (Tokyo, Japan), Acros Organics, Thermo-Fisher Scientific (Geel, Belgium), and Sigma-Aldrich Co. (St Louis,

MO, USA), respectively.

3.2.2. Esterification

Esterification was carried out in an acyl chloride-pyridine system following the procedure given in Chapter 2. The calculated amount of pyridine and acyl chloride based from the stoichiometric ratios given in Table 3- 1 was added into a water-free suspension of nanocellulose. Esterification was then carried out with continuous stirring at a specified temperature for each acyl chloride listed in Table 3- 1.

Table 3- 1. Esterification conditions used to prepare the different types of nanocellulose esters

BC ester	**AcCl:OH ratio***	**Pyr: AcCl ratio****	**T*** (°C)**	**Time (h)**
C2-1100	4	1.5	40	1
C3-1100	4	1.5	50	3
C8-1100	5	3	60	2.5
C10-1100	5	3	60	2.5
C14-1100	5	3	60	2.75
ADM-1100	12	5	70	44
BNZ-1100	8	3	70	6.5
PIV-1100	12	5	70	44
C2-300	4	1.5	50	0.75
C3-300	4	1.5	50	4
C8-300	5	3	60	2.5
C10-300	5	3	60	2.5
C14-300	5	3	60	2.75
ADM-300	12	5	70	48
BNZ-300	8	3	70	7
PIV-300	12	3	70	44

* acyl chloride to hydroxyl molar ratio **pyridine to acyl chloride molar ratio *** temperature

The esterification conditions listed in Table 3- 1 were obtained after testing several conditions with varying acyl chloride to OH ratios, acyl chloride to pyridine ratios and temperature. The progress of the reaction was monitored by drawing out a 2-mL portion

of the reaction mixture at various times, filtering, washing, and oven-drying and finally checking the FTIR spectra. When the area of the carbonyl peak reaches 40 square units, the reaction was stopped by pouring ethanol to the reaction mixture. The reaction mixture was filtered, and washed several times with warm ethanol (about 50°C). The washed nanocellulose ester was further subjected to Soxhlet extraction in 10% dichloromethane in ethanol for 16 h to ensure the removal of residual acyl chloride, pyridine and NMP. Finally, the nanocellulose ester was solvent-exchanged to acetone, then to *t*-butanol, and finally freeze dried for 2 days. The structure of the different BC esters prepared and their corresponding names and abbreviations are shown in Figure 3-1.

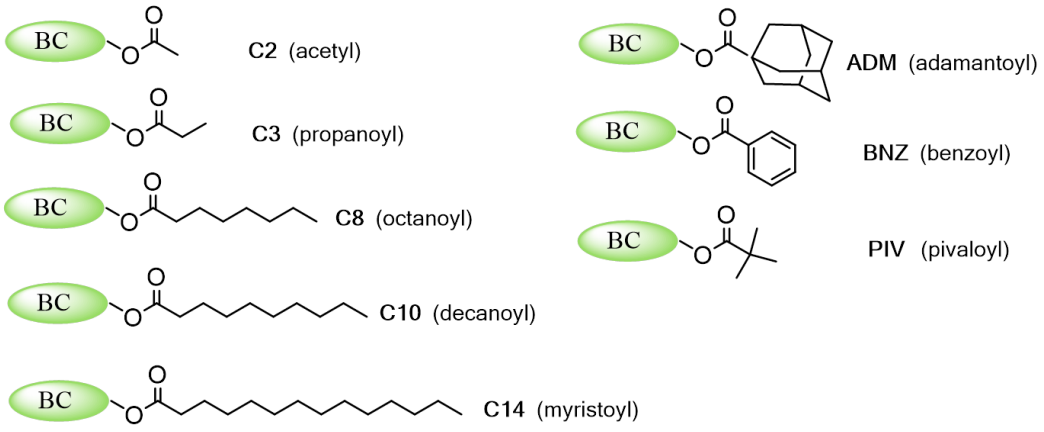

Figure 3-1. The structure of the different nanocellulose esters.

3.2.3. Characterization of nanocellulose esters

DS was determined by saponification method. A 150-mg sample was stirred in 15 mL of ethanol for 20 min at room temperature. To this was added 10 mL of 0.5 M NaOH and the flask was sealed with plastic wrap first, and then capped with aluminum foil to fix the plastic wrap into the flask. The mixture was then transferred to a water bath pre-heated to 70°C and the reaction was kept for 30 min with continuous stirring. The mixture was then cooled and titrated with 0.2M HCl to a phenolphthalein endpoint. A blank sample containing only the untreated BC1100 was also subjected to the same treatment as the modified one. The number of moles of ester calculated from titration data was then used to calculate the DS. The complete removal of the ester groups was

confirmed by the absence of the carbonyl peak in the FTIR spectra of saponified nanocellulose.

The FTIR, DP_v and XRD analysis were carried out following the procedure in Chapter 2. Prior to DP_v and XRD analysis, the nanocellulose esters were hydrolyzed first in alkali solution to remove the ester groups.

3.2.4. Thermogravimetric analysis

Both dynamic and isothermal TGA were performed to measure the thermal stability of the different nanocellulose esters. The procedure followed that in Chapter 2.

3.2.5. Pyrolysis-gas chromatography-mass spectrometry

Low-temperature pyrolysis was performed with a Py3030id double shot pyrolysis (Frontier Laboratories, Ltd., Fukushima, Japan) coupled to a GC/MS system (QP 2010, Shimadzu Scientific Instruments, Tokyo, Japan). A 300-μg sample placed in a metal sample cup was attached to the sampler using a metal stick. The sampler was then attached to the pyrolyzer and purged with helium by loosening the air purge nut for few min before starting the pyrolysis. The heart-cut analysis was programmed to heat the sample for 5 min at 110°C and followed by heating to 280°C at a heating rate of 20°C/min. The evolved volatiles from the initial heating at 110°C were not collected. The evolved gases during the non-isothermal heating process were cryo-focused at the front point of the separation column (UA-5, 30m x 0.25 mm i.d. x 0.25 μm film thickness) by liquid nitrogen supplied from Micro Jet Cryo-Trap (Frontier Laboratories Ltd., Fukushima, Japan). The evolved gases were separated out in the column with a GC oven temperature programmed at 40°C and holding it for 4 min, ramping at 10°C/min to 320°C, and finally holding at this temperature for 4 min. The carrier gas was helium with a flow rate of 1.23mL/min. A split ratio of 1:49 was applied. For MS detection, electron impact ionization system was used with ionization energy set at 0.80kV. The ion source and interface temperature were 200°C and 190°C, respectively. Pyrolysis of each sample was carried out at least two times. The structure of the evolved gas was identified using the NIST 2011 Mass Spectral Library and Software.

3.3. Results and Discussion

3.3.1. Esterification and DP_v

One of the properties affected by esterification conditions is the DP. Esterification in acidic medium at elevated temperature can hydrolyze cellulose and result to esterified cellulose of lower DP. Such effect even inspired other researchers to prepare modified CNCs by concurrent hydrolysis and esterification. Yu et al. (2014) prepared silver-CNC from microcrystalline cellulose (MCC) by concurrent hydrolysis and esterification of MCC followed by redox reaction with silver-ammonia aqueous solution in the same pot. The first step which was the simultaneous hydrolysis and esterification with formic acid catalyzed by HCl was conducted at 90°C for 3h. Spinella et al. (2016) prepared modified CNC from ramie fibers by concurrent hydrolysis and esterification using organic acids catalyzed by HCl and the reaction was carried out at 140°C for 3h.

Because the thermal stability of nanocellulose decreased with decreasing DP_v, the DP_v of the starting nanocellulose was tried to maintain by carrying out esterification at temperatures (40-70°C) much lower than those reported for the preparation of CNC by concurrent hydrolysis and esterification. The reaction temperature was not fixed to 40°C similar to acetylation because it has been reported that increasing chain length and size of the acylating agent decreases the reaction rate due to steric hindrance (Tomé et al. 2011; Uschanov et al. 2011; Vuoti et al. 2013). The slow reaction rate expected for acyl chlorides with longer chain length (C8, C10 and C14) and bulkier groups (ADM, BNZ, and PIV) was offset by increasing the temperature and the amount of acyl chloride as shown in Table 3- 1. Because the increase in acyl chloride favors the formation of acidic condition and the increase in temperature in acidic medium is favorable for hydrolysis; the amount of pyridine was also increased. Pyridine, apart from catalyzing the reaction, also aided in the neutralization of the acidic pyrodinium hydrochloride. Despite the increase in temperature and the amount of acyl chloride, the time needed to reach a carbonyl peak area of 40 was still longer for those with long carbon chain and bulky groups (Table 3- 1). To check whether the esterification conditions caused significant change in DP_v, the nanocellulose was regenerated from its corresponding esters by saponification and the DP_v of the regenerated nanocelluloses were again measured. No significant change in DP_v was observed in all of the samples as presented in Table 3-2.

Table 3- 2. The degree of substitution (DS), viscosity-average degree of polymerization (DP_v) and crystallinity indexes (CrI) of BC1100, BC300 and their esters

Sample	DS	DP	CrI	Sample	DS	DP	CrI
BC-1100	0	1100	93.6	BC-300	0	300	95.5
C2-1100	0.41	1100	94.1	C2-300	0.43	280	95.7
C3-1100	0.42	1170	95.7	C3-300	0.42	289	96.7
C8-1100	0.47	1096	93.9	C8-300	0.46	300	95.4
C10-1100	0.45	1160	94.6	C10-300	0.47	295	93.7
C14-1100	0.44	1159	94.9	C14-300	0.44	300	95.7
ADM-1100	0.45	1056	92.6	ADM-300	0.44	296	94.5
BNZ-1100	0.43	1165	96	BNZ-300	0.42	297	95.1
PIV-1100	0.4	1050	95.2	PIV-300	0.43	292	96.7

3.3.2. FTIR and DS

The extent of esterification, which is evaluated by DS values, can also affect the final properties of the modified nanocellulose. Ifuku et al. (2007) acetylated BC nanofibers with different DS and found that the enhancement in the properties of nanocomposite reinforced with acetylated BC is affected by the DS. Although not in the form of nanocellulose, Jandura et al. (2000) also reported that the thermal stability of esterified cellulose fibers increased with increasing DS. Thus to avoid discrepancies in comparing nanocellulose esters with different DS, nanocellulose esters with similar DS as possible were prepared.

Controlling the DS was made possible by monitoring the change in the FTIR spectra during esterification. Because of similar spectra of the esters of BC1100 and BC300, only the spectra of BC1100 esters are shown in Figure 3-2.

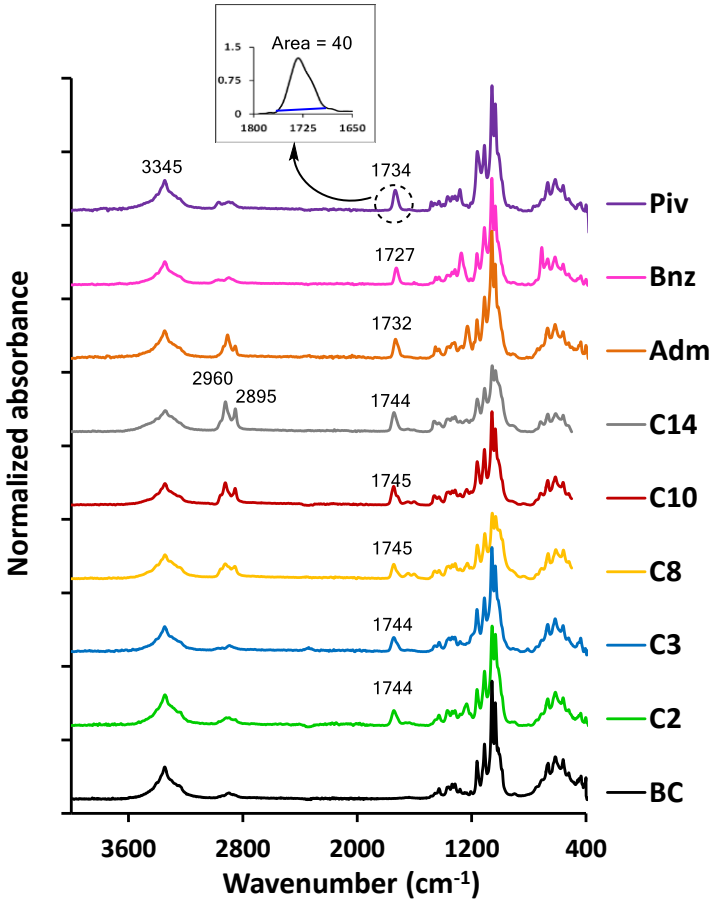

Figure 3-2. FTIR spectra of BC1100 and its esters. The inset shows an enlarged section of the carbonyl peak and the target peak area.

The introduction of an ester group to cellulose changes the FTIR absorption spectra of cellulose. The most distinct change is the appearance of a strong absorption peak around 1745 cm^{-1} which corresponds to the stretching of the carbonyl ester group. With aryl substitution, this peak shifts to lower frequency by about 15-25 cm^{-1} (Pavia et al. 2001) and it was observed in BNZ ester (Figure 3-2). The carbonyl peak of branched PIV and cyclic ADM nanocellulose esters also appeared at a frequency lower than straight-chain esters which was similar to those observed by Heinze et al. (2003) and Xu et al. (2011).

Another peak that also differentiates the nanocellulose esters from the untreated BC1100 is the CH_2 asymmetric and symmetric stretching at 2960 cm^{-1} and 2895 cm^{-1}, respectively (Jandura et al. 2000). The increase in the intensity of CH_2 absorption bands,

however, was only noticeable in esters with long carbon chains and ADM group.

The broad absorption band corresponding to OH groups appearing at 3345 cm^{-1} is also known to change after esterification. The intensity of this band is reported to decrease because of the replacement of the OH groups by ester groups. The decrease in the intensity, however, is observable for highly substituted cellulose esters similar to the report of Labafzadeh et al. (2012) and Abraham et al. (2016) where the DS values were 2 and above. In this study, the decrease in the OH band in the nanocellulose esters is hardly noticeable when compared to the untreated BC1100. Similar behavior was also observed by Lee et al. (2011) and Ávila Ramírez et al. (2014). Accordingly, the small change in the intensity of the OH band after esterification suggests that the modification essentially took place on the surface or in the amorphous fraction of the cellulose (Lee et al. 2011).

Among the changes in absorption peaks attributed to esterification, it is the carbonyl peak that gives a quantifiable change to all of the modified BC and a direct relationship to the DS. The intensity of the carbonyl peak is proportional to the DS; i.e. the higher the DS, the higher is the intensity (Tomé et al. 2011; Ávila Ramírez et al. 2014). Moreover, high correlation between the area of the carbonyl peak and DS values of acetylated BC was observed in Chapter 2. It is with this reason that the area of the carbonyl peak was used as a controlling parameter during esterification. From the equation derived in Chapter 2, the area of carbonyl peak that gives a DS of 0.40 was calculated to be about 40 square units (Figure 3-2). Thus, during esterification, the area of the carbonyl peak was constantly monitored. The carbonyl peak area of the prepared nanocellulose esters on average was recorded to be 40.6 ($\pm$1.3). Since the calibration curve was based only on acetylated nanocellulose, the actual DS was still measured by saponification method to ensure that the DS values fall within a narrow range. As presented in Table 3- 2, the DS values obtained from saponification method did not vary much and were in the range of 0.40 – 0.47. The result showed that the use of FTIR to control the DS during esterification can be reliable when aiming for esterified nanocellulose of nearly the same DS.

3.3.3. Crystallinity

When cellulose is subjected to chemical modification, its crystallinity may vary depending on the extent of modification and reaction conditions. Reports have shown that a change in crystallinity during modification can have an adverse effect to the desired property. Ifuku et al. (2007) reported that extensive acetylation, a DS above 0.78,

increased the coefficient of thermal expansion of acetylated BC and their composites primarily due to the reduction in the degree of crystallinity. Tingaut et al. (2010) acetylated microfibrillated cellulose and observed that thermal stability improved up to an acetyl content of about 10.5% (DS = 0.44) and decreased when the acetyl content was 17% (DS= 0.77). The decrease in thermal stability at higher acetyl content was also attributed to the reduction in crystallinity. Thus, it is of utmost importance that the crystallinity is maintained after modification. The decrease in thermal stability at higher DS is also one of the reasons why esterification was limited to a low DS, about 0.40.

Before XRD analysis, the ester groups were removed by saponification because the different types of ester can contribute a varying effect on crystallinity. If the ester groups were not removed, the XRD pattern of nanocellulose esters will reflect both the effect of reaction conditions and the ester groups attached to the nanocellulose. Figure 3- shows the diffraction patterns of the untreated BC and that of the recovered nanocellulose from their corresponding esters after saponification. Because the patterns of BC300 esters were also similar, only the patterns of BC1100 esters are shown. All of the diffraction patterns show typical cellulose I structure with three distinct peaks at 14.5°, 16.5°, and 22.4° 2θ with assigned Miller indices of (100), (010) and (110); respectively.

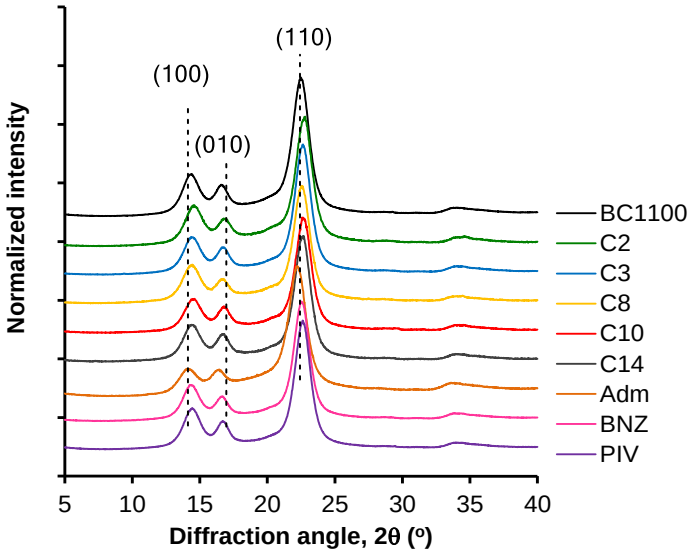

Figure 3-3. XRD patterns of untreated BC1100 and the cellulose regenerated from their corresponding esters after saponification.

As shown in Figure 3-, no significant change in the diffraction pattern after modification was observed, an indication that the crystalline core of the BC after modification was not affected. Consequently, this result is confirmed by the almost similar crystallinity indexes (Table 3- 2) of the untreated BC to that of the modified ones. The crystallinity indexes of BC1100 and BC300 were 93.7(±0.5) and 95.5(±0.8), respectively. The esters of BC1100 and BC300 recorded an average value of 94.6(±1.1) and 95.4(±1.1), respectively.

3.3.4. Thermal stability

Figure 3-4 shows the TG and DTG curves and the values of T_{max} and 5%WLT obtained under dynamic heating of the nanocellulose before and after esterification. All nanocellulose esters showed single step degradation similar to the untreated BC. In general, esterification increased the T_{max} both for BC1100 and BC300 as shown in Figure 3-4. The increase in T_{max} for BC300 was higher than that of the BC1100. BC300 esters registered an average increase in T_{max} of 38 (±6)°C while BC1100 esters increased by 16(±4)°C. The T_{max} values did not vary significantly with the type of esters and the type of nanocellulose. The nearly similar T_{max} values of BC300 and BC1100 esters irrespective of the type of esters suggests that the structure of the ester and the DP_v have no significant effect on the major decomposition temperature of nanocellulose esters. A similar observation was also reported by Uschanov et al. (2011) who reported that the modified forms of microcrystalline cellulose and its whiskers had basically the same decomposition temperatures.

The increase in T_{max} to values around 370°C, however, is not a guarantee that the nanocellulose esters can already be used in high temperature processing. At T_{max}, 50-60% of the starting material had already decomposed. In view of composite preparation, stabilization of nanocellulose at the initial stage of thermal degradation is more important than the increase in T_{max}. The onset of degradation was evaluated from the 5% WLT as shown in Figure 3- 1f.

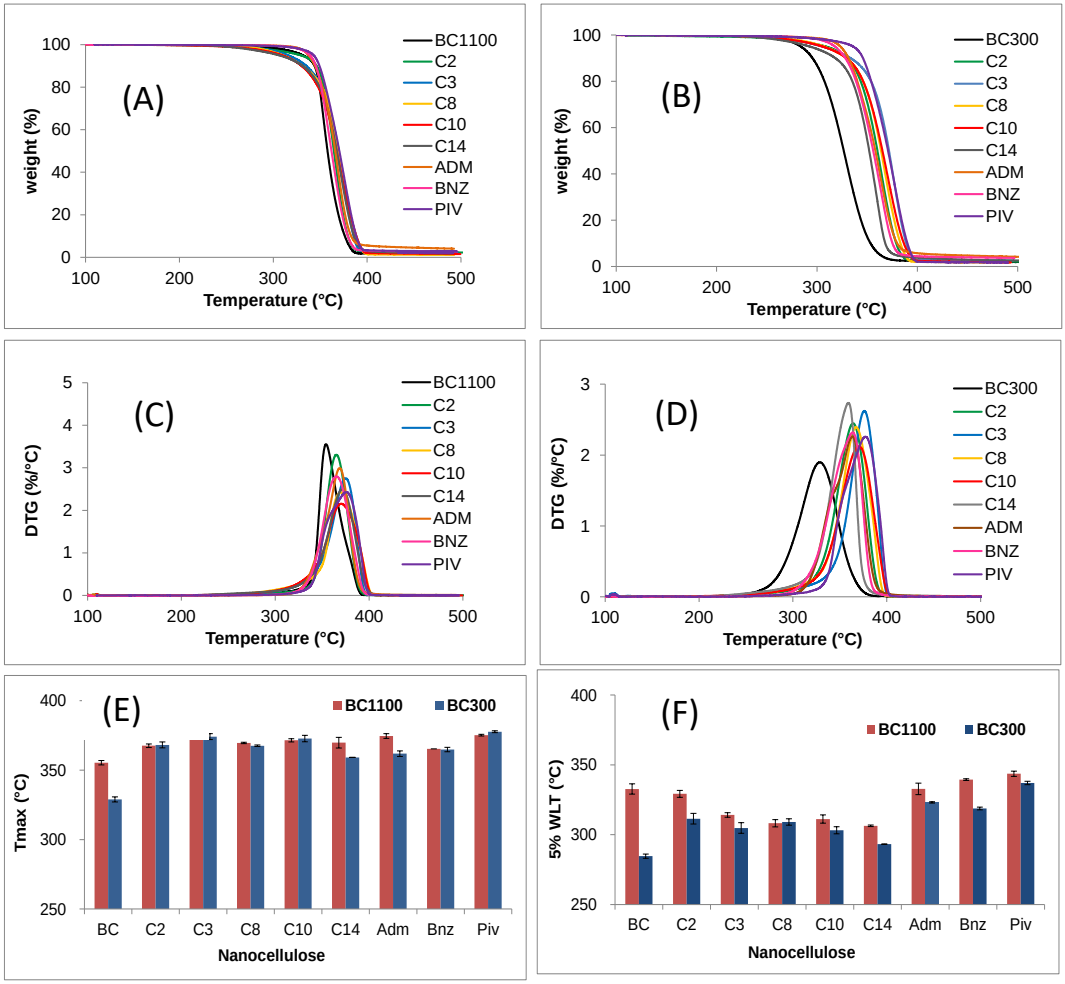

Figure 3- 1. Thermogravimetric (A,B) and derivative thermogravimetric (DTG, C,D) curves of BC1100, BC300, and their esters during dynamic heating, and the measured T_{max} (E) and 5% WLT (F).

The effect of esterification on the 5% WLT varied between BC1100 and BC300 and among the types of esters. Before esterification, the 5%WLT of BC300 was about 48°C lower than that of the BC1100. This big difference in 5%WLT is attributed to the higher number of REs in BC300 than BC1100, which was confirmed in Chapter 2.

The structure of the esters gave varying effect on the 5%WLT of BC1100. Esters with straight carbon chains registered lower 5% WLT than the untreated BC and showed a decreasing trend with increasing chain length. On the other hand, the ADM, BNZ and PIV esters exhibited higher 5% WLT than the untreated BC. For BC300, all esters gave higher 5% WLT than the untreated one. The ADM, BNZ, and PIV esters of BC300 also showed

higher 5%WLT than those of the straight-chain esters. The decreasing trend in 5%WLT with increasing chain length was also observed. A similar trend was observed by Lee et al. (2011) who esterified BC with fatty acids containing 2, 6 and 12 carbon. Janicek et al. (2013) who esterified cellulose fibers with fatty acids of different chain lengths also observed a decreasing extrapolated onset temperature with increasing chain length.

Because compounding of composite is often performed at a fixed temperature, the stability of a material at a fixed temperature for a specific period of time is also important in evaluating the potential of a material as reinforcing filler. The temperature chosen for isothermal heating was the 1%WLT of BC300 which is 250°C. The measured total weight loss (TWL) in percentage also covered the weight loss when the temperature of the furnace was increased from 110 -250°C and holding it isothermal at 250°C for 1h. The higher the TWL, the higher is the rate of degradation.

Figure 3-2 shows the isothermal TG curves of BC1100, BC300 and their esters. Significant difference in TWL was observed between BC1100 and BC300 before esterification. BC1100 registered an average TWL of 1.7%, which is much lower than that recorded for BC300 which gave a TWL of 7.2%. The higher TWL observed in BC300 than in BC1100 supports again the possible contribution of REs to thermal stability. After modification, the TWL of BC300 esters were still generally higher than the BC1100 esters but the difference was not as significant as before esterification.

The effect of the structure of the esters was even more evident from the results of isothermal heating as shown in Figure 3-2. Esterification of BC1100 with straight-chain esters increased the TWL and the weight loss also increased with increasing chain length. Only the esters of ADM, BNZ and PIV showed higher resistance to weight loss than BC1100. Esterification of BC300 showed a decrease in TWL except for C14. A remarkable decrease in TWL was also observed for the ADM, BNZ, and PIV esters of BC300. These bulky esters consistently showed improvement in thermal stability both in the dynamic and isothermal heating and the reason is discussed in the next section.

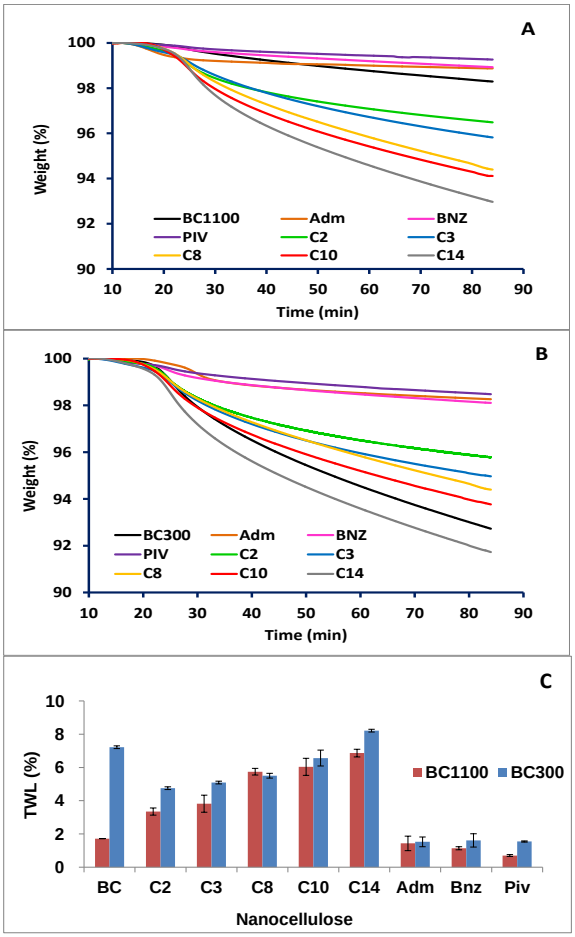

Figure 3-2. Isothermal thermogravimetric curves of BC1100, BC300 and their esters and the measured total weight loss (TWL) in percentage.

3.3.5. Products of low-temperature pyrolysis

Reports on biomass pyrolysis usually focused on fast pyrolysis at high temperature (450-650°C) and very high heating rates (10^3-10^5°C /s) in view of biorefinery applications (Kan et al. 2016) . On the other hand, to understand the events at the initial stage of thermal degradation, low-temperature pyrolysis with a slow heating rate (20°C/min) was performed. The use of PyGCMS enabled the collection and analysis of the evolved gas during low-temperature pyrolysis by GCMS. Initially, pyrolysis was carried out by heating from 110-250°C but the intensity of the chromatogram peaks from this condition was very low, making signal distinction from the noise difficult. The temperature was then increased to 280°C which is about the 5% WLT of BC300. Heating to 280°C liberated enough volatiles that made identification feasible with GCMS.

Figure 3-6 shows the chromatograms of BC1100, BC300 and their corresponding esters after heating from 110 - 280°C. The chromatogram peak labels with their corresponding retention time and compound name are summarized in Table 3-3. Only those peaks that gave similarity index of 90% and above based from the mass spectral comparison in the NIST Library are listed. All compounds gave off CO_2 as one of the products and it was the peak labeled number 1 in each of the chromatograms. CO_2 is considered as one of the primary gases produced during biomass pyrolysis and mainly originates from the decomposition and reforming of carboxyl groups (Qu et al. 2011).

Before esterification, significant difference between the pyrolysis behavior of BC1100 and BC300 was observed. BC300 gave off levoglucosan (LG) while BC1100 did not give significant amount to be detected (Figure 3-6a). This result supports the findings of Shafizadeh et al. (1979) who studied LG production from pyrolysis of cellulosic materials at 400°C under vacuum for 5-9 min. It was reported that higher amount of LG was produced from partially acid-hydrolyzed cotton linters than untreated cotton linters or cotton fabric. The study also reported a good correlation between the T_{max} (reported as DTG peak in their study) and LG formation; i.e., the lower the DTG peak was, the higher the amount of LG formed. It can be recalled from our TG data that the T_{max} of BC300 is also much lower than that of the BC1100.

The susceptibility of BC300 towards LG formation is probably due to the higher number of REs of BC300 than BC1100. To confirm the effect of REs to the formation of LG during low-temperature pyrolysis, the $NaBH_4$-reduced BC300 from Chapter 2 was also pyrolyzed under the same conditions and the chromatogram is also shown in Figure 3-6a. It can be seen that LG was not detected in the $NaBH_4$-reduced BC300. This result shows that the formation of LG is affected by the REs. The role of REs on cellulose pyrolysis has been extensively studied by the group of Matsuoka and co workers. The group reported that cellulose REs are the reactive sites for discoloration at low-temperature pyrolysis and proposed a mechanism for thermal activation of cellulose starting at the REs.

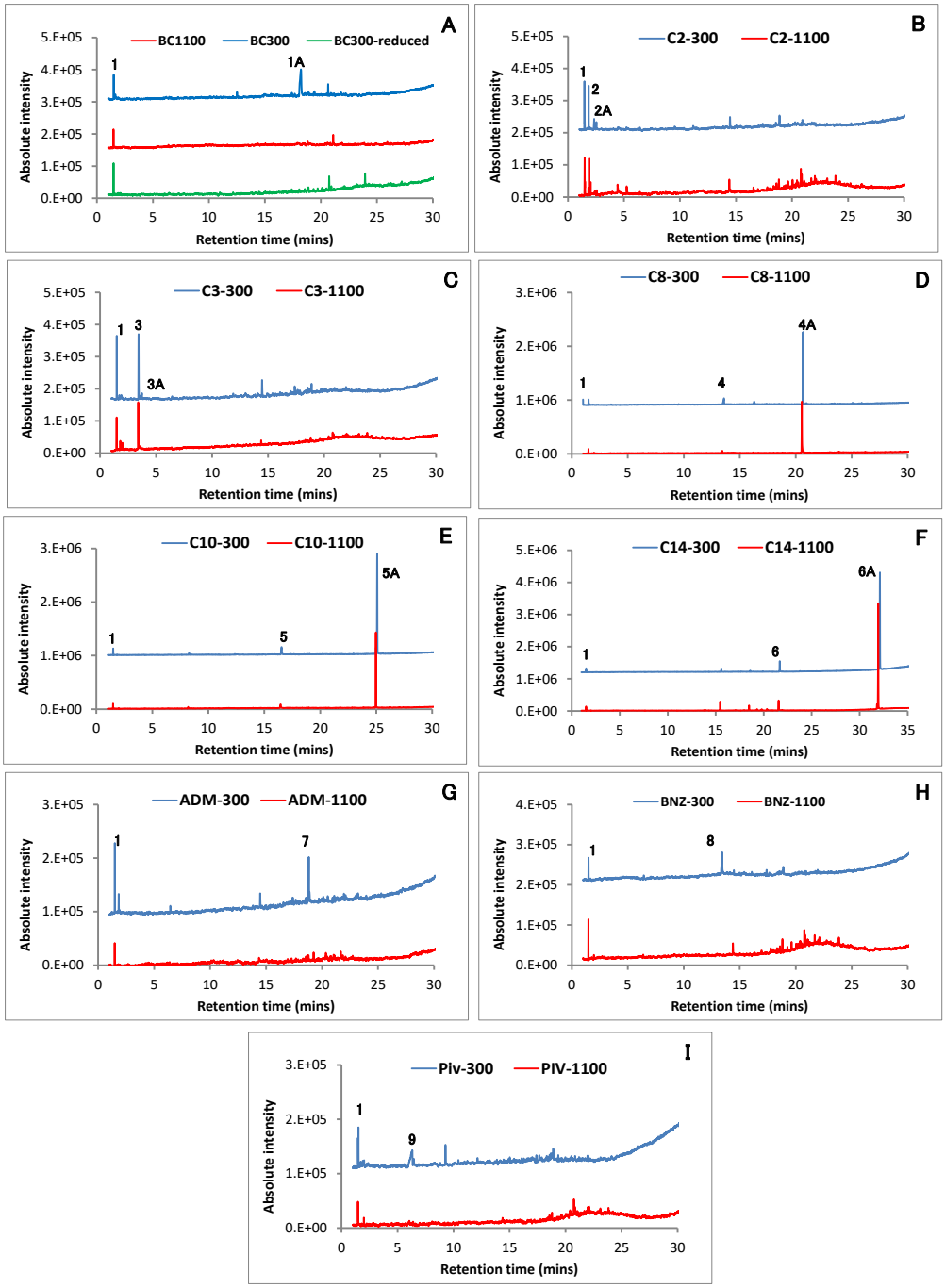

Figure 3-6. Chromatograms of the evolved gas from the low-temperature pyrolysis of BC1100, BC300, and their esters.

The observed difference in the pyrolysis behavior of BC1100 and BC300 suggests that the lower thermal stability of BC300 than BC1100 is associated to the susceptibility of BC300 towards LG formation because of the higher number of REs of BC300 than BC1100. Moreover, it can be deduced that for BC300, the primary decomposition step associated to the initial stage of weight loss during TGA is the formation and release of

LG. During heating, BC300 lost weight earlier than BC1100 by the release of LG resulting to lower 5%WLT and higher TWL than BC1100.

Table 3-3. Peak number, retention times and the corresponding names of the identified products from the low-temperature pyrolysis of BC1100, BC300, and their esters.

Peak number	Retention Time (min)	Compound Name
1	1.50	Carbon dioxide
1A	18.22	Levoglucosan
2	1.85	Acetone
2A	2.54	Acetic Acid
3	3.44	3-Pentanone
3A	3.6	Propanoic acid
4	13.59	Octanoic acid
4A	20.65	8-Pentadecanone
5	16.6	Decanoic acid
5A	24.9	10-nonadecanone
6	21.63	Myristic acid
6A	32.04	14-Heptacosanone
7	18.82	1-Adamantane carboxylic acid
8	13.43	Benzoic acid
9	6.31	Pivalic acid

When the nanocellulose esters were subjected to low-temperature pyrolysis, CO_2 was still one of the main products but LG was not detected in the evolved gas (Figure 3-6). Esterification seems to inhibit LG formation especially for BC300. Considering the structure of LG, the atoms responsible for the formation of a new ring are the carbon atom at C1 and the oxygen atom of the OH group attached to carbon 6. When the OH groups of carbons 1 and 6 are substituted by ester groups, the formation of LG is probably inhibited because of steric hindrance. Moreover, the removal of the ester groups should probably occur first before LG is formed. Indeed, the low-temperature pyrolysis products

of nanocellulose esters yielded only compounds which probably originate from the ester groups such as carboxylic acids and ketones (Figure 3-6 and Table 3-3). The result suggests that at the initial stage of thermal degradation of nanocellulose esters, the removal of the ester groups, which will be termed as deprotection, occurs predominantly before the production of LG.

Deprotection of nanocellulose esters seemed to follow different mechanisms between esters with straight aliphatic chains and with bulky groups ADM, BNZ, and PIV. Considering that the pyrolytic pathway of simple esters occur via elimination reaction to produce alkene and carboxylic acid (Pine 1987), deprotection of nanocellulose esters during low-temperature pyrolysis is expected to give off the equivalent carboxylic acid of the ester group. Indeed, all esters gave off the equivalent carboxylic acids; however, straight-chain nanocellulose esters also gave off symmetrical ketones which were probably formed from the condensation of two ester groups. The release of symmetrical ketones from esters with straight carbon chains was also found to be more dominant than the release of free acids evident from the relatively higher intensity of the peaks corresponding to symmetrical ketones than that for free acids. The formation of symmetrical ketones seems to require less energy than the release of free carboxylic acids.

Recognizing that deprotection is the primary event at the initial stage of thermal degradation, the decreasing 5%WLT with increasing chain length exhibited by nanocellulose esters with straight carbon chain can therefore be attributed to the differences in the molecular weight (MW) of the ester groups that are being removed. For example, the removal of C14 (MW = 211) in the form of an acid or ketone can contribute a higher weight loss than the removal of C2 (MW= 43). This explains why the 5%WLT of C14 is reached at a much lower temperature than that of C2. The same explanation also applies for the trend observed in the TWL of straight-chain esters; i.e. increasing TWL with increasing chain length, during isothermal heating.

In contrast to straight-chain nanocellulose esters, bulky esters of ADM, BNZ, and PIV gave only carboxylic acids during pyrolysis and it was observed only in the BC300 esters. As shown in Figure 3-6g-i, the ADM, BNZ, and PIV esters of BC300 produced adamantane carboxylic acid, benzoic acid, and PIValic acid, respectively. This result shows the higher susceptibility of BC300 esters to undergo deprotection than the BC1100 esters, which probably originated from the REs. The hemiacetal OH at the REs which are

more acidic than the other OH of the glucopyranose ring are easily polarized, thereby exhibiting high chemical reactivity. During esterification, these OH groups at the REs were more likely esterified. When pyrolyzed, the esters at the REs cleave more readily than the ester groups attached to carbon atoms in the 2, 3 and 6 positions of the AGU. The ring oxygen of the glucopyranose and the ester group directly bonded to the anomeric carbon of the RE, can create polarization which makes this region unstable. The high susceptibility of the ester at the REs to be removed could explain why the BC300 esters of ADM, BNZ, and PIV, despite the improvement in thermal stability; still showed lower thermal stability at the initial stage of degradation when compared to their BC1100 counterparts.

Another significant difference observed between the straight-chain esters and the bulky esters is that the resistance displayed by ADM, BNZ, and PIV esters of BC1100 against deprotection was not observed in the straight-chain esters of BC1100; which also produced symmetrical ketones during pyrolysis. The difference in pyrolysis behavior of the bulky BC1100 esters and straight-chain esters at the given heating conditions further support the earlier assumption that the release of symmetrical ketones requires less energy than the release of free acids. The possibly lower energy requirement for the removal of straight-chain esters in the form of symmetrical ketones than the bulky esters of PIV, BNZ and ADM also explain why straight chain nanocellulose esters also consistently showed lower thermal stability at the onset of degradation than those of the bulky nanocellulose esters.

3.3.6. Mechanism of deprotection

From the pyrolysis products, it can be deduced that deprotection of nanocellulose esters can take place in two ways: the direct cleavage of the ester bonds from the cellulose chain to release the equivalent carboxylic acids; and the possible condensation reaction between two esters to produce symmetrical ketones.

The release of carboxylic acids from esters is a typical pyrolytic pathway for simple esters but the formation of symmetrical ketones from nanocellulose esters has not been previously reported elsewhere. Symmetrical ketones were reported to be produced from the pyrolysis of saturated triglycerides which also contains ester groups in a glycerol backbone, a polyol like cellulose (Nichols and Holman 1972) and from acyl lipids (Evershed et al. 1995). In the study of Nichols and Holman (1972) symmetrical ketones

were not the major product which may be attributed to the relatively high temperature (630-650 °C) used during pyrolysis. To check if symmetrical ketone is actually produced from the possible secondary reactions that can take place when the free acids were removed from the cellulose chain, acetic acid and stearic acid were also pyrolyzed under the same conditions. Results showed that these acids only gave off the free acid upon heating and no ketones were produced as shown in Figure 3-7. The methyl ester of stearic acid was also pyrolyzed to determine if condensation reaction can take place from free esters. Similar with the free acids, no symmetrical ketone was also released (Figure 3-7). Thus, the result confirmed that the formation of symmetrical ketone occurs before they are released from the cellulose chain and not after the free acids or free esters are given off. From this viewpoint, a possible mechanism of deprotection at the initial stage of thermal degradation of nanocellulose esters with straight carbon chains is proposed.

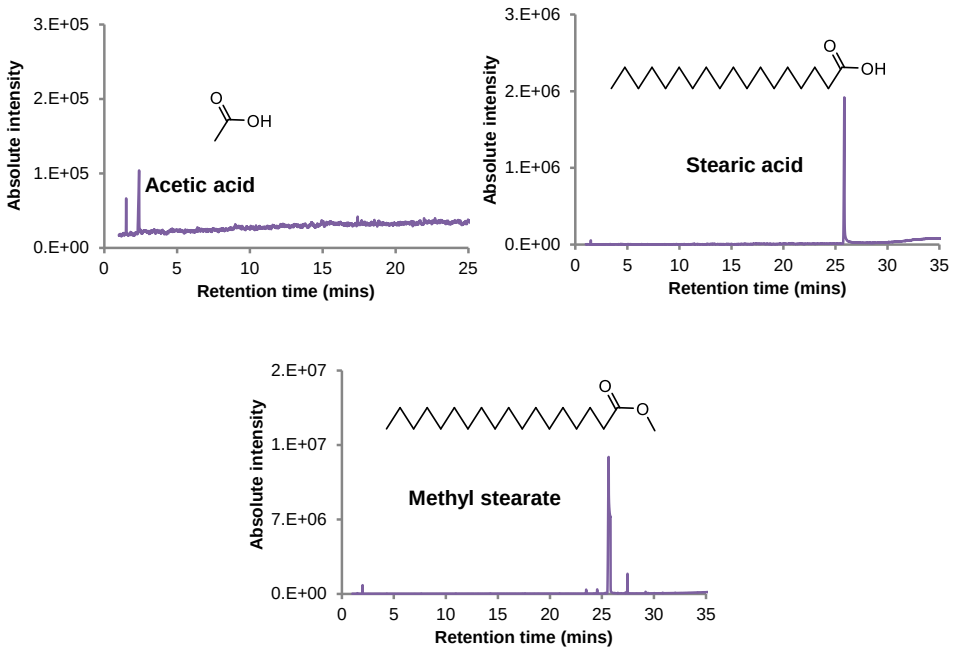

Figure 3-7. Low-temperature pyrolysis products of acetic acid, stearic acid and methyl stearate.

Figure 3-8 shows the proposed deprotection mechanism of nanocellulose esters with straight carbon chains C2, C3, C8, C10 and C14. The mechanism follows the Dieckmann condensation which is the intramolecular condensation of diesters to produce cyclic ß-ketoesters (Wang 2009). The basis of this reaction is the nucleophilic reactivity

of the carbon atom alpha to the carbonyl group (Pine 1987). The first step (Figure 3-8, structure A) in the proposed mechanism is enolization which is the movement of the hydrogen atom (the α-hydrogen atom) attached to the α- carbon to form an enol (Figure 3-8, structure B). The formation of the sp2 hybridized carbon at the alpha position accounts for the nucleophilic reactivity of the α- carbon. This nucleophilic center can attack an electrophilic group; and in the modified nanocellulose esters, the electrophilic group is the nearby carbonyl group of another ester chain. This step forms structure C, a cyclic hemiketal which can undergo ring opening to form a ß-ketoester (D1). Decarboxylation of D1 liberates carbon dioxide and an enol, F, which on rearrangement gives the more stable tautomer, a ketone, and in this case the symmetrical ketone, G. As of the moment, the change in structure of the cellulose chain when D1 undergoes decarboxylation is not yet deduced. If the electron-rich oxygen at the ß-carbon abstract the proton of the OH group attach to the glucose ring in cellulose, the more likely structure that will be formed is an epoxide, E. If the proton in the glucose ring is abstracted as shown in D2, the formation of an enol is more likely, which further rearranges to a ketone.

The absence of symmetrical ketones from the pyrolysis products of ADM, BNZ, and PIV esters can be traced from the proposed mechanism. The first reaction that drives the formation of symmetrical ketones was the enolization initiated by the acidic α-hydrogens. The esters of ADM, BNZ, and PIV lack these α-hydrogens, and thus cannot undergo the same reaction to produce symmetrical ketones. On the other hand, it is still not safe to generalize that all nanocellulose esters without α- hydrogens can exhibit high thermal stability similar to what has been displayed by these three esters. It can be inferred, however, that the thermal stability of nanocellulose esters does depend on how they undergo deprotection; and that the structure of the esters affect the mechanism of deprotection.

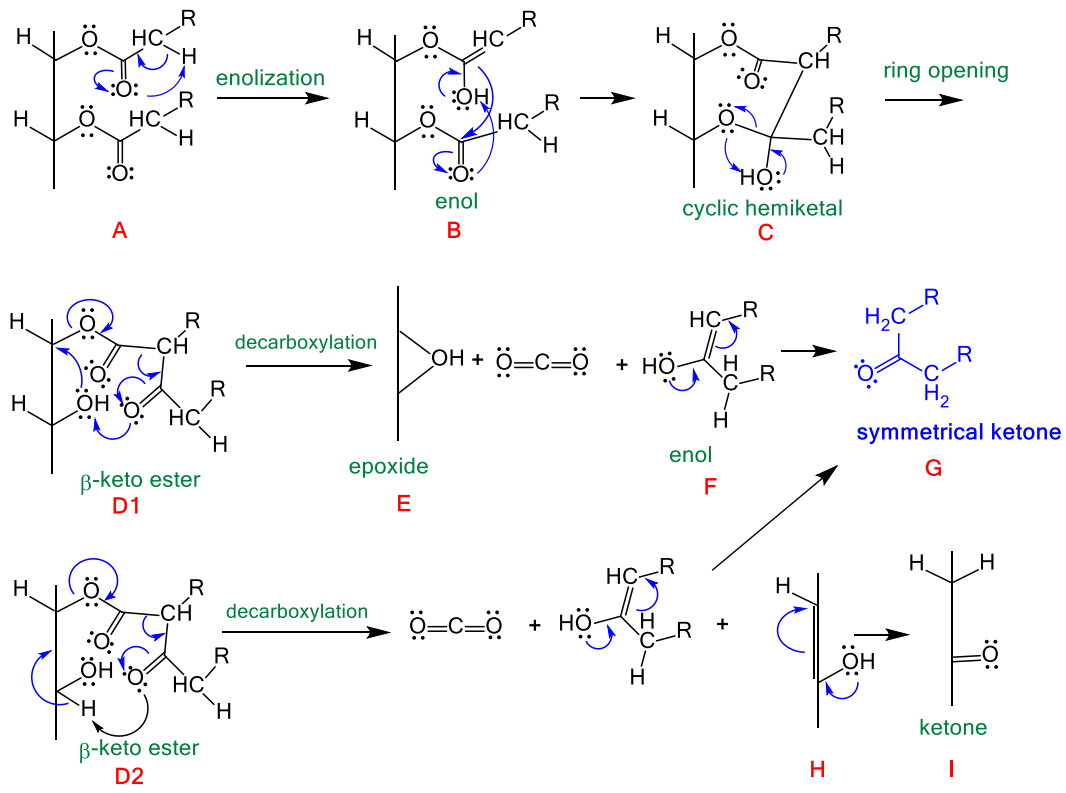

Figure 3- 3. The proposed mechanism of deprotection of nanocellulose esters with straight aliphatic chains during the initial stage of thermal degradation.

3.4. Summary

The esterification conditions used to modify the BC can produce modified nanocellulose without significant change in DPv and crystallinity of the starting material. The DS can also be controlled by monitoring the area of the carbonyl peak in the FTIR spectra. Esterification influenced the thermal stability of nanocellulose. T_{max} increased after esterification and is not affected by the structure of the ester groups. It is the 5% WLT that was affected by the structure of the ester groups. Esters with straight carbon chains (C2, C3, C8, C10 and C14) sped up the onset of degradation while bulky esters (PIV, BNZ, and ADM) delayed the onset of degradation. The products of low-temperature pyrolysis enabled the identification of the possible processes that occur at the onset of thermal degradation of nanocellulose and its esters. The formation of LG and its release is the major process that accounts for the initial weight loss of unmodified BC300. The REs seems to have a catalytic effect toward LG formation. It was not observed in BC1100

which has a higher DP than BC300, and it was inhibited when the REs of BC300 were reduced. LG formation was also inhibited after esterification. Deprotection or the removal of the ester groups occurs during low-temperature pyrolysis of the nanocellulose esters. Based from the structure of the pyrolysis products, two mechanisms of deprotection were deduced: the direct cleavage of the ester bond between nanocellulose and the ester group to produce the equivalent carboxylic acid; and the condensation reaction between two ester groups to produce symmetrical ketones. Straight-chain esters deprotect mainly by condensation reaction which was proposed to be driven by the acidic α-hydrogens. Bulky esters of PIV, BNZ, and ADM which do not possess α-hydrogens deprotect by direct ester bond cleavage. The lower onset of thermal degradation displayed by nanocellulose esters with straight-chain carbon esters than those of the bulky esters was attributed to the possible lower energy required to deprotect by condensation reaction than direct ester bond cleavage. The high improvement in the onset of thermal degradation for the BC1100 esters of PIV, BNZ, and ADM suggest the potential of these esters as reinforcing filler for polymer matrices of high melting point such as nylon 6 or polycarbonates with melting points of 225°C and 250°C, respectively. Finally, the formation of symmetrical ketones through condensation reaction on the surface of the nanocellulose can also open a route for the template synthesis of symmetrical or complex ketones, with nanocellulose or cellulose acting as a template.

3.5. References

Abraham E, Nevo Y, Slattegard R, et al (2016) Highly hydrophobic thermally stable liquid crystalline cellulosic nanomaterials. ACS Sustain Chem Eng 4:1338–1346.

Ávila Ramírez JA, Suriano CJ, Cerrutti P, Foresti ML (2014) Surface esterification of cellulose nanofibers by a simple organocatalytic methodology. Carbohydr Polym 114:416–423.

Evershed RP, Stott AW, Raven A, et al (1995) Formation of long-chain ketones in ancient pottery vessels by pyrolysis of acyl lipids. Tetrahedron Lett 36:8875–8878.

Fahma F, Takemura A, Saito Y (2014) Acetylation and stepwise solvent-exchange to modify hydrophilic cellulose whiskers to polychloroprene-compatible nanofiller. Cellulose 21:2519–2527.

Heinze T, Liebert TF, Pfeiffer KS, Hussain MA (2003) Unconventional cellulose esters :

synthesis , characterization and structure – property relations. Cellulose 10:283–296.

Ifuku S, Nogi M, Abe K, et al (2007) Surface modification of bacterial cellulose nanofibers for property enhancement of optically transparent composites: dependence on acetyl-group DS. Biomacromolecules 8:1973–8.

Jandura P, Riedl B, Kokta B V (2000) Thermal degradation behavior of cellulose fibers partially esterified with some long chain organic acids. Polym Degrad Stab 70:387–394.

Janicek M, Krejci O, Cermak R (2013) Thermal stability of surface-esterified cellulose and its composite with polyolefinic matrix. Cellulose 20:2745–2755.

Kan T, Strezov V, Evans TJ (2016) Lignocellulosic biomass pyrolysis: A review of product properties and effects of pyrolysis parameters. Renew Sustain Energy Rev 57:126–1140.

Kato H, Nakatsubo F, Abe K, Yano H (2015) Crosslinking via sulfur vulcanization of natural rubber and cellulose nanofibers incorporating unsaturated fatty acids. RSC Adv 5:29814–29819.

Labafzadeh SR, Kavakka JS, Sievanen K, et al (2012) Reactive dissolution of cellulose and pulp through acylation in pyridine. Cellulose 243:1295–1304.

Lee K-Y, Quero F, Blaker JJ, et al (2011) Surface only modification of bacterial cellulose nanofibres with organic acids. Cellulose 18:595–605.

Matsuoka S, Kawamoto H, Saka S (2011) Thermal glycosylation and degradation reactions occurring at the reducing ends of cellulose during low-temperature pyrolysis. Carbohydr Res 346:272–9.

Matsuoka S, Kawamoto H, Saka S (2014) What is active cellulose in pyrolysis? An approach based on reactivity of cellulose reducing end. J Anal Appl Pyrolysis 106:138–146.

Matsuoka S, Kawamoto H, Saka S (2016) Reactivity of cellulose reducing end in pyrolysis as studied by methyl glucoside-impregnation. Carbohydr Res 420:46–50.

Menezes AJ, Siqueira G, Curvelo AAS, Dufresne A (2009) Extrusion and characterization of functionalized cellulose whiskers reinforced polyethylene nanocomposites. Polymer (Guildf) 50:4552–4563.

Nichols PC, Holman RT (1972) Pyrolysis of saturated triglycerides. Lipids 7:773–779.

Pavia D, Lampman G, Kriz G (2001) Introduction to Spectroscopy , 3rd edn. Harcourt, Inc., Orlando, USA

Pine SH (1987) Organic Chemistry, Fifth. McGraw-Hill Book Company, Singapore

Qu T, Guo W, Shen L, et al (2011) Experimental study of biomass pyrolysis based on three major components: hemicellulose, cellulose, and lignin. Ind Eng Chem Res 20:388–393.

Shafizadeh F, Furneaux RH, Cochran TG, et al (1979) Production of levoglucosan and glucose from pyrolysis of cellulosic materials. J Appl Polym Sci 23:3525–3539.

Spinella S, Maiorana A, Qian Q, et al (2016) Concurrent cellulose hydrolysis and esterification to prepare a surface-modified cellulose nanocrystal decorated with carboxylic acid moieties. ACS Sustain Chem Eng 4:1538–1150.

Tingaut P, Zimmermann T, Lopez-Suevos F (2010) Synthesis and characterization of bionanocomposites with tunable properties from poly(lactic acid) and acetylated microfibrillated cellulose. Biomacromolecules 11:454–464.

Tomé LC, Freire MG, Rebelo LPN, et al (2011) Surface hydrophobization of bacterial and vegetable cellulose fibers using ionic liquids as solvent media and catalysts. Green Chem 13:2464.

Uschanov P, Johansson LS, Maunu SL, Laine J (2011) Heterogeneous modification of various celluloses with fatty acids. Cellulose 18:393–404.

Vuoti S, Talja R, Johansson L-S, et al (2013) Solvent impact on esterification and film formation ability of nanofibrillated cellulose. Cellulose 20:2359–2370.

Wang Z (2009) Comprehensive Organic Name Reactions and Reagents. John Wiley & Sons, Hoboken, New Jersey, USA

Xu D, Li B, Tate C, Edgar KJ (2011) Studies on regioselective acylation of cellulose with bulky acid chlorides. Cellulose 18:405–419.

Yu HY, Qin ZY, Sun B, et al (2014) One-pot green fabrication and antibacterial activity of thermally stable corn-like CNC/Ag nanocomposites. J Nanoparticle Res 16:1–12.

Chapter 4

Effect of esterification against thermally-induced depolymerization and discoloration of nanocellulose

4.1. Introduction

The full potential of nanocellulose to reinforce a polymer matrix is not fully realized in the actual composite because a reduction in mechanical properties of nanocellulose occurs during processing. The chemical, mechanical and thermal processes involve during the processing of pulp to produce nanocellulose, as well as during compounding to produce the nanocomposites, result to degradation of cellulose, which reduces its reinforcing potential. One such degradation process is depolymerization, which is the breaking of ß(1→4) glycosidic bonds between the glucose units of cellulose. Depolymerization causes the molecular weight (MW) of cellulose to decrease, and so is the degree of polymerization (DP). A reduction in MW (and DP) is associated with a decrease in mechanical properties. Iwamoto et al. (2007) reported that with an increasing number of passes of pulp through a grinder to produce cellulose nanofibers (CNF), the DP decreased as well as the mechanical properties of the corresponding CNF sheets. Bjurhager et al. (2012) studied the state of degradation of an archaeological oak and found out that the tensile strength of holocellulose showed good correlation with the average MW. Berggren et al. (2002) reported that during the alkaline degradation of pulps to remove lignin, the MW distribution of cellulose changed and a large fraction of high-MW cellulose was connected to high fiber strength. Zou et al. (1994) subjected papers to accelerated ageing and found that the loss in fiber strength of papers was primarily due to depolymerization. Clearly, these studies have shown that reduction in mechanical properties can be attributed to depolymerization.

One of the causes of depolymerization of cellulose is exposure to heat. Because of the poor thermal stability of cellulose, heating causes the cellulose chain to depolymerize. Therefore, in view of improving the thermal stability of nanocellulose, the resistance against thermally-induced depolymerization should be evaluated in order to assess the effect on mechanical properties. Moreover, the resistance against thermally-induced depolymerization is viewed to be a more concrete measure of thermal stability than

weight loss resistance because depolymerization can occur even without substantial weight loss (Broido 1973). Thus in this chapter, the thermal stability of nanocellulose esters were evaluated by studying systematically the change in DP and MW distribution of various types of nanocellulose esters during thermal treatment, both in nitrogen and in air. Apart from the change in DP, the effect of esterification on the rate of discoloration of nanocellulose esters was also presented. So far, the resistance of nanocellulose esters against thermally-induced depolymerization and discoloration in nitrogen and in air has not been reported.

From the different types of esters prepared previously, the acetyl (C2), myristoyl (C14), benzoyl (BNZ), and pivaloyl (PIV) esters were selected. C2 and C14 are short- and long-chain esters, respectively, with α-hydrogens. BNZ and PIV are the simplest aromatic and branched esters, respectively, without α-hydrogens. The choice of esters is based on the findings in Chapter 3 that α-hydrogens in the ester groups affect the mechanism of deprotection and the resistance to weight loss. In this chapter, it is aimed to understand the effect of the structure of the esters on the DP of the residual cellulose after heating. The findings of this study can provide information on how the structure of the esters affect thermally-induced depolymerization and what type of ester can possibly provide a maximum reinforcing effect and still maintain their color even after the action of heat during processing.

4.2. Materials and Methods

4.2.1. Sample preparation

Films were prepared from the esters by hot-pressing. A calculated mass of nanocellulose ester or BC to achieve a film with a weight distribution of about 10 mg/cm^2 was suspended in ethanol. The suspension was then vacuum- filtered in a 0.1 micron membrane filter. The wet mat was sandwiched between two metal plates and hot-pressed under a pressure of 0.5MPa at 110^{o}C for 12 min.

4.2.2. Heat treatment

A film of 2cm x 2cm x 0.15mm was heated in a glass tube oven, Sibata GTO 2000 (Souka, Japan). The oven was pre-heated at a desired temperature (250, 280, and 300^{o}C) and the air inside was replaced with nitrogen using a three-way stopcock attached to a vacuum pump and a nitrogen gas source. The film, placed in an upright position in a glass

vial (22 mm inner diameter), was then inserted quickly into the glass tube oven using the metal stick holder. Replacement of air to nitrogen was repeated again at least three times which took approximately 2 min. After 1 h, the glass vial containing the film was taken out and immediately cooled by blowing nitrogen gas. To ensure that each sample is subjected to similar heating conditions, only one sample placed in nearly the same position as possible inside the glass tube oven was heated at a time. For heating in air condition, the replacement of air with nitrogen was removed from the procedure.

4.2.3. DP determination

The DP of the residual cellulose after thermal treatment was determined by viscometry following the procedure in Chapter 1 and gel permeation chromatography (GPC). Before DP determination, the heat-treated film was alkali-treated to remove the remaining ester groups. To 120-mg heat-treated films in a test tube, 10 mL of ethanol was added and the mixture was stirred until the film was dispersed in the mixture. Then, 10 mL of 0.50M NaOH was added to hydrolyze the ester groups and slightly capped. The mixture was transferred to a water bath pre-heated to 60^{o}C and kept it for 2h. The mixture was kept at room temperature overnight to ensure complete hydrolysis. The mixture was neutralized with 0.50 M HCl, filtered and washed repeatedly with ethanol, and finally with water. The recovered nanocellulose was then freeze dried.

Analysis of DP by GPC followed the procedure reported by Evans et al. (1989) and Bali et al. (2013). The nanocellulose was derivatized to carbamates by tricarbanilation. Prior to tricarbanilation, the freeze dried nanocellulose was dried in vacuum over P_2O_5 at 60^{o}C overnight. A 7.5-mg sample was placed in a reaction flask and capped with rubber cork. Anhydrous pyridine (2 mL) and phenyl isocyanate (0.3 mL) were added and the reaction mixture was kept for 48h at 70^{o}C. Methanol (0.5 mL) was then added to quench the excess phenyl isocyanate and the mixture was cooled. The obtained cellulose tricarbamate was precipitated in 50 mL of 7:3 methanol and water solution and collected by centrifugation at 3500 rpm for 15 min. The precipitate was washed twice with 25 mL of methanol:water mixture (7:3) followed by washing with 25 mL of water three times, and then freeze dried.

To prepare the sample for the GPC analysis, 1 mg of the freeze-dried cellulose tricarbanilate was further vacuum dried over P_2O_5 overnight at 60^{o}C. Then 1 mL of GPC-grade THF was added to solubilize the sample. The solution was filtered using a

disposable syringe filter unit (0.5 μm PTFE) prior the GPC analysis. At least two samples per treatment were analyzed for GPC. The GPC analysis was done using LC-20AT (Shimadzu Scientific Instruments, Kyoto, Japan) liquid chromatograph system equipped with a guard column (Shodex KF-G), a series of analytical columns (KF-804-L and KF-803-L, Shodex, Tokyo Japan), and an SPD-20A UV_{236nm} detector. A volume of 50μL was injected and separation was carried out at a flow rate of 1 mL/min at 40^{o}C with THF as an eluent. A calibration curve was constructed using Supelco polystyrene standards (Sigma Aldrich, St Louis, MO, USA) with narrow molecular weight distributions (MWD). The DP values were obtained by dividing the MW of tricarbanilated cellulose with the MW of tricarbanilated anhydroglucose unit (MW= 519).

4.2.4. Color test

The change in color was measured using a spectrophotometric color difference meter (NF333; Nippon Denshoku Industries Co., Ltd., Tokyo, Japan) equipped with a pen type movable optical sensor with a measurement diameter of 8 mm. The instrument was calibrated with white and black standard plates. CIELAB parameters (L*, a*, b*) were determined using a multicolored LED in reflectance mode at a viewing field angle of 10°. At least 6 measurements at 3 different locations in each side of the film were measured and two films were analyzed per heating treatment. The overall color change (∆E) was determined using the equation $\Delta E = [(\Delta L^*)^2 + (\Delta a^*)^2 + (\Delta b^*)^2]^{1/2}$ where the ∆L*, ∆a*, and ∆b* were the difference between the L*, a*, b*; respectively; of original BC and that of the heat-treated samples.

4.3. Results and Discussion

4.3.1. Thermal treatment and DP_v

The change in DP as affected by heating was first determined using viscometry. This method is relatively easy, fast, convenient, widely used in industrial applications, and can be used for monitoring cellulose degradation during process steps but yielding relative data (Oberlerchner et al. 2015).

Figure 4-1 shows the change in (DP_v) of BC and its esters after heating at various temperatures. The corresponding weight losses are also presented.

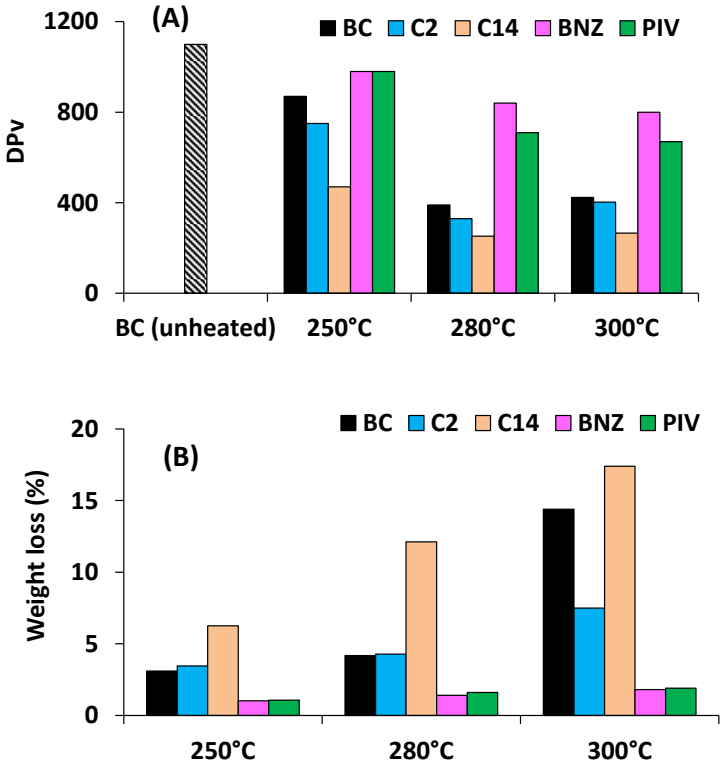

Figure 4-1. Viscosity-average degree of polymerization (DP_v, A) and the corresponding percentage weight losses (B) of BC and its esters after heating at different temperatures for 1h in nitrogen.

With increasing heating temperature, DP_v decreased while the percent weight loss increased. The effect of esterification on DP_v also varied. The C2 and C14 esters gave lower DP_v than BC, with C14 registering the lowest DP_v at all heating temperatures; while the BNZ and PIV esters consistently showed higher resistance against thermal depolymerization than the untreated BC. At 300^{o}C, the DP_v of BNZ and PIV only decreased to 800 and 670, respectively, while BC decreased to 400. The weight losses of BNZ and PIV were also significantly lower than those of the BC, C2 and C14. It should be noted also that at 300^{o}C, the weight losses of BC, C2 and C14 significantly increased but their DP_v values were almost similar to that observed at 280^{o}C and even showed a slight increase. This unusual result can probably be traced from the limitation of viscometry. Accordingly, the Mark-Houwink-Sakurada (MHS) parameters used to calculate MW from intrinsic viscosity are known to vary with small molecules, thereby

leading to errors in viscosity measurement (Oberlerchner et al. 2015). Another limitation of viscometry is the lack of information about MWD. If the MWD is too wide, the contribution of fewer cellulose chains that are either too long or too short cannot be resolved from viscosity measurement. If the MWD is known, the mechanism of fragmentation of cellulose chains can be further understood. To resolve these issues and also to confirm the resistance against depolymerization exhibited by BNZ and PIV, another technique of MW determination was used.

4.3.2. Thermal treatment and the change in MWD

To obtain MWD, separation of cellulose chains is required and this was achieved by size exclusion chromatography or more often referred to as gel permeation chromatography (GPC). From the MWD curve, various types of average MW can be obtained. Two of these are the M_w or the weight-average MW and the M_n or the number-average MW. The respective DP values obtained from these two types of MW are the DP_w and DP_n, respectively. The ratio of M_w to M_n (or DP_w to DPn) gives the measure of dispersity of the distribution and is given the notation polydispersity index (PDI).

Figure 4-2 shows the MWD of the carbamate derivatives of BC recovered from their corresponding esters after heat-treatment at various temperatures. For comparison, the MWD of original, unheated BC is superimposed and the values of DP_w, DPn and PDI are also presented. The MWD of unheated BC shows a large proportion of high MW cellulose chains. Heating caused these high MW chains to depolymerize as shown by the shifting of the MWD curves of heat-treated BC and its esters to low MW region with increasing temperature.

The MWD curves of untreated BC shows its susceptibility towards depolymerization. At 250°C, the MWD curve still showed a unimodal distribution but showed narrower peak and wider base, an indication of a decrease in high-MW chains and an increase in low-MW chains. This distribution was confirmed by the decrease in the DP_w and DP_n by 24% and 59% , respectively; and an increase in the PDI by 85%. At 280°C, the MWD curve showed shouldering at the low-MW region. The DP_w was almost the same as to heating at 250°C but the DP_n decreased dramatically by 79% which resulted in a very high PDI value of 11. This result suggests that when cellulose undergoes chain scission to produce low-MW fragments, the low-MW fragments are probably more susceptible to depolymerization and produces even shorter cellulose

chains with continuous heating. Contrary to the result obtained from viscometry, a drastic decrease in DP was observed at 300°C. The peak of the MWD curve completely moved to low MW-region resulting to a DP_w of 491 and a DP_n of 71. The PDI (about 7) was lower than that recorded at 280°C; an indication that the high-MW cellulose chains have also been fragmented thus narrowing the dispersity.

The effect of esterification on the MWD after thermal treatment varied. C2 and C14 esters which have α-hydrogens displayed different thermal behavior. Esterification with C14 seemed to speed up chain scission causing the MWD of C14 to shift drastically to the low-MW region just by heating at 250^{o}C. The DP_w and DP_n of C14 were also lower than those of the unmodified BC. The large decrease in the MW of C14 is probably due to the formation of carboxylic acids when heated. Although, deprotection of C14 at lower temperature primarily released symmetrical ketones, with further heating these ketones probably degrade into free carboxylic acids which initiate acid-catalyzed chain scission. The catalytic effect of free carboxylic acids is probably more pronounced in C14 than in C2 because of the low volatility of long chain fatty acids, myristic acid in the case of C14. For C2 esters, the acetic acid produced is volatile enough to be easily released from the fibers, and thus inhibiting acid-catalyzed chain scission.

Acid-catalyzed depolymerization of cellulose was reported by Yang, Wei, & Lickfield, (2000), who investigated the change in MW and mechanical strength of cotton fabric impregnated with various types of polycarboxylic acids. It was found that the decrease in mechanical strength of the cotton fabric was attributed to acid-catalyzed depolymerization, which increased with increasing ionization constant of the acid. Although not using cellulose but cellobiose as a model compound, the study of Kayser et al., (2013) also demonstrated the acid-catalyzed scission of glycosidic bonds in cellobiose by the action of various mineral, mono- and dicarboxylic acids.

Even though previous reports confirmed that depolymerization can be catalyzed by carboxylic acids, the hypothesis that the difference in the volatility between acetic and myristic acid had caused the difference in their effect on the extent of depolymerization during heat treatment is still not validated. To confirm this hypothesis, BC films were impregnated with acetic acid or myristic acid by soaking the films in 1M ethanolic solution of each acid for 6 hours, patting dry the excess solution with lint free tissue, and drying overnight at 40^{o}C. The acid-impregnated BC films and untreated BC were then subjected to a heat-treatment in air at 250^{o}C for 1.5h, redispersed in ethanol and washed

to remove any excess acids, dried and analyzed for its DP_v. From a DP_v of 1100, the DP_v of untreated BC, acetic acid- and myristic acid-impregnated BC decreased to 400, 380, and 270, respectively, after heat-treatment. Although the extensive depolymerization could mostly be due to heat treatment, a clear difference between the DP_v of acetic acid- and myristic acid-impregnated BC was still observed. The extent of depolymerization of myristic acid-impregnated BC was higher than that of the acetic-acid impregnated BC, which is possibly due to the difference in the boiling points of the two acids. Acetic acid which boils at 118^{o}C must have volatilized easily during heat treatment at 250^{o}C, while myristic acid which boils at 250^{o}C must have been retained more in the fibers and with continued heating, had caused more degradation than acetic acid did. This same rationale is possibly the reason why the extent of depolymerization of C14 ester was higher than that of C2 ester and of the untreated BC. The findings also suggest that the nature of the by-products of thermal degradation, such as volatility, can also affect the rate of thermally-induced depolymerization.

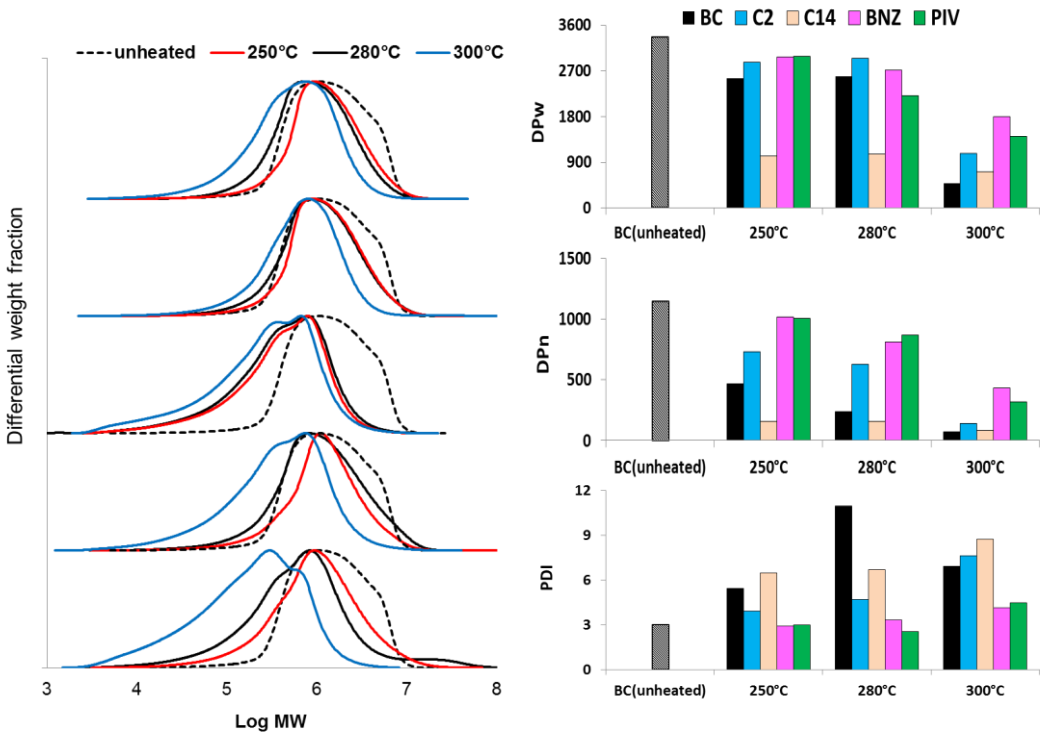

Figure 4-2. Differential MWD of the carbamate derivatives of BC and its esters after heating at various temperatures for 1h and the values of DPw, DPn, and polydispersity index (PDI) expressed to non-derivatized cellulose.

While C14 showed poor resistance, BNZ and PIV esters consistently exhibited improved resistance against thermally-induced depolymerization similar with the result from viscometry. These esters gave higher DP_w and lower PDI than BC, C2, and C14. This result suggests that even after heating, BNZ and PIV esters have a more uniform distribution of high-MW cellulose chains than those of BC, C2, and C14. It can be recalled that BNZ and PIV esters showed improved thermal stability attributed to the absence of α-hydrogens which possibly drive the removal of ester groups by Dieckmann condensation. Interestingly, these esters also showed higher resistance against depolymerization than C2 and C14 esters. It seemed to show that thermally-induced depolymerization is also influenced by the stability of the ester groups.

The inhibition of depolymerization because of the esterified surface hydroxyl groups can be attributed to the prevention of hydrogen-bond rearrangement on the surface molecules of cellulose crystallite. Matsuoka, Kawamoto, & Saka, (2014) proposed that the breaking of the C3–OH···O5 hydrogen bond, along with proton donation to C1–O through hydrogen-bond rearrangement or hydrogen bonding with other molecules were proposed to be important in promoting depolymerization during pyrolysis. Considering that hydrogen-bond rearrangement on the surface of cellulose molecules, indeed, play a role in the depolymerization of cellulose, esterification of the surface hydroxyl groups must have prevented the formation of hydrogen bonds, and the more difficult to remove the ester group is, the lesser the chance of hydrogen-bond rearrangement.

4.3.3. Thermal treatment and discoloration

When cellulose is subjected to heat, the most prominent change visible to the eyes is discoloration. Figure 4-3 shows the heat-treated films after 1 h in nitrogen at different heating temperatures. By visual inspection, no significant change in color was observed up to 280 ^{o}C for BC and the esters of PIV and BNZ while slight yellowing was observed for C2 and C14. At 300 ^{o}C, the unmodified BC clearly showed a higher degree of discoloration than any of the BC esters, with the BNZ and PIV displaying the highest resistance against thermal discoloration.

Quantitatively, the observed color changes can be expressed as CIELAB parameters L*, a* and b*. L* is a measure of lightness in the scale of 0 to 100. A decrease in L* denotes darkening of a material. The a* and b* parameters are the color coordinates (+a* for red; -a* for green, +b* for yellow and –b* for blue) under any testing condition. From

these CIELAB parameters, the overall color change, ∆E, can be calculated. The higher the value of ∆E, the higher is the degree of deviation from the original color. In this paper, ∆E values were calculated in reference to the untreated BC before heat treatment. The CIELAB parameters and ∆E values of the films after heat treatment are shown in Figure 4-3. The values of a* and b* increased with increasing temperature, an indication of increasing degree of redness and yellowness of the films, respectively. The L* values decreased with increasing temperature, with the lowest value measured in untreated BC. C2 and C14 esters gave lower L* than BNZ and PIV esters, which even up to 300^{o}C recorded L* values of about 90. From the values of ∆E, the overall resistance against discoloration is clearly exhibited by the BNZ and PIV esters. It can be recalled that BNZ and PIV ester bonds were found to be more stable than C2 and C14 ester bonds because of the absence of acidic alpha hydrogen. It appears that the stability of the ester bonds affects not only weight loss resistance but also the mechanism of thermal discoloration.

The high resistance of BNZ and PIV against thermal discoloration can be due to their resistance against depolymerization, which inhibits the formation of REs. Discoloration of cellulose has been reported to be due to the formation of chromophores which require “reactive spots” for degradation and condensation reactions(Rosenau et al. 2014). These “reactive spots” can only be carbonyl groups and in pure cellulose like BC, the carbonyl groups exist in their masked hemiacetal form at the REs. Similarly, a previous study of Matsuoka, Kawamoto, & Saka, (2011) revealed that REs are active sites for thermal discoloration in cellulose. Thus, if depolymerization is inhibited, the formation of REs which can be active sites for thermal discoloration is also suppressed.

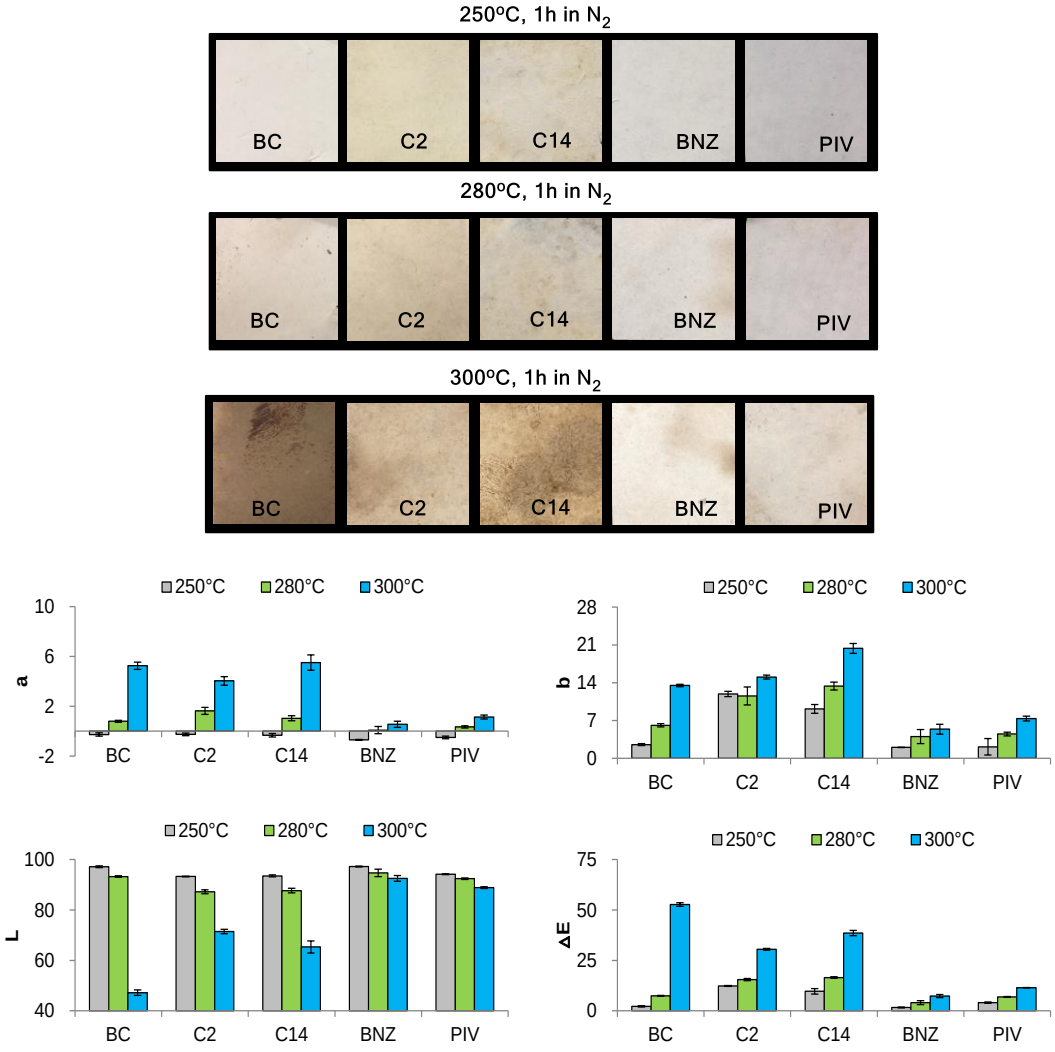

Figure 4-3. Color changes of BC and its esters after heating at different temperatures for 1h in nitrogen and their respective CIELAB parameters and the overall change in color (ΔE).

4.3.4. Thermal degradation in air

Investigation of thermal stability in air is important because in actual application compounding is done in air and not in an inert atmosphere. Figure 4-4 shows the comparison of the MWD of BC and its esters heated in air and in nitrogen at 250^{o}C. The rate of degradation in air is higher than that in nitrogen. Oxidative reactions are reported to be responsible for accelerated rates of weight loss and depolymerization of cellulose in air at temperatures below 300^{o}C (Shafizadeh and Bradbury 1979). It was proposed that oxygen initiates the abstraction of hydrogen from cellulose molecules with the formation of hydrogen peroxy radicals during the early stage of thermal degradation in air (Mamleev et al. 2007).

Despite the increase in the rate of depolymerization in air, BNZ and PIV still gave higher resistance than BC, C2 and C14. The degradation of C14 was in fact very drastic resulting to very low DP_w and DP_n values. The MWD curve of C14 also showed a bimodal distribution with a small peak at low-MW region. The rate of depolymerization of C2 in air was also higher than BNZ and PIV. Although the DP_w of C2 was not very far from that of BNZ and PIV, it was the DP_n that displayed a clear difference from the BNZ and PIV. The DP_n of C2 in air was 66% and 58% lower than the DP_n of BNZ and PIV, respectively. The large decrease in the DP_n of C2 resulted to wide dispersity with a PDI of 7.9. The higher resistance against depolymerization displayed by BNZ and PIV esters than those of C2 and C14 in air suggests that thermal degradation of nanocellulose esters in air is still possibly influenced by the presence of α- hydrogens in the structure of the ester groups.

A previous report on the thermal-oxidative degradation of ^{14}C-labeled cellulose revealed that oxidative products such as CO_2, CO, formic acid and formaldehyde were found to originate mainly from the pyran ring due to the rupture of C1–C2 bond (Kozmina et al. 1963) and not from the acetyl groups. The acetyl groups were in fact stable against oxidation. From their findings it is possible that during thermal degradation of cellulose esters in air, depolymerization most likely depends on the stability of the pyran ring which is influenced by the type of ester groups attached to it. The high resistance displayed by BNZ and PIV against thermally-induced depolymerization both in air and nitrogen suggests that BNZ and PIV may have a higher stabilizing effect on the pyran ring than that of C2 and C14; but the mechanism still needs to be resolved.

Overall, the stability of BC esters towards thermally-induced depolymerization increased in the order of C14<C2<PIV<BNZ. The trend is the same whether heating is done in air or nitrogen, or the DP determination is done by viscometry or GPC. The absolute DP values, however, were significantly different. The calculated DP_v values were significantly lower than DP_w. Although it was commonly assumed that M_v is approximate of M_w, and thus $DP_v \approx DP_w$, our results showed otherwise. M_v and M_w can differ significantly depending on the Mark-Houwink-Sakurada parameters used and on the MWD of the sample (Evans and Wallis 1989). Nevertheless, the results suggest that for rapid monitoring of the change in MW during cellulose degradation, viscometry can be used in cellulosic samples with low MWD to give relative data.

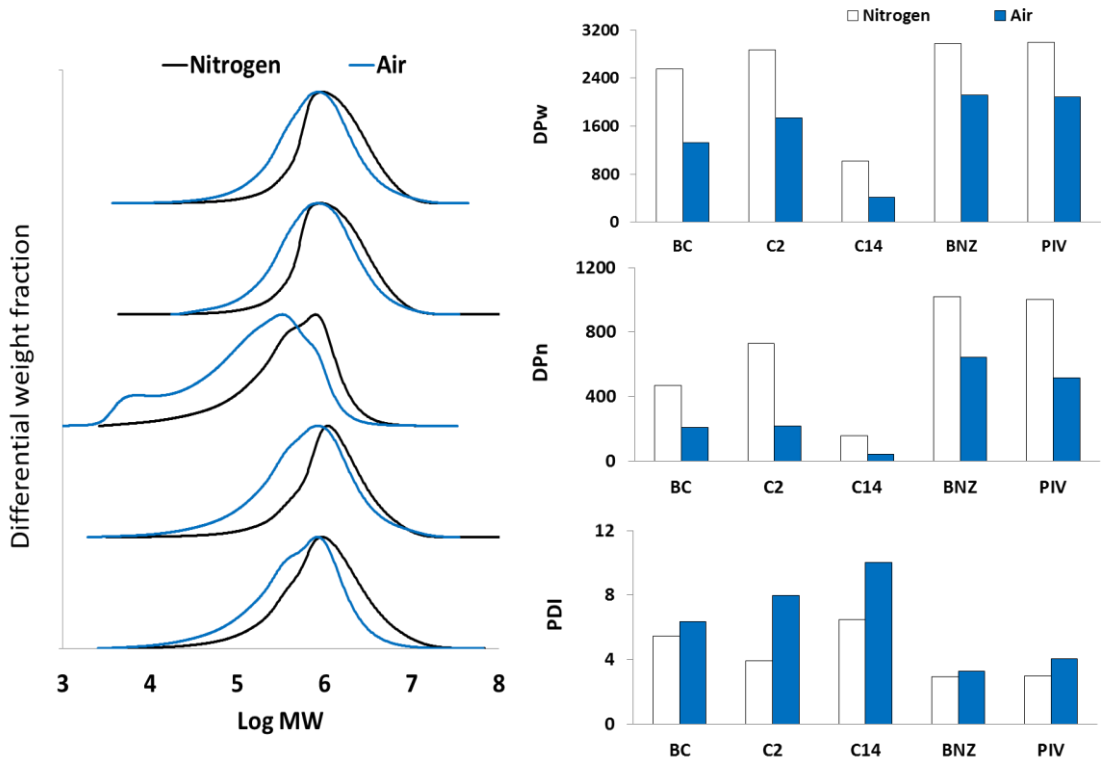

Figure 4-4. Differential MWD of the carbamate derivatives of BC and their esters after heating in nitrogen and air at 250^{o}C for 1h, and the values of DPw, DPn and PDI expressed to non-derivatized cellulose.

The change in color of BC and its esters after heating in air is shown in Figure 4-5. The values of ΔE in comparison to those heated in nitrogen are also presented. Similar to the change in MW, discoloration was also more enhanced in air than in nitrogen. Higher ΔE was observed in air than in nitrogen at any heating temperature. The higher discoloration observed in air can be attributed to the increased rate of depolymerization in air. Moreover, oxidative reactions may also produce different types of chromophores and thus speeds up discoloration. Oxygen was reported to intensively react to the products of thermal depolymerization of cellulose (Mamleev et al. 2007) which may produce chromophores as by-products. Nevertheless, the BNZ and PIV esters still showed higher resistance against thermal discoloration both in air and nitrogen than the untreated BC, C2 and C14.

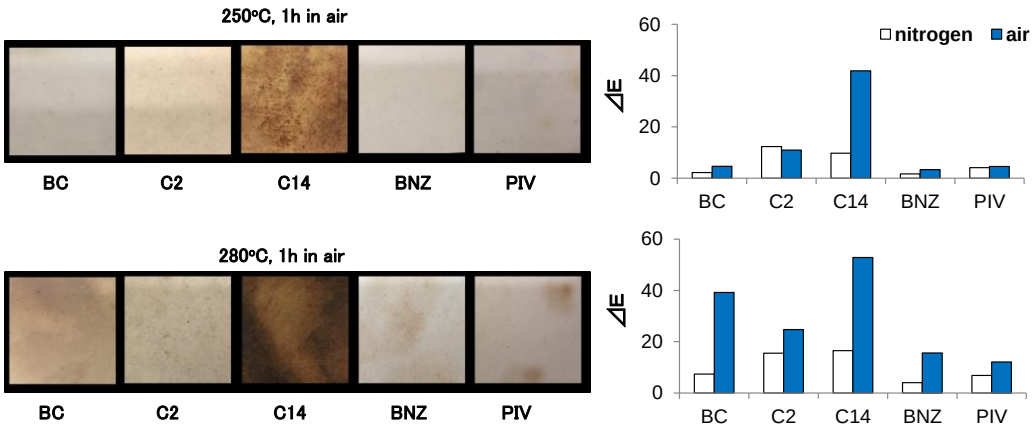

Figure 4-5. Heat-treated films of BC and its esters in air and comparison of the overall change in color (△E) of films heated in air and in nitrogen.

4.4. Summary

Esterification alters the rate of thermally-induced depolymerization of nanocellulose. An increase or decrease in the rate of depolymerization depends on the structure of the ester groups. BNZ and PIV esters without α-hydrogens showed higher resistance against depolymerization than C2 and C14 esters with α-hydrogens. The effect of α-hydrogen on the rate of depolymerization can be traced from its role in the mechanism of ester removal. The resistance of BNZ and PIV esters against depolymerization was also complemented by its resistance against discoloration. The delay of depolymerization translates to the inhibition of the formation of REs which can be active sites for thermal discoloration. The similar thermal behavior of nanocellulose esters in air and in nitrogen suggests that α-hydrogens do play a role in the mechanism of thermal degradation in air. The superior stability displayed by BNZ and PIV against depolymerization and discoloration both in air and nitrogen suggests that these two esters have the potential to sustain high mechanical properties yet maintain their colors despite being subjected to heat during processing. The apparent high M_w coupled with low PDI make it a good candidate as reinforcing filler of high thermal stability.

4.5. REFERENCES

Bali G, Foston MB, O'Neill HM, et al (2013) The effect of deuteration on the structure of bacterial cellulose. Carbohydr Res 374:82–88.

Berggren R, Molin U, Berthold F, et al (2002) Alkaline degradation of birch and spruce: Influence of degradation conditions on molecular mass distributions and fibre strength. Carbohydr Polym 51:255–264.

Bjurhager I, Halonen H, Lindfors EL, et al (2012) State of degradation in archeological oak from the 17th century vasa ship: Substantial strength loss correlates with reduction in (holo)cellulose molecular weight. Biomacromolecules 13:2521–2527.

Broido A (1973) Molecular weight decrease in the early pyrolysis of crystalline and amorphous cellulose. J Appl Polym Sci 17:3627–3635.

Evans R, Wallis AFA (1989) Cellulose molecular weights determined by viscometry. J Appl Polym Sci 37:2331–2340.

Evans R, Wearne RH, Wallis AFA (1989) Molecular weight distribution of cellulose as its tricarbanilate by high performance size exclusion chromatography. J Appl Polym Sci 37:3291–3303.

Iwamoto S, Nakagaito AN, Yano H (2007) Nano-fibrillation of pulp fibers for the processing of transparent nanocomposites. Appl Phys A 89:461–466.

Kayser H, Rodriguez-Ropero F, Leitner W, et al (2013) Mechanistic comparison of saccharide depolymerization catalyzed by dicarboxylic acids and glycosidases. RSC Adv 3:9273–9278.

Kozmina OP, Khripunov AK, Kurlyankina VI (1963) The mechanism of the oxidation of cellulose esters with oxygen--XIX. The oxidation of acetyl cellulose labelled with radioactive carbon in the acetyl groups and in the pyran ring. Polym Sci USSR 5:1232–1234.

Mamleev V, Bourbigot S, Yvon J (2007) Kinetic analysis of the thermal decomposition of cellulose: The main step of mass loss. J Anal Appl Pyrolysis 80:151–165.

Matsuoka S, Kawamoto H, Saka S (2014) What is active cellulose in pyrolysis? An approach based on reactivity of cellulose reducing end. J Anal Appl Pyrolysis 106:138–146.

Matsuoka S, Kawamoto H, Saka S (2011) Reducing end-group of cellulose as a reactive site for thermal discoloration. Polym Degrad Stab 96:1242–1247.

Oberlerchner JT, Rosenau T, Potthast A (2015) Overview of methods for the direct molar mass determination of cellulose. Molecules 20:10313–10341.

Rosenau T, Potthast A, Krainz K, et al (2014) Chromophores in cellulosics, XI: Isolation and identification of residual chromophores from bacterial cellulose. Cellulose 21:2271–2283.

Shafizadeh F, Bradbury .A. G. W. (1979) Thermal degradation of cellulose in air and nitrogen at low temperatures. J Appl Polym Sci 23:1431–1442.

Yang CQ, Wei W, Lickfield GC (2000) Strength of Durable Press Finished Cotton Fabric. 910–915.

Zou X, Gurnagul N, Uesaka T, Bouchard J (1994) Accelerated aging of papers of pure cellulose: mechanism of cellulose degradation and paper embrittlement. Polym Degrad Stab 43:393–402.

Chapter 5

Wood-based cellulose esters and their thermal stability

5.1. Introduction

The cellulose use for industrial applications is derived mainly from plants, and mostly from woods. Even though wood cellulose has the same chemical structure as BC, they have different structural organization and properties. Wood cellulose exhibits lower mechanical properties, crystallinity and water holding capacity than BC (Martínez-Sanz et al. 2011). Nevertheless, wood still remains as the most viable source of nanocellulose, because wood is cheaper and more abundant than BC or any other sources of cellulose.

Another distinct difference between wood cellulose and BC is their purity. While BC is essentially pure cellulose; wood-based cellulose is always associated with other biopolymers. In the plant cell walls, cellulose is always surrounded by hemicellulose and lignin, which both acts like a polymer matrix, forming a natural composite. Hemicellulose is a heterogeneous polysaccharide representing about 20-30% of the weight of dry wood and the composition and distribution varies with the type of woods (Sjöström 1993). Softwoods comprise about 20% galactoglucomannans and 5-10% arabinoglucurunoxylan while hardwoods contain mainly glucurunoxylan, which covers 15-30% of the weight of dry wood (Sjöström 1993). Lignin is a heterogeneous, highly complex polymer consisting of various phenylpropane units (Yokoi et al. 1999).

Isolating cellulose in the form of pulp from wood requires a combination of mechanical and chemical treatments. Kraft pulping, which cooks the wood chips in a hot solution of NaOH and Na_2S in a pressurized vessel, is the most commonly used process in producing pulps from wood. Kraft pulping depolymerizes lignin and partially hydrolyzes and solubilizes the hemicellulose (Hubbe et al. 2008). Because the pulp fibers produced still contains fairly large amount of hemicellulose and lignin, kraft pulping is often followed by acidic bleaching to further remove the lignin (Sjöholm 2004). The bleached kraft pulp, however, still contains hemicellulose and this residual hemicellulose can affect the properties of the bleached kraft pulps, and the subsequent nanocellulose produced from them.

One of the properties affected by the existence of hemicellulose in pulps is thermal stability. Hemicellulose, which is completely amorphous and has a lower DP (100-200) (Sjöholm 2004) has a lower thermal stability than cellulose. Yang et al. (2007) reported the pyrolysis behavior of biomass components and reported that hemicellulose decomposition ranged from 220-315^{o}C while that of cellulose was 315-400^{o}C. Werner et al. (2014) studied the thermal decomposition of various commercially available hemicelluloses and compared it to microcrystalline cellulose (MCC) and reported that MCC is the most thermally stable among the polysaccharides. The thermal stability of hemicelluloses also varied, xylan being the least thermally stable and glucan-based hemicellulose to be the most stable among the hemicelluloses. Pulp fibers containing hemicelluloses and lignin have also been shown to exhibit lower thermal stability than fibers that were subjected to chemical treatments to remove lignin and hemicelluloses (Alemdar and Sain 2008; Jonoobi et al. 2009; Barreto et al. 2011). Even after acetylation of bleached kraft pulps, the 10% and 50% weight loss temperature was also found to decrease with increasing xylan content (Peredo et al. 2015).

It is apparent from previous reports that the poor thermal stability of hemicellulose can contribute a destabilizing effect on the thermal properties of pulps. Thus, thermal stabilization of wood-based cellulosic pulps and nanocelluloses must also consider the effect of hemicellulose. In this chapter the effect of esterification on the thermal stability of Nadelholz bleached kraft pulps (NBKP) and wood cellulose nanofibers (WCNF) derived from NBKP was investigated in order to understand the role of hemicellulose in thermal stabilization. Because hemicellulose is also a polysaccharide with abundant hydroxyl groups that can be substituted with ester groups, it is viewed that complete esterification of hemicellulose can contribute a significant improvement in thermal stability.

5.2. Materials and Methods

5.2.1. Preparation of WCNF

NBKP with 14% hemicellulose was used as a raw material for the preparation of WCNF. Fibrillation was done by passing 1% aqueous suspension of NBKP four times through a grinder (MKCA6-3; Masuko Sangyo Co., Saitama, Japan) at 1,500 rpm. The first and second passes were performed with a clearance gauge of -0.5 and -1.0,

respectively; while the last two passes was set at -2.5, from the zero position.

5.2.2. Esterification

The esterification of NBKP and WCNF followed the procedure given in Chapter 3. Similar with Chapter 4, only the esters of C2, C14, BNZ and PIV were selected for further investigation. Table 5-1 gives the esterification conditions of the various esters prepared. To obtain samples with different DS, samples were collected at different time intervals during esterification.

Table 5- 1. Esterification conditions for NBKP and WCNF.

Sample	**AcCl:OH ratio***	**Pyr: AcCl ratio****	**T*** (°C)**
C2-NBKP	2	2	60
C14-NBKP	2	3	60
BNZ-NBKP	4	3	60
PIV-NBKP	5	5	70
BNZ-WCNF	2	2	50

* acyl chloride to hydroxyl molar ratio **pyridine to acyl chloride molar ratio *** temperature

5.2.3. Characterization

Films of untreated and esterified NBKP or WCNF were prepared by hot-pressing. Characterization of their morphology, DP, and thermal stability followed the procedure given in previous chapters.

5.3. Results and Discussion

5.3.1. Morphology, crystallinity and reactivity of NBKP and WCNF

The morphology of NBKP and WCNF is shown in Figure 5-1. The mechanical disintegration of NBKP fibers, which initially have an average width of about 25 μm, resulted to thin nanofibers with an average width of about 20 nm. The DP_v also decreased from 900 to 700 after fibrillation.

The x-ray diffractograms of NBKP and WCNF as shown in Figure 5-1 display a typical pattern for cellulose I. The overlapping peaks at 2θ = 14.2° and 16.6° were assigned the Miller indices of (100) and (010); respectively, while the prominent peak at 2θ = 22.4° was assigned the Miller index of (110). The crystallinity index of NBKP was 85.7, which decreased to 76.4 after grinding.

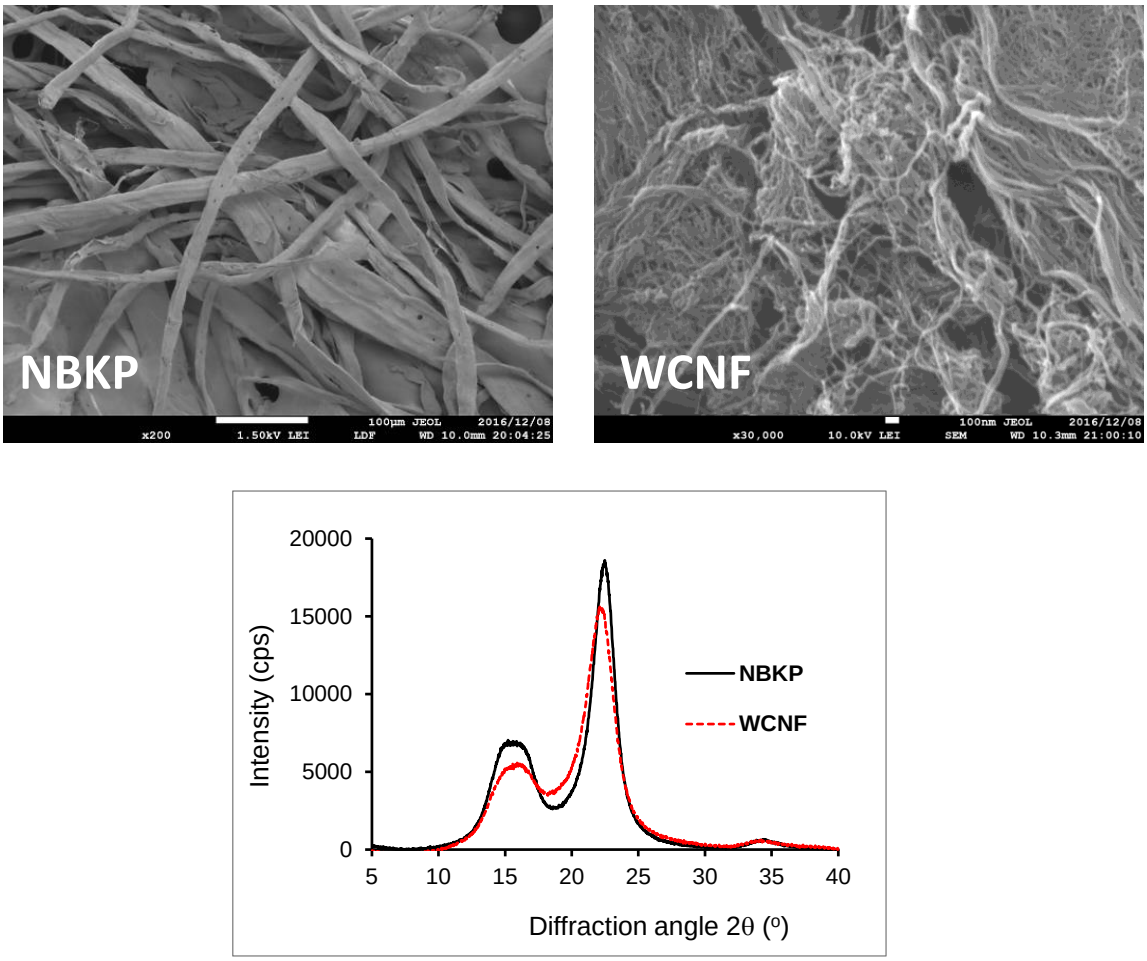

Figure 5-1. FESEM images at 30,000 times magnification and x-ray diffractograms of NBKP and WCNF before esterification. Scale bars represent 1µm and 100 nm for NBKP and WCNF, respectively.

Figure 5-2 shows the change in DS during the time-series esterification of NBKP. pivaloylation gave the slowest rate despite having the highest concentration of acyl chloride and pyridine. At 10-hr reaction time, the DS reached only 0.40. Extending the reaction time up to 30 h increased the DS to about 0.6. Even though WCNF had lower

concentration of acylating agent and reaction temperature than NBKP, the progree of reaction of WCNF was almost similar to that of the NBKP; an indication of increased reactivity after fibrillation. The increase in surface area and amorphous content after fibrillation must have contributed to the increase in reactive hydroxyl groups of WCNF, thereby increasing its reactivity.

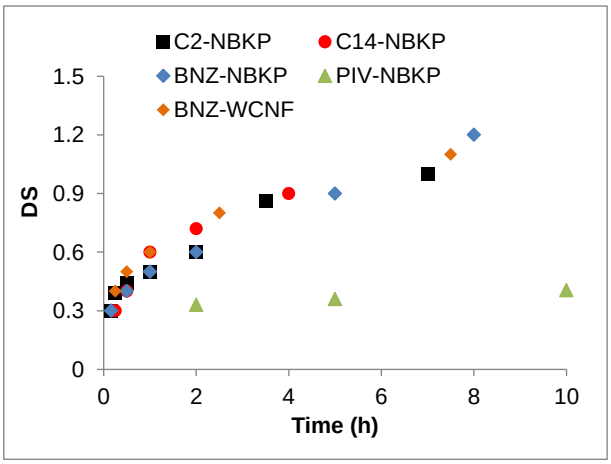

Figure 5-2. Change in DS of NBKP and WCNF with time during esterification.

5.3.2. Thermal stability of NBKP esters

Based on the hemicellulose content of NBKP, which is about 14% and the assumption that the percentage distribution of galactoglucomannan and arabinoglucuronoxylan in softwoods are 20% and 10%, respectively; the theoretical DS to fully esterify the hemicellulose was calculated to be about 0.4. From this calculation, the NBKP esters with a DS of 0.3, 0.6, and 0.9 were selected for thermal analysis.

Figure 5-3 shows the dynamic heating curves, the temperature at 1% and 5% weight loss, and T_{max} values of NBKP and its esters with different DS. Similar with BC, esterification did not change the single-step degradation of NBKP. Regardless of the DS values and the type of esters, thermal stability of NBKP improved after esterification. T_{max} increased but the structure of the esters as well as the DS showed no varying effect on T_{max}, which was also observed in BC. The onset of degradation, however, is influenced by the type of ester and the DS value. In general, the 1% WLT did not show improvement after esterification at DS 0.3, and even decreased with increasing DS for C14. At DS 0.6, the BNZ and PIV esters displayed 25^{o}C increase in 1% WLT and the values were higher than those of C2 and C14. The low degree of improvement at DS 0.3 indicates that

esterification of hemicellulose and amorphous cellulose was still incomplete. At DS 0.6, apart from esterifying the hemicellulose, the extent of esterification must have also covered the amorphous part of the cellulose; thus a significant increase in the onset temperature was observed. At DS 0.9, the onset of degradation temperature decreased, which suggests the possibility of esterifying the crystalline core at this DS value.

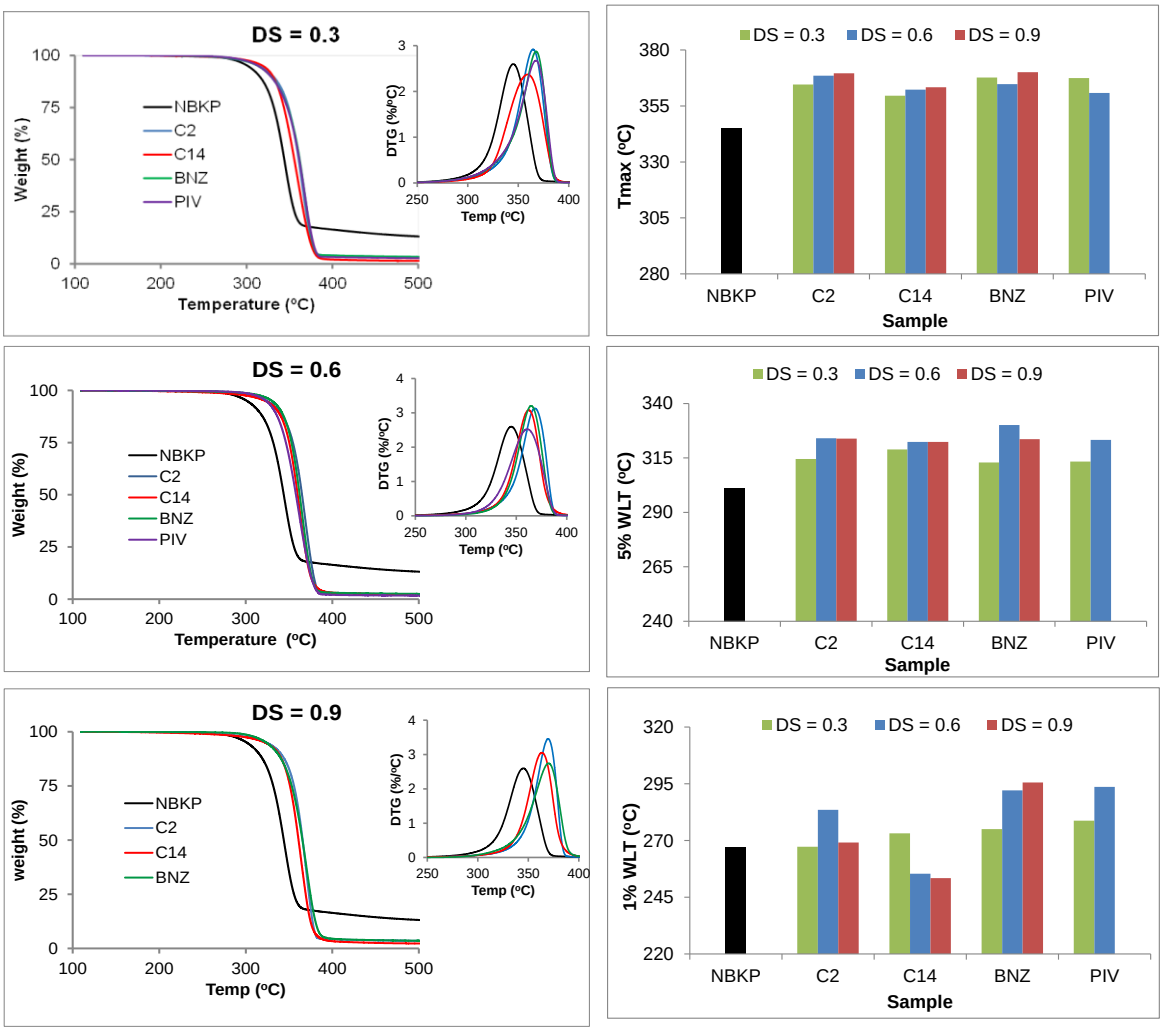

Figure 5-3. Dynamic heating curves, T_{max}, and 5% and 1% weight loss temperature of NBKP esters with different degree of substitution (DS) values.

The effect of DS and the structure of the ester were also observed in the results of isothermal heating presented in Figure 5-1. Esterification improved the weight loss resistance of NBKP, which registered higher TWL and 1% weight loss time ($t_{1\%}$) than NBKP esters. At DS 0.3, the structure of the esters did not show varying effect; the TWL

only decreased by 5.8% and the $t_{1\%}$ was only extended by 14%. At DS 0.6 and 0.9, the effect of structure of the ester is very pronounced. BNZ and PIV both showed higher weight loss resistance than C2 and C14. This result is in agreement with the findings in Chapter 3 wherein esters having α-hydrogens showed lower weight-loss resistance than esters without α-hydrogens. Furthermore, a significant improvement in weight loss resistance was observed relative to a DS of 0.3. At DS 0.6, the TWL of BNZ and PIV decreased by 57% and $t_{1\%}$ was extended 2.1 times longer than the untreated NBKP. This result suggests the importance of completely esterifying the hemicellulose and the amorphous cellulose. Extensive esterification, however, resulted to a decrease in weight loss resistance. At DS 0.9, C2 and C14 esters showed an increase in TWL relative to DS 0.6. In fact, C14 even recorded higher TWL than the untreated NBKP.

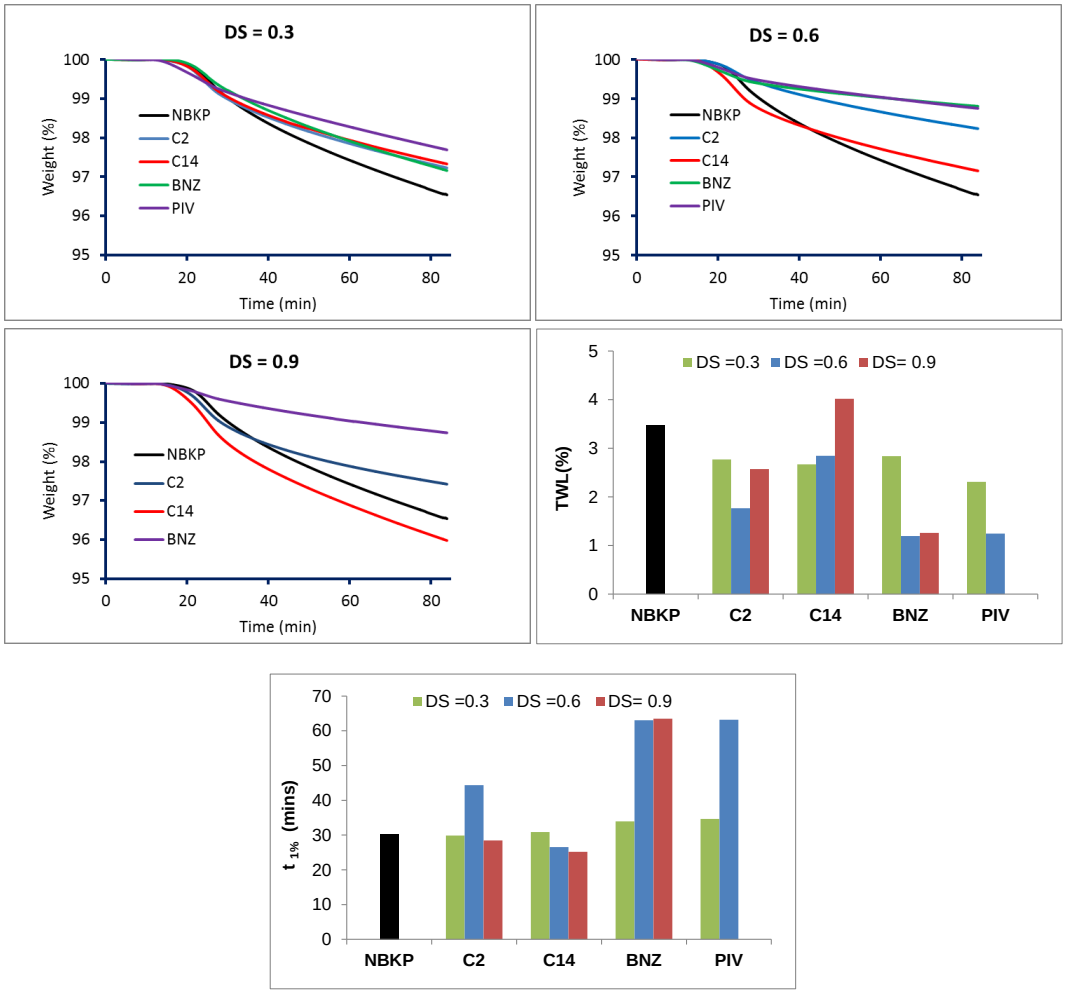

Figure 5-1. Isothermal heating curves, total weight loss, and 1% weight loss time of NBKP and its esters with different degree of substitution (DS).

5.3.3. Thermal stability of benzoylated WCNF

Because of higher reaction rate of benzoylation over pivaloylation, benzoylation was chosen for further investigation on its effect on WCNF. The TG curves of benzoylated WCNF at various DS are shown in Figure 5-5. Benzoylation improved the thermal stability of WCNF but the DS did not show any significant effect. The 1% WLT, 5% WLT, and T_{max} were higher than untreated WCNF on average by 24°C, 20°C and 25°C; respectively. Similarly, the weight loss resistance also improved after benzoylation and was not affected by varying the DS. Considering that the event occurring at the initial stage of thermal weight loss is the removal of the benzoyl group as observed in Chapter 3, the findings suggest that the number of benzoyl esters being removed seems to be not dependent on the number of benzoyl groups attached to the cellulose chains.

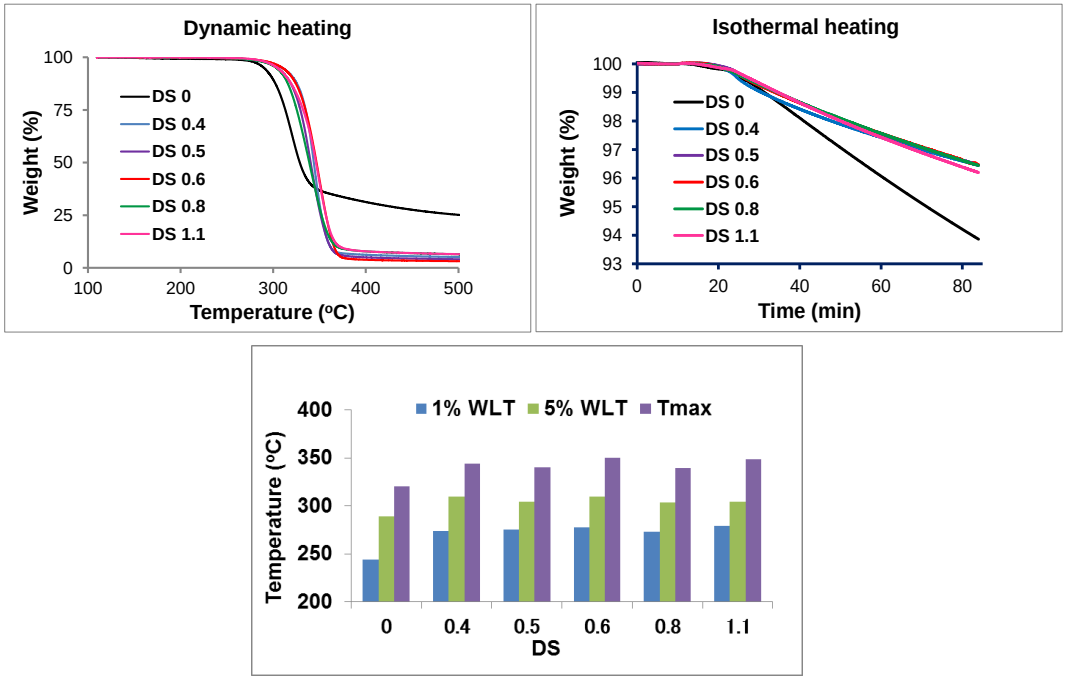

Figure 5-5. TG curves and data of WCNF and its benzoyl esters with different degree of substitution (DS) values.

Apart from improvement in weight-loss resistance, benzoylation also improved the resistance against thermally-induced discoloration. The residue after isothermal TGA as shown in Figure 5-6 clearly differentiates the color of untreated WCNF film from benzoylated films. The presence of hemicellulose and the mechanical fibrillation which increased the number of REs most likely contribute to the poor discoloration resistance of

untreated WCNF. Although not in the form of pulps, Adorjan et al. (2005) reported that hemicellulose contributed to the formation of chromophores (color-bearing compounds) in cellulose dissolved in N-methylmorpholine-N-oxide monohydrate because of the higher rates of pentoses to form chromophores than hexoses. Moreover, the same report also confirmed that protection of the REs by glycosylation inhibits the formation of chromophores. Thus, the resistance of benzoylated WCNF can probably be attributed to the possible benzoylation of the REs of hemicellulose and amorphous cellulose.

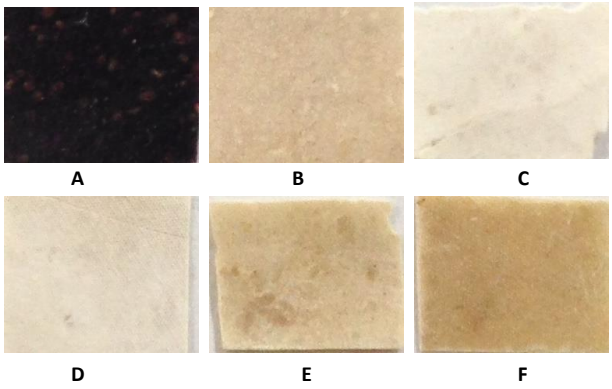

Figure 5-6. The residue of untreated WCNF (a) and benzoylated WCNF with a DS of 0.4 (b), 0.5 (c), 0.6 (d), 0.8 (e) and 1.1 (f) after isothermal TGA at 250^{o}C for 1h in nitrogen.

To determine the resistance against thermally-induced depolymerization, WCNF and benzoylated WCNF at DS 0.6 were subjected to thermal treatment. Because the residue of WCNF at 1-hour heating in nitrogen at 250^{o}C was significantly discolored (Figure 5-6) the thermal treatment was limited to 0.5 h only but done in air in order to simulate the atmospheric condition used in industries when processing composites. As shown in Figure 5-7, benzoylated WCNF showed improved resistance against thermally-induced depolymerization similar to the result of benzoylated BC in Chapter 4. The MWD curve of untreated BC shifts to the low-molecular weight region more than that of the benzoylated WCNF after thermal treatment. The DPw of benzoylated WCNF (4400) is much higher than that of the WCNF (1300), an indication of possible depolymerization of long-chain cellulose in WCNF during thermal treatment. The thermal resistance against discoloration is further confirmed after thermal treatment in air. The discoloration of WCNF films in air is more apparent than that of the benzoylated WCNF.

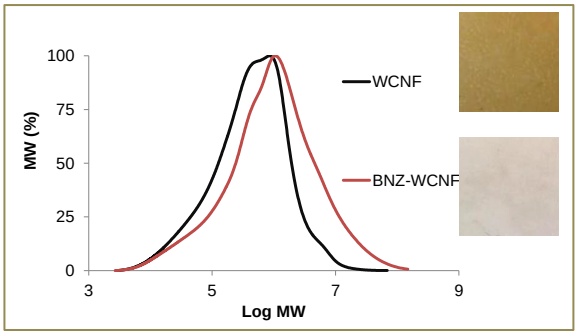

Figure 5-7. Molecular weight distribution curves of WCNF and benzoylated WCNF at DS 0.6 after heat treatment in air for 0.5h. Inset is the films after heat treatment.

5.3.4. Comparisons of thermal stability

Figure 5-8 shows the comparison of the thermal stability of BC nanofibers (BC1100), BC nanocrystals (BC300), NBKP, WCNF and their benzoylated derivatives. The data were obtained from the TG analysis of films prepared from each samples. Because the ultimate goal of thermal stabilization is to increase the temperature at the onset of degradation, only the 1% and 5% WLT are presented. Before benzoylation, BC1100, having the highest DPv, also showed the highest 1% and 5% WLT. Although the DPv of WCNF (700) is much higher than BC300, WCNF recorded the lowest 1% and 5% WLT. The presence of hemicellulose which has a much lower DP than BC300 could have contributed to the poor thermal stability of WCNF. Moreover, mechanical fibrillation must have also depolymerized and degraded the cellulose, producing more REs or decreasing the crystallinity. After benzoylation, the 1% and 5% WLT increased in all of the samples. Interestingly, NBKP gave almost similar 1% and 5% WLT as the BC1100 at DS 0.6. On the other hand, benzoylated WCNF only showed similar thermal stability as the benzoylated BC300. Because the WCNF was prepared by passing the NBKP four times to a grinder, degradation of cellulose and hemicellulose must have occurred, thus recovering a 1% and 5% WLT similar to BC was not achieved. Similar thermal stability as that of BC could have been achieved by WCNF if milder fibrillation process was adapted. Nevertheless, the increase in the 1% WLT of WCNF by more than 20^{o}C already increases the range of potential processing temperature for WCNF.

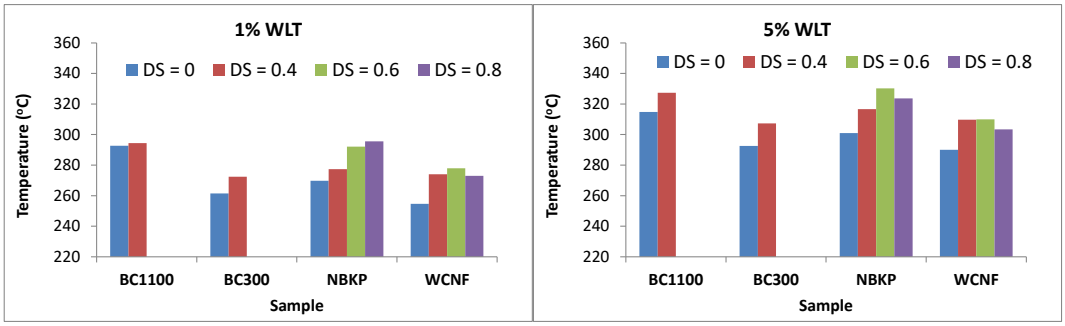

Figure 5-8. Comparisons of the onset of degradation temperatures of BC, NBKP, WCNF and its esters.

5.4. Summary

This chapter explored the potential of esterification in improving the thermal stability of wood-based cellulosic pulps (NBKP) and nanofibers (WCNF). Initially, different types of ester groups (C2, C14, BNZ and PIV) were introduced to NBKP at various DS. Esterification increased the T_{max} but the structure of the esters and the DS did not show significant variation on the T_{max}. The onset of degradation temperature, represented by the 1% and 5% WLT, and the resistance to weight loss during isothermal heating, varied with the DS. The optimum DS, which possibly esterified the hemicellulose and amorphous cellulose completely, was found to be 0.6. The BNZ and PIV esters consistently gave higher onset of degradation temperatures and resistance to weight loss than C2 and C14 esters.

Benzoylation, which has a faster reaction rate than pivaloylation, was then chosen to modify WCNF. The thermal stability of WCNF improved after benzoylation and the degree of improvement was not affected by varying the DS from 0.4-1.1. Improved resistance against thermal discoloration and depolymerization was also displayed by benzoylated WCNF.

When the thermal stability of benzoylated NBKP and WCNF were compared with that of the benzoylated BC1100 and BC300, benzoylated NBKP exhibited similar thermal stability as that of benzoylated BC1100. Benzoylated WCNF, on the other hand, only showed similar thermal stability as benzoylated BC300.

5.5. References

Adorjan I, Potthast A, Rosenau T, et al (2005) Discoloration of cellulose solutions in *N* -methylmorpholine- *N* -oxide (Lyocell). Part 1 : Studies on model compounds and pulps. Cellulose 12:51–57.

Alemdar A, Sain M (2008) Isolation and characterization of nanofibers from agricultural residues: wheat straw and soy hulls. Bioresour Technol 99:1664–71.

Barreto ACH, Rosa DS, Fechine PBA, Mazzetto SE (2011) Properties of sisal fibers treated by alkali solution and their application into cardanol-based biocomposites. Compos Part A Appl Sci Manuf 42:492–500.

Hubbe MA, Rojas OJ, Lucia LA, et al (2008) Cellulosic nanocomposites: a review. 3:929–980.

Jonoobi M, Harun J, Shakeri A, Misra M (2009) Chemical composition, crystallinity, and thermal degradation of bleached and unbleached kenaf bast (Hibiscus cannabinus) pulp and nanofibers. BioResources 4:626–639.

Martínez-Sanz M, Lopez-Rubio A, Lagaron JM (2011) Optimization of the nanofabrication by acid hydrolysis of bacterial cellulose nanowhiskers. Carbohydr Polym 85:228–236.

Peredo K, Reyes H, Escobar D, et al (2015) Acetylation of bleached Kraft pulp: Effect of xylan content on properties of acetylated compounds. Carbohydr Polym 117:1014–1020.

Sjöholm E (2004) Size Exclusion Chromatography of Cellulose and Cellulose Derivatives. In: Handbook of size exclusion chromatography. Marcel Dekker, Inc., New York, USA, pp 331–352

Sjöström E (1993) Wood Chemistry: Fundamentals and Applications, Second Edi. Academic Press, Inc., San Diego, CA, USA

Werner K, Pommer L, Broström M (2014) Thermal decomposition of hemicelluloses. J Anal Appl Pyrolysis 110:130–137.

Yang H, Yan R, Chen H, et al (2007) Characteristics of hemicellulose, cellulose and lignin pyrolysis. Fuel 86:1781–1788.

Yokoi H, Ishida Y, Ohtani H, et al (1999) Characterization of within-tree variation of lignin components in *Eucalyptus camaldulensis* by pyrolysis–gas chromatography. Analyst 124:669–674.

Chapter 6

Conclusions and Future Perspectives

6.1. Conclusions

With the goal of expanding the application of nanocellulose to high processing temperatures of thermoplastics with high melting points, this study investigated the factors affecting thermal stability and the effect of esterification on the thermal stability of various types of nanocellulose. To understand the thermal stabilization of pure cellulose, BC was initially used as a starting material to eliminate the effect of hemicellulose. The effect of DP and acetylation on the thermal stability of BC was evaluated in Chapter 2. Furthermore, the structure of the esters was varied and the degradation mechanism was deduced to understand how the structure of the esters affects thermal degradation (Chapter 3). The effect of esterification on thermally-induced depolymerization and discoloration of BC was further investigated in Chapter 4. After understanding the effect of esterification on the thermal stability of pure cellulose, wood-based cellulosic pulps and nanofibers were used to understand the effect of hemicellulose (Chapter 5).

The major observations presented in Chapters 2 to 5, can be summarized as follows:

- The thermal stability of BC with similar degree of crystallinity but different DP_v decreased with decreasing DP_v due to an increase in the number of REs as DP_v decreased.
- Acetylation improved the thermal stability of BC indicated by the higher 5% WLT and T_{max} of acetylated BC than untreated BC; and the degree of improvement increased with decreasing DP_v. The possible protection of REs contributed to the high degree of improvement in the thermal stability of BC with low DP_v.
- T_{max} of BC esters increased but the structure of the esters and DP_v have no significant effect on the values of T_{max}.
- The initial stage of degradation of BC is characterized by levoglucosan formation, which was observed in BC with low DP_v because of the possible catalytic effect of REs towards levoglucosan formation. When BC is esterified, levoglucosan formation was inhibited.
- Deprotection or the removal of the ester groups occurs at the onset of thermal degradation of BC esters, and two mechanisms of deprotection were proposed: (1)

the direct cleavage of the ester bond between nanocellulose and the ester group to produce the equivalent carboxylic acid; and (2) the condensation reaction between two ester groups to produce symmetrical ketones.

- Straight-chain esters (C2, C3, C8, C10 and C14) deprotect mainly by condensation reaction which was proposed to be driven by the acidic α-hydrogens. Bulky esters of BNZ, ADM, and PIV, which do not possess α-hydrogens deprotect by direct ester bond cleavage.
- The structure of the ester groups affects the onset of degradation, primarily attributed to the difference in the mechanism of deprotection. Esters with straight carbon chain sped up the onset of degradation while bulky esters (ADM, BNZ and PIV) delayed the onset of degradation.
- BNZ and PIV esters of BC did not only show improved resistance against thermal weight loss but also against thermally-induced depolymerization and discoloration.
- Esterification of wood-based pulps, NBKP, improved thermal stability and the degree of improvement depends on the DS. The DS that possibly esterified the hemicellulose and amorphous cellulose was found to give the highest degree of improvement.
- Benzoylation improved the resistance of WCNF against thermal weight loss, thermally-induced depolymerization and discoloration. The DS did not show significant effect on the thermal stability of benzoylated WCNF.

6.2. Future Perspectives

Thermal stabilization of nanocellulose, especially those derived from plant resources, is a challenging goal because their thermal stability is affected by several factors. Taking into consideration the effect of DP, it is recommended that to avoid severe decrease in thermal stability of nanocellulose, one must avoid processes that will cause severe depolymerization during the preparation of nanocellulose. Even though a high degree of improvement in thermal stability of low-DP nanocellulose can be achieved after esterification, still, the esterified low-DP nanocelluloses cannot surpass the thermal stability of high-DP nanocelluloses, especially if comparing the temperature at the onset of degradation. Thus, to be able to prepare thermally stable WCNF, the process of preparing WCNF must first be optimized in the future so that subsequent chemical modification will be more effective.

Finally, this study must have answered several questions about thermal stabilization of nanocellulose by esterification but also opened up new issues left unanswered but possibly worth considering for further studies. Investigation on the structure of the residual cellulose after ester removal is recommended in order to understand how the change in the structure of residual cellulose affects the resistance or susceptibility of cellulose against thermally-induced depolymerization and discoloration. The mechanism of thermal degradation of esterified hemicellulose is also worth investigating in order to clarify the role of hemicellulose on thermal stabilization of wood-based nanocellulose.

Acknowledgments

This study would have not been possible without the people who wholeheartedly helped me in so many ways.

First and foremost, I am thankful to Prof. Hiroyuki Yano, my research advisor, for accepting me as his PhD student. His guidance, suggestions, and words of encouragements helped me a lot in conducting this research.

I am also very grateful to Prof. Fumiaki Nakatsubo, who patiently taught me a lot of experimental techniques in chemical modification of cellulose and related compounds. His expertise in organic chemistry contributed greatly to the realization of this study.

I also wish to extend my gratitude to my examiners; Prof. Tsunehisa Kimura and Prof. Toshiyuki Takano, for their valuable comments that helped in improving this manuscript.

My heartfelt gratitude also goes to all the members of the Laboratory of Active Bio-based Materials (LABM) who helped me in so many little ways, which when summed up altogether contributed a lot in making my stay at LABM easier, more convenient and memorable. I wish to thank specifically Kitano san, Igarashi san, Homma san, Ando san, Omura san, Abe sensei, Chuchu san, Subir san, and Ishimaru san.

I also wish to acknowledge my Filipino and foreign friends here in Kyoto, especially Josko, Dalton, Vince and Master san, who gave me all the laughs and fun moments when not in the laboratory.

The scholarship grant from Monbukagusho (Ministry of Education, Culture, Sports, Science and Technology) is gratefully acknowledged.

My university in the Philippines, Central Luzon State University, especially the members of the Chemistry Department, is thanked for their continued support.

Finally, I also owe my greatest thanks to my family, especially my older sister, who has always been supportive and helpful to me. And the person who added a different color to my stay here in Japan, Paavo, is warmly thanked for all the discussions that ranged from mundane topics to more scientific and technical issues, as well as to all the side trips and fun. His family is also warmly thanked for their endearing words of encouragements.

I THANK YOU all for making one of my dreams a reality.

Melissa B. Agustin
Kyoto University, January 2017

List of Publications

The contents of this thesis have been described in the following publications:

1. "The thermal stability of nanocellulose and its acetates with different degree of polymerization", Melissa B. Agustin, Fumiaki Nakatsubo, Hiroyuki Yano, *Cellulose* **2016**, 23[1], 451–464 (**Chapter 2**)
2. "Products of low-temperature pyrolysis of nanocellulose esters and implications for the mechanism of thermal stabilization" Melissa B. Agustin, Fumiaki Nakatsubo, Hiroyuki Yano, *Cellulose* **2016**, 23[5], 2887–2903 (**Chapter 3**)
3. "Improved resistance of chemically-modified nanocellulose against thermally-induced depolymerization " Melissa B. Agustin, Fumiaki Nakatsubo, Hiroyuki Yano, (Accepted for publication to *Carbohydrate Polymers*) (**Chapter 4)**